Analysis of Critical Infrastructure Interactions

Kevin Paul Schneider

A dissertation submitted in partial fulfillment of the
requirements for the degree of

Doctor of Philosophy

University of Washington

2005

Program Authorized to Offer Degree: Electrical Engineering

University of Washington
Graduate School

This is to certify that I have examined this copy of a doctoral dissertation by

Kevin Paul Schneider

and have found that it is complete and satisfactory in all respects,
and that any and all revisions required by the final
examining committee have been made.

Chair of the Supervisory Committee:

____
Chen-Ching Liu

Reading Committee:

____
Chen-Ching Liu

____
Kai Strunz

____
Lawrence Jones

Date: ______________________

University of Washington

Abstract

Analysis of Critical Infrastructure Interactions

Kevin Paul Schneider

Chairperson of the Supervisory Committee:
Professor Chen-Ching Liu
Department of Electrical Engineering

The modern power infrastructure has evolved from small isolated circuits into an expansive interconnected system that is dependent on multiple supporting infrastructures. One of the most significant and potentially detrimental supporting infrastructures to interact with power systems is telecommunications. Currently there are no established analytic techniques that enable system operators or planners to analyze the interactions that occur at the seam between these two critical infrastructures.

Until the late 1960's there were few interactions between the power and telecommunications infrastructures. This changed with the Northeastern blackout of 1965 which began the large scale integration of power and communications systems. For the following 20 years the addition of communications systems increased the overall reliability of power systems and allowed for new operational paradigms. However, within the past 20 years there have been an increasing number of blackouts that involve elements of the telecommunications infrastructure. This is due in part to the increased system level integration that has occurred without a corresponding increase in analysis.

This dissertation presents a method for analyzing and assessing potential

vulnerabilities that affect the interface of the power and telecommunications infrastructures. The presented method is used to analyze two existing Special Protection Systems as well as the topology identification component of the North East Pacific Times-series Underwater Networked Experiment Energy Management System. These systems are analyzed for potential vulnerabilities that affect the interface of the power and telecommunications infrastructures and could initiate or contribute to catastrophic blackouts. While it is not possible to stop the occurrence of catastrophic blackouts the proposed vulnerability assessment method can help to reduce their rate of occurrence and minimize their severity when they do occur.

Table of Contents

List of Figures

Figure Number Page

List of Tables

Table Number Page

Acknowledgements

The list of people and organizations that have helped me to reach this point is considerable and I apologize if there is anyone who I fail to mention.

First I would like to thank Professor Paul Boynton who allowed me to work with his research group while I was an undergraduate in the Physics Department. Within this research group Dr. Michael Moore and Keven McKenney spent considerable time aiding me in my work as an undergraduate.

When I first started graduate school my work was made possible by the Grainger Foundation, who generously supported my work for the first year and a half. Their support allowed me to explore areas of research that I otherwise would not have been able to.

Soon after beginning Graduate School I had the good fortune to work with the NEPTUNE power group. Within that group I would like to than Professor Chen-Ching Liu, Dr. Bruce Howe, Dr. Harold Kirkham, Professor Mohammad El-Sharkawi, Tim McGinnis, and Phil Lancaster, all of whom helped me to see how a collaborative effort can work successfully. The work on the NEPTUNE power system was funded by the National Science Foundation with the grant, "Development of a power system for cabled ocean Observatories", OCE-0116750.

I have also has the privilege of working with the Advance Power Technologies Center at the University of Washington. This industrial consortium has been generous enough to support my work for the past year and a half. Working with this group has shown me the value of collaborative efforts between academia and industry. The APT Center is supported by AREVA T&D, The Bonneville Power Administration, CESI, LS Industrial Systems, PJM, and Réseau de Transport d`Eletricité.

I owe a special debt of gratitude to Professor Chen-Ching Liu who has been my advisor for the past four and a half years. He has aided me throughout my studies and helped me to become a better scholar and engineer. Without his guidance this work

may never have been completed.

Finally, I would like to thank my dad who has given me the character to succeed at so many things in life. Without his guidance over the years my life would not be what it is today. For this I am eternally grateful.

Chapter 1: Introduction

Proper operation of the electric power infrastructure is an essential element of modern society. In addition to electricity, society is equally dependant on other infrastructures such as banking, health care, natural gas, oil, telecommunications, transportation, water, and waste disposal [1]. When any of these infrastructures fails to operate correctly, the cost to society in terms of lost productivity and additional expenditure of resources is substantial. This is especially true of the power infrastructure which is the lynch pin that allows for the proper operation of the other critical infrastructures.

While the power industry provides services that are essential for the proper operation of every other major infrastructure, it is by no means independent of these other infrastructures [2]. This fact has become increasingly evident in the past forty years as the power industry has begun to make extensive use of emerging telecommunications technologies. One of the motivating factors for the greater integration of communications systems is the concurrent advance that has been made in computer capabilities. The combination of powerful computers and high speed communications systems allows modern power systems to perform complex tasks that were not possible forty years ago. Accompanying these new abilities are new modes of failures within power systems. Traditional vulnerabilities to events such as natural disasters and single point equipment failures are now joined by new vulnerabilities that arise due to the interaction of the power and telecommunications infrastructures.

With the introduction of competitive economic markets the operating philosophies of the vertically integrated monopoly have begun to give way to new philosophies that push systems closer to their physical limits. In part, it is these economic pressures that have created interest in the interface of the power and telecommunications infrastructures. The initial work that has been performed to examine the interface has concentrated more on increasing the allowable operating limits of the power system and less on the potential consequences of failures at the interface. As a result, there has been no systematic analysis of potential vulnerabilities.

The risk of not fully examining potential vulnerabilities is that events occurring at the interface can affect large areas due to the interconnected design of modern power systems. Although there have been major blackouts that were the result of events at the interface of these infrastructures [3], there has been little substantive work to analyze the role of the communications systems. This dissertation will develop a systematic method for the analysis of interactions that affect the interface of the power and telecommunications infrastructures in order to identify potential vulnerabilities. Once potential vulnerabilities have been identified they can be properly addressed so that the vulnerability can be mitigated or completely eliminated.

1.1 Power System Vulnerabilities

Power systems are vulnerable to events that originate from a number of sources including but not limited to: natural disasters, human error, gaming in the electricity markets, sabotage, and communications system failures. Any one of these sources can be either a triggering cause or a contributing factor to a catastrophic outage.

1.1.1 Natural Disasters

Natural disasters can have a variety of effects on power systems, ranging from damage to individual components to widespread outages. The manifestation of natural disasters varies greatly by geographic location. In order to understand the impact of natural disasters on power systems a number of situations will be examined.

In the northern latitudes of North America freezing rain and snow can lead to excessive mechanical stresses on transmission lines and their support towers. While transmission line towers are engineered to support snow and ice in addition to the dynamic load of the cable, extremely severe storms can cause an accumulation of ice which exceeds the failure stress of the towers. One such event occurred from January 5th-10th 1998 in the Hydro-Québec power system [3]. Starting on January 5th freezing rain and snow began accumulating on the support towers for 230-kV, 315-kV, and 735-kV transmission lines throughout the Hydro-Québec system. By the morning of January 6th several 735-kV transmission line towers had collapsed, removing their lines from service and shifting power flows to the lower 230-kV and 315-kV lines. Over the next few days the intensity of the storm continued and additional transmission lines fell. By the 10th of January over one hundred and twenty towers within the 735-kV system had collapsed together with over two hundred towers in the 230-kV and 315-kV systems. In all, service to approximately 1.4 million customers was interrupted. Due to the severity of damage and the large geographic area affected, it was not until February 8th that service was restored to all customers.

In the Southeastern United States tropical storms and hurricanes are major concerns for local area residents, as well as power system operators. When the wind speed of a tropical storm reaches seventy-four miles per hour it is reclassified as a category 1 hurricane. These high winds can cause transmission lines to swing into each other resulting in intermittent phase to phase faults, an effect known as "line galloping". Additionally, trees can fall into power lines and debris can be thrown into sub-stations. On October 3rd 2002 Hurricane Lili caused widespread damage and outages to customers of Cleco Power [3]. Approximately 164,500 customers across Louisiana and Mississippi were affected. More recently Hurricane Katrina devastated Louisiana and portions of other Southern States in August of 2005. The full extent of the damage still has not been assessed at the time of this writing but it is by far the most devastating Hurricane on record.

Large earthquakes have been some of the most destructive natural disasters in recorded history. The effects on power systems can range from toppled transmission line towers to physically damaged generation units, nuclear units being of particular concern. On October 17th 1989 at 10:04 Pacific Daylight Time a magnitude 6.9 earthquake struck the San Francisco area. Extensive damage to the power system resulted in the loss of service to 1.4 million Pacific Gas and Electric (PG&E) customers [3]. Fortunately the Pacific AC Intertie with the Pacific Northwest was not damaged, or the extent of the blackout would have been much more severe.

Snow storms, hurricanes, and earthquakes are the natural disasters which are most commonly associated with blackouts. Other less common events can also have severe impacts on power systems. Solar flares on the surface of the sun can result in magnetic storms in the earth's atmosphere. Since transmission systems operate on the propagation of electromagnetic waves, magnetic storms can make a significant impact. On March 18th 1989 at 2:45 a.m. five transmission lines from the James Bay generation complex in the Hydro-Québec system were tripped due to a solar magnetic storm [3]. The loss of the five transmission lines isolated 9,450 MW of generation from the rest of the system, at a time when the total system load was approximately 21,350 MW. The isolation of over 44% of the system generation was not a contingency that the system was able to survive. As a result 19,400 MW of load within the Hydro-Québec system was lost as well as the export of 1,325 MW. Only 625 MW of islanded load was not interrupted.

The actions of small animals are a natural occurrence which can also adversely impact the operation of a power system. On March 26th 1985 woodpecker damage to a tree resulted in a fault on a 230-kV transmission line in the Florida Power Company (FPC) service area [3]. The breakers on either side of the fault tripped during the initial fault and then reclosed. Due to slow clearing time of the fault, generation at the Anclote and Bartlow generation plants was lost and Pinellas County was isolated from the rest of the system. In this case, the actions of a single small bird resulted in the interruption of service to 170,000 FPC customers.

From these examples it can be seen that even modern power systems are vulnerable to natural disasters. Due to the severity and broad reach of natural disasters they have the potential to cause catastrophic blackouts. Natural disasters cannot be prevented, but their impact on power systems can be minimized through proper planning, robust system designs, and adequate training for personnel who operate the systems.

1.1.2 Human Error

Human error is very different from deliberate acts of sabotage. Human error occurs when operators make every attempt to properly plan and operate a system, but due to lack of situation awareness or mistakes, the system is incorrectly planned or operated. Human error is becoming a more significant factor as power systems become larger and more complex.

Errors in power system planning can range from providing inadequate reactive power support in an area to misjudging economic markets and constructing new generation in areas where the load demand fails to meet expectations. Possibly one of the largest planning miscalculations in the power industry was the rush to build nuclear power plants in the 1960's. Through a combination of immature technologies, negative public perception, and decreasing electricity demands due to conservation, those who invested in nuclear power plants lost substantial sums of money. Presently there are just over one hundred non-military nuclear power plants in the United States providing approximately 20% of the nation's electricity [4]. There has been no new construction of nuclear power plants in the last two decades.

With the ever increasing size of operating areas it is becoming more difficult for operators to maintain situational awareness. With the loss of situational awareness comes the possibility that operators may take actions that do not benefit the system. This has been seen when operators are reluctant to shed small amounts of load in order to maintain overall system stability. Emerging economic factors place even more stress on not interrupting power to customers. The result is that in an attempt to maintain customer service in a local area, catastrophic blackouts can occur.

Human error will always play a role in the planning and operation of power systems. Through adequate training of planners and operators and the development of robust systems, the impact of human error can be minimized.

1.1.3 Market Gaming

In an ideal economic market no single participant controls enough of the market to have “market power”, meaning that no single participant can significantly affect the price of goods. One aspect of market gaming is an attempt by an individual or group of individuals to utilize their share of the market in an attempt to manipulate the market price, regardless of the negative effect these actions may have on the market as a whole. One possible way to achieve this would be to limit the amount of available generation in a region by performing unnecessary maintenance on major generators. If there is a small gap between the supply and demand in the region the idling of key generators could be enough to result in massive price spikes. Similar results could be achieved by purposely congesting transmission lines into an area that is generation deficient. If the demand in an area outstrips available supply rolling blackouts or a total system collapse could result.

The only effective way to ensure that market gaming does not adversely effect the power system is to have proper regulatory policies and oversight in place to prevent harmful market gaming.

1.1.4 Sabotage

Sabotage is the direct, or indirect, attempt to cause damage to the power infrastructure. Direct attacks have taken the form of damaged transmission towers while indirect attacks took the form of the terrorist attacks of September 11th 2001, which destroyed the sub-stations in the basements of the World Trade Centers.

On July 24th 1989 at 08:22 Eastern Standard Time the Baker-Broadford 765-kV transmission line in the Appalachian Power system tripped open [3]. Subsequent investigation revealed that tower #255 near Elkhorn City, Kentucky, had been toppled by explosives placed on two of the four tower legs. The loss of the Baker-Bradford line was a single contingency event and as such no load was lost. But as a result of the loss of the 765-kV line, increased power flows across Pennsylvania, Virginia, and West Virginia required coordinated curtailments of scheduled transactions.

On September 19th 1990 at 22:20 Eastern Standard Time an off-duty Hydro-Québec employee deliberately grounded a transformer bank at the Hertel sub-station [3]. Two 315-kV lines, seven 735-kV lines, and four static compensators were affected by the grounding. 200,000 customers accounting for 4,000 MW of load lost service during the event, power was restored by 22:35 Eastern Standard Time.

Due to the highly distributed nature of power systems it is impractical to provide physical security for every generator, sub-station, and transmission line. Currently the best solution is to provide security at key central locations and to plan and operate the system so that acts of sabotage can be isolated to small areas and load loss minimized.

1.1.5 Information and Communications System Failures

Information and communications system failures are perhaps the most complex to analyze because of the interactions between the two infrastructures. Since the Northeastern blackout of 1965 power systems have relied significantly on the telecommunications infrastructures. In the wake of the 1965 blackout engineers struggled to deal with the aftermath and the implications of an event that had been previously considered impossible. The evolution of the modern computerized Energy

Management System (EMS), which makes extensive use of communications systems, can be traced back to the 1965 blackout [5].

In 1997, under the Clinton administration, the President's Commission on Critical Infrastructure Protection published [1]. It was noted that: "The exponential growth of information system networks that interconnect the business, administrative, and operational systems contributes to system vulnerability." It is the interactions between the telecommunications and power infrastructures, and the resulting potential vulnerabilities at their interfaces, which is the focus of this dissertation.

1.2 Significant Power System Blackouts

Blackouts have occurred since the operation of the first complete power system in September 1882. In an attempt to track the occurrence of blackouts the United Stated Department Of Energy (DOE) has establish criteria for the reporting of blackouts [6]. Form EIA-417 must be submitted to the DOE Operations Center if any one of the following criteria applies to an event:

1. Uncontrolled loss of 300 MW or more of firm system load for more than 15 minutes from a single incident.
2. Load shedding of 100 MW or more implemented under emergency operational policy.
3. System-wide voltage reductions of 3 percent or more.
4. Public appeal to reduce the use of electricity for purposes of maintaining the continuity of the electric power system.
5. Actual or suspected physical attacks that could impact electric power system adequacy or reliability; or vandalism, which targets components of any security system.
6. Actual or suspected cyber or communications attacks that could impact electric power system adequacy or vulnerability.

7. Fuel supply emergencies that could impact electric power system adequacy or reliability.

8. Loss of electric service to more than 50,000 customers for 1 hour or more.

9. Complete operational failure or shut-down of the transmission and/or distribution electrical system.

The North American Reliability Council (NERC)[1] Disturbance Analysis Working Group (DAWG) has compiled blackout data which has been reported to the DOE under the requirements of [6]. This database contains information dating back to 1984.

In an attempt to understand the characteristics of blackouts, the analyses of seven blackouts are reviewed in Appendix 2. The analysis of Appendix 2 is a review of reports that have been published by government organizations and power companies.

What can be seen from the reports is that contributory events in the telecommunications infrastructure are becoming more common. In the 1960's and 1970's there were no significant blackouts which could be attributed to interaction of the power and telecommunications infrastructures. In the 1980's and 1990's this began to change as communications systems were more widely used as integral power system components. It is the evolving interaction between the power infrastructure and these communications systems which is of interest.

1.3 Overview of Power System Infrastructure

In order to completely understand the interactions between power and communications systems it is necessary to have a thorough understanding of modern power systems. In particular two aspects of the power infrastructure will be examined,

---

[1] On August 8th 2005 the Energy Policy Act of 2005 was signed into law. This legislation authorized the formation of an Electric Reliability Organization (ERO) with the ability to enforce compliance with reliability standards. NERC will become the ERO for the U.S. and Canada.

Special Protection Systems (SPSs) and EMSs. Both of these system types will be introduced in this chapter and then further addressed with specific examples in their own subsequent chapters.

1.3.1 Overview of Special Protection Systems

SPSs are designed to detect a set of predetermined system conditions and to generate appropriate control signals. Generally the predetermined system conditions correspond to situations which place undesired stress on the power system. While continuous actions such as High Voltage Direct Current (HVDC) control can be performed, the vast majority of SPSs are discontinuous actions such as breaker operations, load shedding, and generator tripping. One of the most common motivations for installing SPSs is to defer the capital investment associated with expansion of transmission systems [17-19]. For the same reasons dedicated communications systems are rarely installed specifically for a SPS, instead existing legacy systems are often pressed into service. This is slowly changing as more utilities install newer fiber optic systems.

In contrast to local protection systems which generally operate equipment in the same area where measurements are made, SPSs can operate equipment which is spatially disparate from the sensing points. As a consequence of this characteristic communications systems are an integral part of many SPSs. Generally measurements are made throughout the system and collected at a central control center. At the control center the inputs are evaluated and control signals are sent to remote equipment. In Appendix 2 a number of SPSs were encountered when examining blackouts, Appendix 3 examines five specific SPS in detail in order to place their operation in the context of overall power system operations.

1.3.2 Overview of Energy Management Systems

Since the New York Blackout of 1965 power system operators have had an increased awareness of the necessity of properly coordinating power systems. In order to coordinate power systems spanning hundreds and sometimes thousands of miles, an extensive telecommunications infrastructure was necessary. As a direct result of the 1965 blackout the electric power industry saw the emergence of the computerized EMS which utilized the existing legacy telecommunications infrastructure. Even with the legacy telecommunications infrastructure that existed during the 1960's the design of an EMS was limited by computer technology. Due to the available computers of the time these early systems could only perform a relatively few number of calculations per second. In order to compensate for the limited abilities of the hardware, software was highly optimized and tailored specifically to a given hardware platform in order to perform larger and more complex calculations. The result of the software optimization was that the various components of the EMSs were so interdependent that the architecture was “closed” [26-28]. A closed architecture system is shown in Figure 1.1.

The architecture of the earlier systems was closed in the sense that systems were not able to be upgraded or modified in a piecemeal manner due to the extensive interdependence of the components. Instead, entire systems had to be replaced every five to ten years or risk using out of date technology. In addition, the O&M cost for the older legacy systems was considerable. Adding to the O&M cost, vendors could go out of business and the utilities would then have to have their own in-house team of full time engineers as well as supplies of spare parts. For these reasons, and others, modern EMS designs have focused on an “open” architecture concept, shown in Figure 1.2.

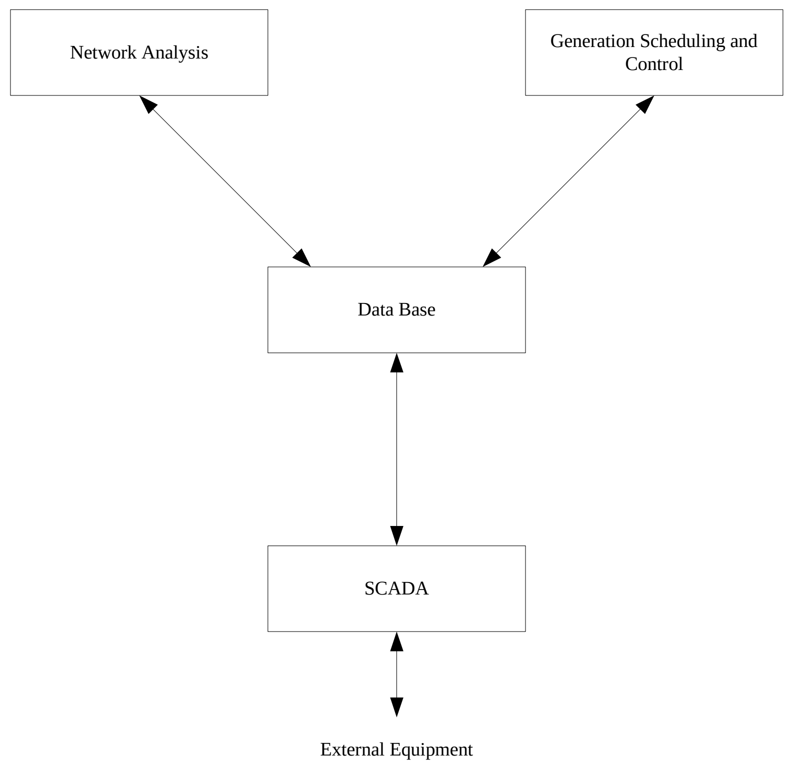

Figure 1.1: Closed EMS architecture

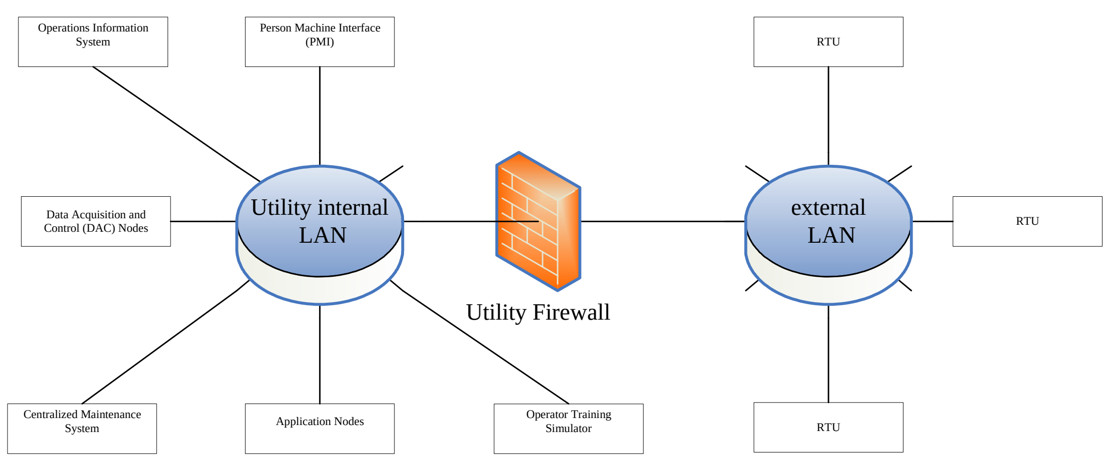

Figure 1.2: Open EMS architecture

While the open architecture concepts are still relatively new, there are five major concepts that distinguish the new architecture from the older closed architecture designs. They are:

- Portability: Refers to ability of the software to run on different software and hardware platforms.
- Interoperability: Refers to the ability to run different software and different hardware together in the same network.
- Expandability: Refers to the ability to increase the size of the system as well as the scope of the software.
- Modularity: Refers to the ability to add new software functions without adversely affecting the rest of the system.
- Scalability: Refers to the ability to apply the same software to systems of various sizes.

With the open architecture concept and the computational power of modern computers the interactions between power and telecommunications infrastructures have become more complex. State estimation and topology identification are two of the functions within a modern EMS that require extensive interactions between these infrastructures. For both state estimation and topology identification the power system may not be able to directly obtain all of the state information of the power system. As a result the available information is transmitted to a central control center via a Supervisory Control And Data Acquisition (SCADA) system using the telecommunications infrastructure, where the information is processed. The relevant control signals are then dispatched back to the power system via SCADA which again makes use of the telecommunications infrastructure. Even with the open architecture designs that have been implemented there is a significant reliance on the telecommunications infrastructure.

1.4 Current Methods of Modeling Infrastructure Interfaces

In recent years it has become increasingly apparent that there is a mutual reliance among the critical infrastructures upon which society is built. A 1997 report in the United States by the President's Commission on Critical Infrastructure Protection titled "Critical Foundations: Protecting America's Infrastructure" cited eight critical infrastructures as being: "…so vital that their incapacity or destruction would have a debilitating impact on our defense and economic security" [1]. The eight critical infrastructures were: transportation, oil and gas production and storage, water supply, emergency services, government services, banking and finance, electrical power, and telecommunications. What was not discussed in significant detail was that disruptions in one critical infrastructure can have catastrophic consequences in other infrastructures.

Despite its importance, there currently is limited literature pertaining directly to the issue of interaction between infrastructures. One representation for infrastructure interdependencies that has attempted to lay a non-analytical foundation describing these interactions is found in [28] and [39]. Building on the work of [28] and [29] the authors of [30] have attempted to analytically describe the interactions using marked Petri Net (PN) models. The work presented in [28-30] has attempted to examine interactions among the eight critical infrastructures in a general context so that all eight could be tied together into a single model.

While the infrastructure of natural gas distribution is important to gas turbine plants, it is not probable that the loss of supply at a single generation facility will result in a catastrophic blackout; the same statement is not true of the telecommunications infrastructure. A single failure within the telecommunications infrastructure can interact with the power infrastructure in such a way that the result is a catastrophic blackout. For this reason the interactions between the power and telecommunications infrastructures are of significant importance to power system operations [31].

Currently there are very few published articles that address the issue of interactions between the power and telecommunications interface, and none that attempt to analytically describe the interactions. What can be found in available literature is an understanding of the limitations of the current telecommunications infrastructure as well as proposals for new communications system architectures; these projects include GridWise™, GridStat and the Eastern Interconnect Phasor Project (EIPP) [32-34]. The projects include the installation of new communications lines and the implementation of new software protocols. Within these new architectures the concept of Quality of Service (QoS) is prominent; QoS address the issues of bandwidth, reliability, and latencies. As with the majority of the work that has been previously done these projects treat the operation of the power and telecommunications infrastructures independently for the purposes of analysis.

While articles may not be specifically published utilities do have methods for assessing their communications systems. One such company is the Bonneville Power Administration (BPA) which makes extensive use communications system intensive SPSs [35]. In lieu of a formal analysis of the interaction of the power and telecommunications infrastructures BPA applies a set of assumptions. In particular, based on past experience they have found that their communications system has a maximum latency of 40 milliseconds. Based on this number all communications signals are assumed to take less than 40 milliseconds to be transported from source to destination. The maximum value is then used when performing simulations and system planning involving the communications system. With respect to redundancy the telecommunications infrastructure used by BPA was designed so that there are always two parallel paths. This redundancy is only applied to the communications paths and not necessarily to component level functions. There is no formal analysis for the effects of communications signals with higher than expected latencies or failures at the component level.

This dissertation will develop an analytic method for the analysis of interactions that affect the interface of the power and telecommunications infrastructures in order to identify potential vulnerabilities. The analytic method will make use of a process by which the two infrastructures are combines into a single model. The goal of this vulnerability assessment will be to limit the occurrence of catastrophic blackouts and to minimize their affect when they do occur.

The remainder of this dissertation is divided into three chapters. Chapter 2 introduces PN models and discusses how they can be used to examine infrastructure interactions. This chapter forms the vulnerability assessment method that will be used in subsequent chapters to analyze SPSs and EMS functions. Chapter 3 uses PN models to evaluate two existing SPSs and to identify potential vulnerabilities at the infrastructure interfaces. Chapter 4 examines one of the specific energy management functions of the North East Pacific Times-series Underwater Networked Experiment (NEPTUNE) and applies Petri Net models to its operation. Chapter 5 contains the concluding remarks for this dissertation.

Chapter 2: Modeling of Infrastructure Interfaces

Petri Nets are a graphical and mathematical tool developed by Carl Adam Petri and presented in his 1962 Doctoral Dissertation [37]. Since their introduction marked PN models have found a variety of applications [38-41], including the modeling of critical infrastructures [28], [42], and [43]. As was noted in the previous chapter these attempts to model infrastructure interactions were generalized to large scale system events such as disruptions in the natural gas supply.

This chapter will begin with a review of the basic concepts used in marked PN models and then examine their applications to power systems. Based on these concepts, and new techniques presented in this chapter, an analytic method for the analysis of interactions that affect the interface of the power and telecommunications infrastructures will be presented. This method will then be applied in subsequent chapters to analyze potential vulnerabilities in SPSs and EMS functions which could contribute to catastrophic blackouts.

2.1 Petri Net Structure

From [38] the graphical representation of a marked PN model has places P, transitions T, input and output arcs A, and an initial marking M_o.

$$PN \equiv (P, T, A, M_o) \tag{2.1}$$

Where:

$$P = \{p_1, p_2, \ldots . p_n\}$$
$$T = \{t_1, t_2, \ldots, t_m\}$$
$$A \subset \{P \times T\} \cup \{T \times P\}$$
$$M_O = \{\mu_1, \mu_2, \ldots, \mu_n\}$$

Additionally, the probability of a transition firing, the Transition Probability (TP), and the time required for a transition to occur, the Transition Time (TT), will be added to reflect the probability of a transition occurring, as well as the finite time necessary for a transition to occur.

$$PN \equiv \left(P, T, A, M_o, TP_i, TT_i\right) \tag{2.2}$$

Where:

TP_i : Percent chance of the ith transition occurring

TT_i : Time require for the ith transition to occur

2.1.1 Place Nodes

For each piece of equipment in the power and communications systems there will be a number of P nodes to indicating the possible states. Examples of P nodes include: “breaker open”, “breaker closed”, “signal in transit”, and “load shedding signal at load shedding computer”.

Since there are system characteristics that are not determined by any single piece of equipment, “global P nodes” will be used to represent global system characteristics. Examples of global P nodes will include: “generation and load matched”, “generation deficiency”, and “control computer available”.

Another type of P node is a “source/sink” node which contains an initial marking which will not change regardless of the number of markings moved into or out of it. In effect the node has an infinite number of markings. This type of P node is important when modeling devices that rely on a control element. For example, the generation of a control signal may require the control computer to be operational but the generation of the control signal does not make the control computer non-operational. Therefore in order to enable certain transitions source/sink P nodes are used. A complete failure of the control element can be modeled by not marking the P node in the initial marking.

2.1.2 Transition Nodes

For every action that affects a state represented by a P node there will be a number of associated T nodes. A T node is “enabled” if each of the input P nodes contains a number of markings equal to the weight of the input arc. Only enabled T nodes are able to “fire”. The firing of a T node will be determined by the TP once a node is enabled.

Every T node will have an associated TP which reflects the stochastic characteristics of physical systems. For example, for a given relay there may only be a 99.999985% chance of proper operation. These values can be taken directly from Failures In Time (FIT) rates or determined empirically for physical components. Individual TPs can also be set to 0.0 or 1.0 in order to examine the system responses to the failure of specific equipment. Furthermore, a T node may be fired based on the calculations of a relay or other computer. For example, an enabled T node will only fire, TP=1.0, if a differential current measurement is greater than 50 amps, otherwise TP=0.0.

Each T node will also have an associated TT to reflect the finite time necessary for events to occur. Examples of transition times include, “time necessary for breaker contacts to physically separate”, “time required for a packet of information to propagate along a fiber optic cable”, and “computational time required for the control computer to process a signal”.

2.1.3 Weighted Connecting Arcs

Connecting arcs determine which P nodes are affected by the firing of a T node. When a T node fires it moves a number of markings based on the weight of the connecting arc. Different arcs will have different weights based on their function within the system. The weight of a connecting arc is shown in a PN model by an adjacent positive integer value. Connecting arcs are where the interfaces between the power and telecommunications infrastructures are represented. Arcs between T nodes of the telecommunications infrastructures and P nodes of the power infrastructure will be of the most interest.

2.2 Algebraic Representation of Petri Net Models

With the individual components of a marked PN model defined, a simple example will be examined in order to develop the algebraic representation. Figure 2.1 shows a diagram of the operation of two breakers isolating a single phase to ground fault; the associated marked PN model is shown in Figure 2.2. Each side of the transmission line has a relay, R1 and R2, which sense the fault and generated trip signals for the associated breakers, B1 and B2 respectively.

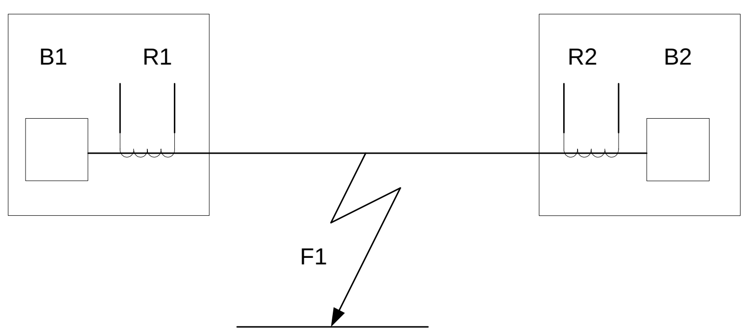

Figure 2.1: Diagram of a phase to ground fault

Within the PN model of Figure 2.2 there are two parallel marking paths, each one representing the operation of one of the two breakers. The only way that the fault can be cleared, and the model returned to the initial un-faulted marking M_o, is for both of the breakers to operate properly. Following the work of [37], the coincidence matrix for Figure 2.2 is constructed (2.3).

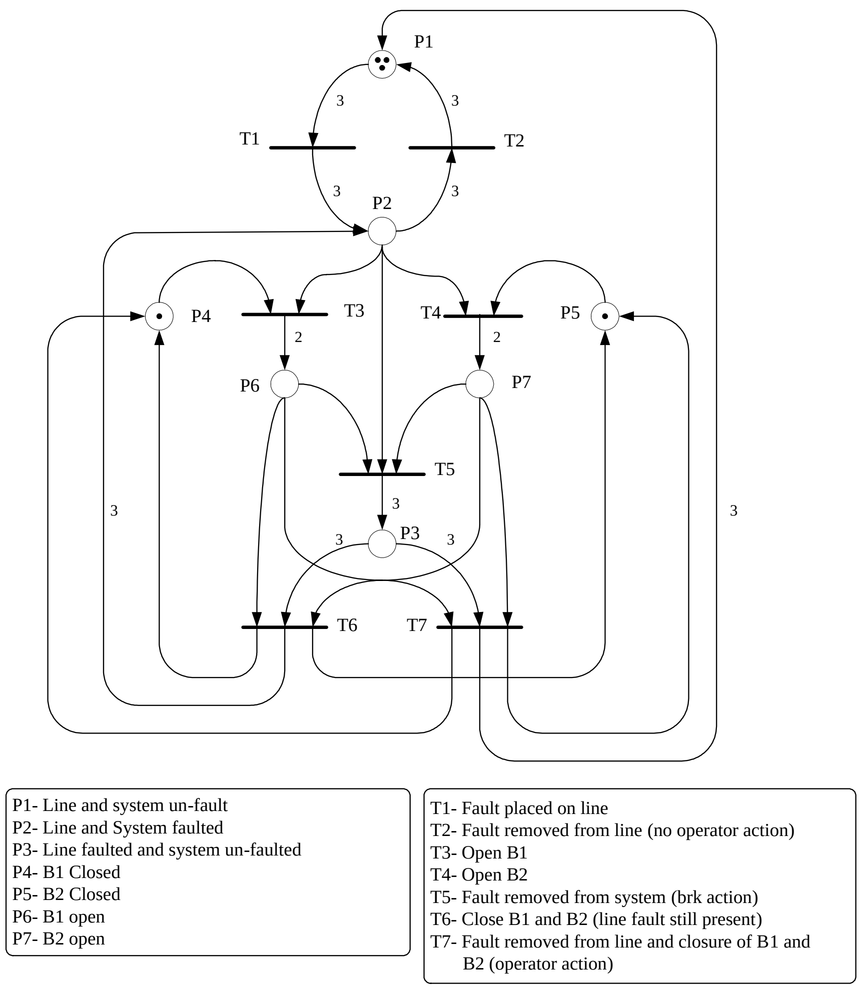

Figure 2.2: PN model for diagram of Figure 2.1

$$C^T = \begin{bmatrix} -3 & 3 & 0 & 0 & 0 & 0 & 3 \\ 3 & -3 & -1 & -1 & -1 & 3 & 0 \\ 0 & -1 & 0 & 0 & 3 & -3 & -3 \\ 0 & 0 & -1 & 0 & 0 & 1 & 1 \\ 0 & 0 & 0 & -1 & 0 & 1 & 1 \\ 0 & 0 & 2 & 0 & -1 & -1 & -1 \\ 0 & 0 & 0 & 2 & -1 & -1 & -1 \end{bmatrix} \tag{2.3}$$

The coincidence matrix of (2.3) is the algebraic representation of the movement of markings for the PN model of Figure 2.2. The entries show which P node are connected to which T nodes and the weight of the connecting arc. For example, the entry of -1 at (3,2) indicates that when T node 3 fires, P node 2 loses 1 marking.

2.3 Reachability of Petri Net Models

Using the coincidence matrix of (2.3) it is possible to determine the final marking, given the initial marking, and the firing matrix.

$$M_f = \left(M_o + \left(C^T U_k\right)\right) \tag{2.4}$$

Where:

M_f : Final marking

M_o : Initial marking

U_k : Firing matrix

The firing matrix is a column vector containing an entry for each of the T nodes that fire. It is also possible for a T node to fire more than once, in which case the entry would be an integer value greater than one. In [39] it is shown that if there exists a firing sequence, U_k, which transforms M_o to M_f then (2.5) holds true.

$$B_f \Delta M = 0 \tag{2.5}$$

Where:

$$B_f = \left[I \quad | \quad -C_{11}{}^T \quad \left(C_{12}{}^T\right)^{-1} \right]$$
$$\Delta M = M_f - M_o$$

By examining all of the possible markings that satisfy (2.5) the reachability graph for the PN model of Figure 2.2 can be generated, shown in Figure 2.3. The reachability graph of Figure 2.3 assumes that the TP of each transition is 1.0 and that there are no requirements on TTs.

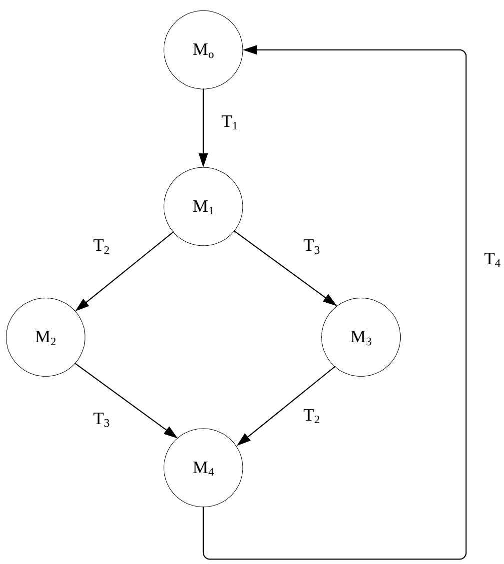

$$M_0 = \begin{bmatrix} 2 & 1 & 0 & 1 & 0 & 0 \end{bmatrix}^T$$
$$M_1 = \begin{bmatrix} 0 & 1 & 2 & 1 & 0 & 0 \end{bmatrix}^T$$
$$M_2 = \begin{bmatrix} 0 & 0 & 1 & 1 & 2 & 0 \end{bmatrix}^T$$
$$M_3 = \begin{bmatrix} 0 & 0 & 1 & 1 & 0 & 2 \end{bmatrix}^T$$
$$M_4 = \begin{bmatrix} 0 & 0 & 0 & 0 & 2 & 2 \end{bmatrix}^T$$

Figure 2.3: Reachability graph for the PN model of Figure 2.2

If the final desired marking is the same as the initial marking, and the trivial null firing matrix solution is not acceptable, then it is necessary to find a firing matrix that is T-invariant. T-invariants are found by finding non-trivial solutions to (2.6).

$$CU_k = 0 \tag{2.6}$$

T-invariant solutions are a necessary set of solutions if the issue of system restoration is to be addressed. In the case of the model in Figure 2.2, only a T-invariant solution will restore the system to an un-faulted condition after a fault has occurred. The only integer value T-invariant of interest for the model of Figure 2.2 is shown in (2.7).

$$U_k = \begin{bmatrix}1 & 1 & 1 & 1\end{bmatrix}^T \tag{2.7}$$

2.4 Total Transition Probability and Total Transition Time

Once the integer value firing matrix is known it is possible to calculate a Total Transition Probability (TTP) and Total Transition Time (TTT). The TTP is the product of the individual serial TPs for the T nodes which fire and the TTT is the sum of the individual serial TTs for T nodes which fire.

$$TTP = \prod_{\substack{i=1 \\ i \neq m}}^{n} TP_i \tag{2.8}$$

$$TTT = \sum_{\substack{i=1 \\ i \neq m}}^{n} TT_i \tag{2.9}$$

where:

n : number of T nodes in the system
m : nodes which do not fire

The TTP can also be converted to Total Non Transition Probability (TNTP), where TNTP=1-TTP. This is a convenient compact form when the TTP is close to a unity value.

2.5 Petri Net Models with Communications Systems

The limitation to a model such as that seen in Figure 2.2 is that it does not account for the operation of a communications systems. From section 1.3.1 it is clear that SPSs often make extensive use of communications systems. Therefore, this section will introduce the modeling of communications systems integrated into power systems, in the framework of a single PN model. The model seen in Figure 2.2 will be modified so that it includes a communications system, shown in Figure 2.4. This will allow for a comparison of the model before and after the addition of the communications system elements.

Using the same fault scenario that was presented in Figure 2.1, Figure 2.5 shows a PN model that includes the necessary communications between the relay and the breaker. For this example it is assumed that the relay transmits a trip signal to the breaker which has a receiver, Figure 2.4. While this is generally not the case in a sub-station it is instructive to see how power and communications systems interact. In particular the difference between the PN models of Figure 2.1 and Figure 2.5 can be examined.

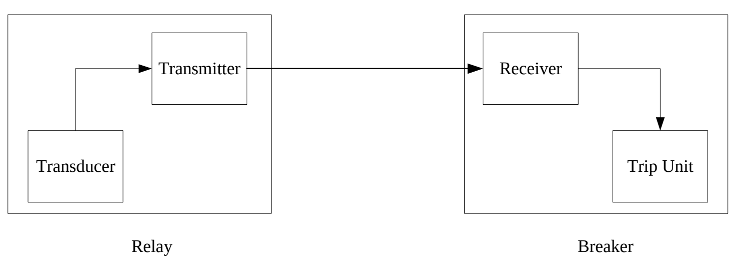

Figure 2.4: Communications path from relay to breaker

An important aspect of the PN model of Figure 2.5 is that the interfaces between the power and telecommunications infrastructure are clearly visible, and marked. The ability to see the infrastructure interfaces lends insight into the potential problem that can arise due to infrastructure interactions. Once the interfaces have been identified, further analytic study can be performed.

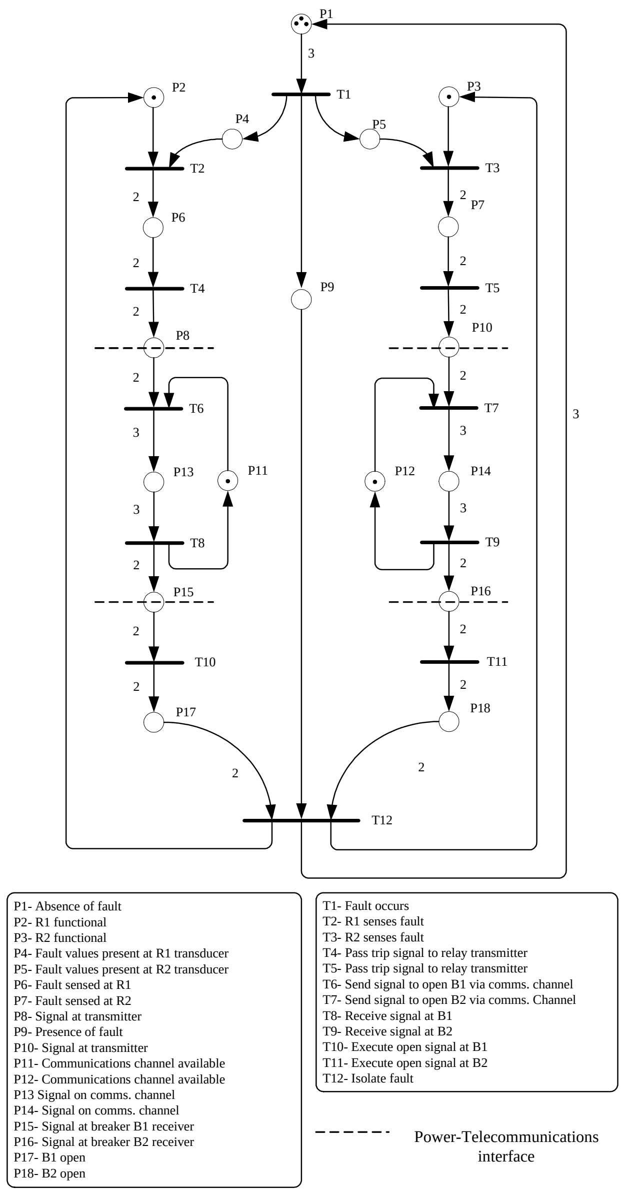

Figure 2.5: PN model with communications system information

The first step in the analysis is to construct the coincidence matrix as was done in (2.3) for the system of Figure 2.1.

$$C^T = \begin{bmatrix} -3 & 0 & 0 & 0 & 0 & 0 & 0 & 0 & 0 & 0 & 0 & 3 \\ 0 & -1 & 0 & 0 & 0 & 0 & 0 & 0 & 0 & 0 & 0 & 1 \\ 0 & 0 & -1 & 0 & 0 & 0 & 0 & 0 & 0 & 0 & 0 & 1 \\ 1 & -1 & 0 & 0 & 0 & 0 & 0 & 0 & 0 & 0 & 0 & 0 \\ 1 & 0 & -1 & 0 & 0 & 0 & 0 & 0 & 0 & 0 & 0 & 0 \\ 0 & 2 & 0 & -2 & 0 & 0 & 0 & 0 & 0 & 0 & 0 & 0 \\ 0 & 0 & 2 & 0 & -2 & 0 & 0 & 0 & 0 & 0 & 0 & 0 \\ 0 & 0 & 0 & 2 & 0 & -2 & 0 & 0 & 0 & 0 & 0 & 0 \\ 1 & 0 & 0 & 0 & 0 & 0 & 0 & 0 & 0 & 0 & 0 & 1 \\ 0 & 0 & 0 & 0 & 2 & 0 & -2 & 0 & 0 & 0 & 0 & 0 \\ 0 & 0 & 0 & 0 & -1 & 0 & 1 & 0 & 0 & 0 & 0 & 0 \\ 0 & 0 & 0 & 0 & 0 & -1 & 0 & 1 & 0 & 0 & 0 & 0 \\ 0 & 0 & 0 & 0 & -3 & 0 & 3 & 0 & 0 & 0 & 0 & 0 \\ 0 & 0 & 0 & 0 & 0 & -3 & 0 & 3 & 0 & 0 & 0 & 0 \\ 0 & 0 & 0 & 0 & 0 & 0 & 2 & 0 & -2 & 0 & 0 & 0 \\ 0 & 0 & 0 & 0 & 0 & 0 & 0 & 2 & 0 & -2 & 0 & 0 \\ 0 & 0 & 0 & 0 & 0 & 0 & 0 & 0 & 0 & 2 & 0 & -2 \\ 0 & 0 & 0 & 0 & 0 & 0 & 0 & 0 & 0 & 0 & 2 & -2 \end{bmatrix} \qquad (2.10)$$

From the coincidence matrix the integer T-invariant firing sequences can be determined, in the case of (2.10) there is only one of interest, shown in (2.11).

$$U_k = [1 \quad 1 \quad 1 \quad 1 \quad 1 \quad 1 \quad 1 \quad 1 \quad 1 \quad 1 \quad 1 \quad 1]^T \qquad (2.11)$$

2.5.1 Decomposition of the Coincidence Matrix

While the basic coincidence matrix is useful for determining reachability of a PN model, a simple reordering of the indices can yield an even more insightful form (2.12).

$$\tilde{C}^T = \left[\begin{array}{ccc|ccc|c} C_{S1-comms} & & & & & & \\ & C_{S1} & & & 0 & & \\ & & & & & & \\ \hline & & & C_{S2-comms} & & & \\ & 0 & & & C_{S2} & & \\ & & & & & & \\ \hline & 0 & & & 0 & & C_{S3} \end{array}\right] \tag{2.12}$$

Where:

C_{S1} :Sub-matrix of $\tilde{C}^T$, involving only R1-B1

C_{S2} :Sub-matrix of $\tilde{C}^T$, involving only R2-B2

$C_{S1-comms}$:Sub-matrix of C_{S1} involving only the telecommunications infrastructure

$C_{S2-comms}$:Sub-matrix of C_{S2} involving only the telecommunications infrastructure

C_{S3} :Sub-matrix of $\tilde{C}^T$, involving only the power infrastructure

Reordering the elements of (2.10) into the form of (2.12) yields (2.13). Equation (2.13) contains the information of (2.10) in the form of (2.12). The reordered form of (2.12) and (2.13) is useful because it isolates the operations into specific groups. For example, C_{S1} and C_{S2} isolate the actions that occur in concurrent and unconnected paths, indicating that the operation of the two breakers, B1 and B2, are in no way coupled. Additionally, the sub-matrices $C_{S1-comms}$ and $C_{S2-comms}$ isolate only the operations that occur within the telecommunications infrastructure and in no way directly influence the power infrastructure.

$$\tilde{C}^T = \left[\begin{array}{ccccc|ccccc|cc}
-2 & 0 & 0 & 2 & 0 & 0 & 0 & 0 & 0 & 0 & 0 & 0 \\
-1 & 1 & 0 & 0 & 0 & 0 & 0 & 0 & 0 & 0 & 0 & 0 \\
3 & -3 & 0 & 0 & 0 & 0 & 0 & 0 & 0 & 0 & 0 & 0 \\
0 & 2 & 0 & 0 & -2 & 0 & 0 & 0 & 0 & 0 & 0 & 0 \\
0 & 0 & -1 & 0 & 0 & 0 & 0 & 0 & 0 & 0 & 0 & 1 \\
0 & 0 & -1 & 0 & 0 & 0 & 0 & 0 & 0 & 0 & 1 & 0 \\
0 & 0 & 2 & -2 & 0 & 0 & 0 & 0 & 0 & 0 & 0 & 0 \\
0 & 0 & 0 & 0 & 2 & 0 & 0 & 0 & 0 & 0 & 0 & -2 \\
\hline
0 & 0 & 0 & 0 & 0 & -2 & 0 & 0 & 2 & 0 & 0 & 0 \\
0 & 0 & 0 & 0 & 0 & -1 & 1 & 0 & 0 & 0 & 0 & 0 \\
0 & 0 & 0 & 0 & 0 & 3 & -3 & 0 & 0 & 0 & 0 & 0 \\
0 & 0 & 0 & 0 & 0 & 0 & 2 & 0 & 0 & -2 & 0 & 0 \\
0 & 0 & 0 & 0 & 0 & 0 & 0 & -1 & 0 & 0 & 0 & 1 \\
0 & 0 & 0 & 0 & 0 & 0 & 0 & -1 & 0 & 0 & 1 & 0 \\
0 & 0 & 0 & 0 & 0 & 0 & 0 & 2 & -2 & 0 & 0 & 0 \\
0 & 0 & 0 & 0 & 0 & 0 & 0 & 0 & 0 & 2 & 0 & -2 \\
\hline
0 & 0 & 0 & 0 & 0 & 0 & 0 & 0 & 0 & 0 & -3 & 3 \\
0 & 0 & 0 & 0 & 0 & 0 & 0 & 0 & 0 & 0 & 1 & -1
\end{array}\right] \quad (2.13)$$

With concurrent paths in a PN model the size of the reachability graph will rapidly expand if the paths are not simultaneously considered. For this reason, during the construction of the reachability graph it will be assumed that the transitions in the concurrent paths occur simultaneously, e.g. TP_6 and TP_7 fire at the same time. This synchronization of events is a valid assumption since as was seen in (2.9) the actions necessary to operate one breaker do not influence the actions necessary to operate the other breaker, shown by the decoupled nature of C_{S1} and C_{S2}.

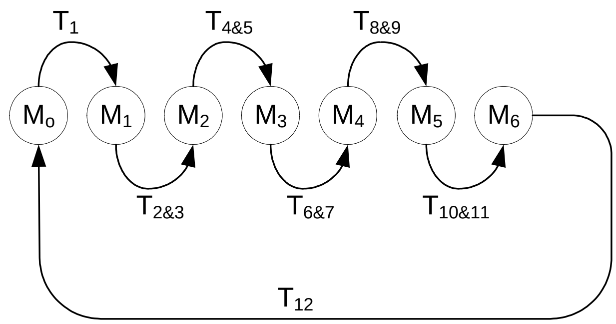

$$M_1 = [0\ 1\ 1\ 1\ 1\ 0\ 0\ 0\ 1\ 0\ 1\ 1\ 0\ 0\ 0\ 0\ 0\ 0]^T$$
$$M_0 = [3\ 1\ 1\ 0\ 0\ 0\ 0\ 0\ 0\ 0\ 1\ 1\ 0\ 0\ 0\ 0\ 0\ 0]^T$$
$$M_2 = [0\ 0\ 0\ 0\ 0\ 2\ 2\ 0\ 1\ 0\ 1\ 1\ 0\ 0\ 0\ 0\ 0\ 0]^T$$
$$M_3 = [0\ 0\ 0\ 0\ 0\ 0\ 0\ 2\ 1\ 2\ 1\ 1\ 0\ 0\ 0\ 0\ 0\ 0]^T$$
$$M_4 = [0\ 0\ 0\ 0\ 0\ 0\ 0\ 0\ 1\ 0\ 0\ 0\ 3\ 3\ 0\ 0\ 0\ 0]^T$$
$$M_5 = [0\ 0\ 0\ 0\ 0\ 0\ 0\ 0\ 1\ 0\ 1\ 1\ 0\ 0\ 2\ 2\ 0\ 0]^T$$
$$M_6 = [0\ 0\ 0\ 0\ 0\ 0\ 0\ 0\ 1\ 0\ 1\ 1\ 0\ 0\ 0\ 0\ 2\ 2]^T$$

Figure 2.6: Reachability graph of the PN model in Figure 2.5

Once the reachability graph has been constructed it is possible to calculate the TTP to determine the probability of successful fault isolation. In addition it will be possible to identify potential vulnerabilities at the power and telecommunications interface.

Equation (2.14) gives the probability of the post fault transition from the initial faulted conditions to a state where the fault is completely isolated, the TTP. Since there is only a single T-invariant firing solution and all concurrent paths are considered simultaneously, the probability calculation is the product of all the TPs.

$$TTP = P(M_1 \mid M_0) = \prod_{i=2}^{12} TP_i \tag{2.14}$$

In order to calculate (2.14) there must be an associated TP for each of the transitions, as given by the T-invariant firing matrix. A transition is dependant on a specific piece of equipment functioning properly. Each piece of equipment will have an associated firing probability for that particular time in its life. The firing probability as a function of equipment age will vary based on the type of equipment, age, and history of use. For the purposes of this example the firing probabilities, as well as firing times, will be treated as known constants, Table 2.1. The values of Table 2.1 are assumed values and do not represent any particular type of equipment. Furthermore, the transition times are only given place holding variables with no numerical values. Since transition T_1 is the occurrence of a fault, it will be assumed to have a value of 1.0 in order to initiate the sequence.

Table 2.1: T-Node TPs and TTs for the PN model of Figure 2.5

T-node	TP	TT	T-node	TP	TT
1	1.000	TT_1	7	.99751	TT_7
2	.99452	TT_2	8	.99158	TT_8
3	.99612	TT_3	9	.94685	TT_9
4	.99486	TT_4	10	.99942	TT_{10}
5	.99321	TT_5	11	.99845	TT_{11}
6	.99742	TT_6	12	.99999	TT_{12}

Using the values of Table 2.1, and equation (2.14), the probability of correctly isolating a fault, the TTP, is 0.912436; the corresponding TNTP is 0.087564. If the minimum allowable probability of operation is set as 0.95 then changes have to be made to achieve this. These changes would most likely take the form of a repair or the replacement of the communication receiver on B1 since it has a significantly lower TP that any other component. In this particular case it was assumed that the receiver associated with TP_8 has aged to the point where the failure rate was beginning to increase, thus TPs decreases.

Additional, the issue of redundancy must be addressed. In transmission systems it is common to have N-1 reliability and in some cases N-2 reliability. The same is generally true of the communications systems used by power systems. In order to examine the level of redundancy in the system, the sub-matrices of (2.13) are examined.

As was noted in the previous section, arranging the entries of the coincidence matrix in the form of (2.12) allows for isolation of specific groups of operations. This in turn allows for the analysis of selected portions of the model. For example, in order to examine only the communications operations that occur between R1 and B1 of Figure 2.4, sub-matrix $C_{S1-comms}$ is examined, shown in (2.13).

In [35] it was shown that a Petri net is completely controllable or completely reachable if the coincidence matrix is of full rank; the same is true for sub-matrices. The rank of the $C_{S1-comms}$ matrix can be determined by using the Singular Value Decomposition (SVD) of $C_{S1-comms}$, which is rank 2, full rank. This implies that there are no path choices in the PN model. The lack of path choices is be a clear indication of a lack of redundancy in the communications system.

$$C_{S1-comms} = \begin{bmatrix} -2 & 0 \\ -1 & 1 \\ 3 & -3 \\ 0 & 2 \end{bmatrix} \tag{2.13}$$

2.5.2 Evaluation of Parallel Communications Paths

One potential solution to the low TTP is to add a second channel for communications between the relay and the breaker. This is a desirable solution since simply replacing the receiver associated with TP_8 does not give redundancy, only increase the TP.

Figure 2.7 shows a PN model similar to that of Figure 2.5 but with redundant channels of communications. The associated coincidence matrix in the form of (2.12) is shown in (2.16).

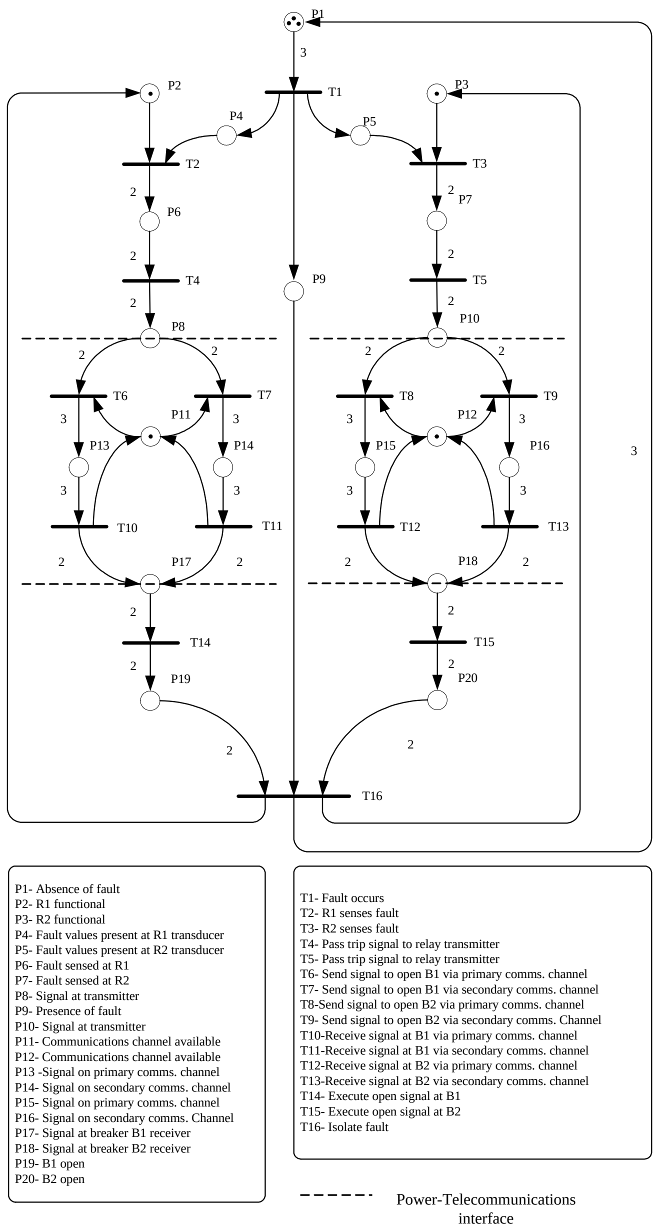

Figure 2.7: PN model with redundant communications

In the PN model of Figure 2.5 each of the relays has two transmitters with an associated communications link. Each of these links is then in turn connected to one of two receivers at the breaker. This system ensures that there is complete redundancy in the communications between the relay and the associated breaker. The two communications paths are completely independent of each other. The signal from one transmitter cannot be routed to the adjacent communications channel, and as such cannot be received by the alternate receiver. This arrangement is represented in the model of Figure 2.7.

$$\tilde{C}^T = \left[\begin{array}{ccccccc|ccccccc|cc}
-2 & -2 & 0 & 0 & 0 & -2 & 0 & 0 & 0 & 0 & 0 & 0 & 0 & 0 & 0 & 0 \\
-1 & -1 & 1 & 1 & 0 & 0 & 0 & 0 & 0 & 0 & 0 & 0 & 0 & 0 & 0 & 0 \\
3 & 0 & -3 & 0 & 0 & 0 & 0 & 0 & 0 & 0 & 0 & 0 & 0 & 0 & 0 & 0 \\
0 & 3 & 0 & -3 & 0 & 0 & 0 & 0 & 0 & 0 & 0 & 0 & 0 & 0 & 0 & 0 \\
0 & 0 & 2 & 2 & 0 & 0 & -2 & 0 & 0 & 0 & 0 & 0 & 0 & 0 & 0 & 0 \\
0 & 0 & 0 & 0 & -1 & 0 & 0 & 0 & 0 & 0 & 0 & 0 & 0 & 0 & 0 & 1 \\
0 & 0 & 0 & 0 & -1 & 0 & 0 & 0 & 0 & 0 & 0 & 0 & 0 & 0 & 1 & 0 \\
0 & 0 & 0 & 0 & 2 & 2 & 0 & 0 & 0 & 0 & 0 & 0 & 0 & 0 & 0 & 0 \\
0 & 0 & 0 & 0 & 0 & 0 & 2 & 0 & 0 & 0 & 0 & 0 & 0 & 0 & 0 & 0 \\
\hline
0 & 0 & 0 & 0 & 0 & 0 & 0 & -2 & -2 & 0 & 0 & 0 & -2 & 0 & 0 & 0 \\
0 & 0 & 0 & 0 & 0 & 0 & 0 & -1 & -1 & 1 & 1 & 0 & 0 & 0 & 0 & 0 \\
0 & 0 & 0 & 0 & 0 & 0 & 0 & 3 & 0 & -3 & 0 & 0 & 0 & 0 & 0 & 0 \\
0 & 0 & 0 & 0 & 0 & 0 & 0 & 0 & 3 & 0 & -3 & 0 & 0 & 0 & 0 & 0 \\
0 & 0 & 0 & 0 & 0 & 0 & 0 & 0 & 0 & 2 & 2 & 0 & 0 & -2 & 0 & 0 \\
0 & 0 & 0 & 0 & 0 & 0 & 0 & 0 & 0 & 0 & 0 & -1 & 0 & 0 & 0 & 1 \\
0 & 0 & 0 & 0 & 0 & 0 & 0 & 0 & 0 & 0 & 0 & -1 & 0 & 0 & 1 & 0 \\
0 & 0 & 0 & 0 & 0 & 0 & 0 & 0 & 0 & 0 & 0 & 2 & 2 & 0 & 0 & 0 \\
0 & 0 & 0 & 0 & 0 & 0 & 0 & 0 & 0 & 0 & 0 & 0 & 0 & 2 & 0 & 0 \\
\hline
0 & 0 & 0 & 0 & 0 & 0 & 0 & 0 & 0 & 0 & 0 & 0 & 0 & 0 & -3 & 3 \\
0 & 0 & 0 & 0 & 0 & 0 & 0 & 0 & 0 & 0 & 0 & 0 & 0 & 0 & 1 & -1
\end{array}\right] \qquad (2.16)$$

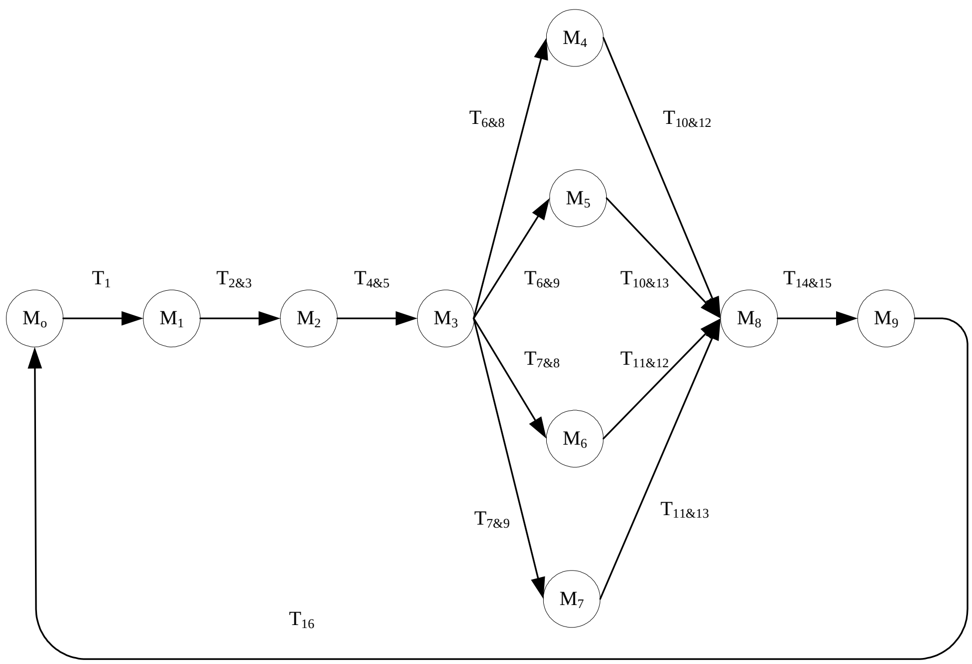

$$M_0 = [3\ 1\ 1\ 0\ 0\ 0\ 0\ 0\ 0\ 0\ 1\ 1\ 0\ 0\ 0\ 0\ 0\ 0\ 0\ 0]^T$$
$$M_1 = [0\ 1\ 1\ 1\ 1\ 0\ 0\ 0\ 1\ 0\ 1\ 1\ 0\ 0\ 0\ 0\ 0\ 0\ 0\ 0]^T$$
$$M_2 = [0\ 0\ 0\ 0\ 0\ 2\ 2\ 0\ 1\ 0\ 1\ 1\ 0\ 0\ 0\ 0\ 0\ 0\ 0\ 0]^T$$
$$M_3 = [0\ 0\ 0\ 0\ 0\ 0\ 0\ 2\ 1\ 2\ 1\ 1\ 0\ 0\ 0\ 0\ 0\ 0\ 0\ 0]^T$$
$$M_4 = [0\ 0\ 0\ 0\ 0\ 0\ 0\ 0\ 1\ 0\ 0\ 0\ 3\ 0\ 3\ 0\ 0\ 0\ 0\ 0]^T$$
$$M_5 = [0\ 0\ 0\ 0\ 0\ 0\ 0\ 0\ 1\ 0\ 0\ 0\ 3\ 0\ 0\ 3\ 0\ 0\ 0\ 0]^T$$
$$M_6 = [0\ 0\ 0\ 0\ 0\ 0\ 0\ 0\ 1\ 0\ 0\ 0\ 0\ 3\ 3\ 0\ 0\ 0\ 0\ 0]^T$$
$$M_7 = [0\ 0\ 0\ 0\ 0\ 0\ 0\ 0\ 1\ 0\ 0\ 0\ 0\ 3\ 0\ 3\ 0\ 0\ 0\ 0]^T$$
$$M_8 = [0\ 0\ 0\ 0\ 0\ 0\ 0\ 0\ 1\ 0\ 1\ 1\ 0\ 0\ 0\ 0\ 2\ 2\ 0\ 0]^T$$
$$M_9 = [0\ 0\ 0\ 0\ 0\ 0\ 0\ 0\ 1\ 0\ 1\ 1\ 0\ 0\ 0\ 0\ 0\ 0\ 2\ 2]^T$$

Figure 2.8: Reachability graph of the PN model in Figure 2.7

From (2.16) the reachability graph of the PN model in Figure 2.7 is constructed, and shown in Figure 2.8. While the issue of concurrent events is resolved as previously described, branching does occur because of the redundant communications channels. Each of the breakers can be opened by a signal from either its primary or secondary receiver, resulting in four possible combinations. The T-invariant firing sequences for the reachability graph of Figure 2.8 are given by (2.17).

$$\begin{aligned}
U_k &= [1\ \ 1\ \ 1\ \ 1\ \ 1\ \ 1\ \ 0\ \ 1\ \ 0\ \ 1\ \ 0\ \ 1\ \ 0\ \ 1\ \ 1\ \ 1]^T \\
U_k &= [1\ \ 1\ \ 1\ \ 1\ \ 1\ \ 1\ \ 0\ \ 0\ \ 1\ \ 1\ \ 0\ \ 0\ \ 1\ \ 1\ \ 1\ \ 1]^T \\
U_k &= [1\ \ 1\ \ 1\ \ 1\ \ 1\ \ 0\ \ 1\ \ 1\ \ 0\ \ 0\ \ 1\ \ 1\ \ 0\ \ 1\ \ 1\ \ 1]^T \\
U_k &= [1\ \ 1\ \ 1\ \ 1\ \ 1\ \ 0\ \ 1\ \ 0\ \ 1\ \ 0\ \ 1\ \ 0\ \ 1\ \ 1\ \ 1\ \ 1]^T
\end{aligned} \tag{2.17}$$

The introduction of redundancy can be seen in the multiple T-invariant firing sequences of (2.17), as well as the ranks of the $C_{S1-comms}$ and $C_{S2-comms}$ matrices of (2.18), both of which are only rank 3.

$$C_{S1-comms} = \begin{bmatrix} -2 & -2 & 0 & 0 \\ -1 & -1 & 1 & 1 \\ 3 & 0 & -3 & 0 \\ 0 & 3 & 0 & -3 \\ 0 & 0 & 2 & 2 \end{bmatrix} \tag{2.18}$$

Since there are parallel paths on the reachability graph, the calculation to determine the probability of successful fault isolation is not as straightforward as in (2.14). Additionally, since there are two possible paths the total fault isolation time will be dependant on which communications channels is utilized, i.e. which path is taken on the reachability graph. Table 2.2 gives the TPs and TTs for the PN model of Figure 2.7.

Table 2.2: T-node TPs and TTs for the PN model of Figure 2.7

T-node	TP	TT	T-node	TP	TT
1	1.000	TT_1	9	0.99765	TT_9
2	0.99452	TT_2	10	0.99158	TT_{10}
3	0.99612	TT_3	11	0.99524	TT_{11}
4	0.99486	TT_4	12	0.99624	TT_{12}
5	0.99321	TT_5	13	0.94685	TT_{13}
6	0.99742	TT_6	14	0.99942	TT_{14}
7	0.99865	TT_7	15	0.99845	TT_{15}
8	0.99751	TT_8	16	0.99999	TT_{16}

Since there are parallel paths that the markings can follow it is necessary to correctly determine the probability of parallel events. This is done using the well known probability axiom of (2.19). The probability of correctly isolating the fault, with either of the communications channels, is given by (2.20) while the total time to isolate the fault is determined in Table 2.3.

$$P(A \cup B) = P(A) + P(B) - P(A \cap B) \tag{2.19}$$

$$\begin{pmatrix} TTP = \\ P(M_1 \mid M_0) \end{pmatrix} = \left(\begin{array}{l} TP_1 \cdot TP_{16} \cdot \\ \left(\left(\begin{array}{l} \left(TP_2 \cdot TP_4 \cdot TP_{14} \cdot \begin{pmatrix} TP_6 \cdot TP_{10} + TP_7 \cdot TP_{11} - \\ TP_6 \cdot TP_{10} \cdot TP_7 \cdot TP_{11} \end{pmatrix} \right) + \\ \left(TP_3 \cdot TP_5 \cdot TP_{15} \cdot \begin{pmatrix} TP_8 \cdot TP_{12} + TP_9 \cdot TP_{13} - \\ TP_8 \cdot TP_{12} \cdot TP_9 \cdot TP_{13} \end{pmatrix} \right) \end{array} \right) - \\ \left(\begin{array}{l} TP_2 \cdot TP_4 \cdot TP_{14} \cdot TP_3 \cdot TP_5 \cdot TP_{15} \cdot \\ \begin{pmatrix} TP_6 \cdot TP_{10} + TP_7 \cdot TP_{11} - \\ TP_6 \cdot TP_{10} \cdot TP_7 \cdot TP_{11} \end{pmatrix} \cdot \\ \begin{pmatrix} TP_8 \cdot TP_{12} + TP_9 \cdot TP_{13} - \\ TP_8 \cdot TP_{12} \cdot TP_9 \cdot TP_{13} \end{pmatrix} \end{array} \right) \right) \end{array} \right) \tag{2.20}$$

Table 2.3: Calculation of fault isolation times for the PN model of Figure 2.7

Combination of communications channels	Time required to isolate fault (milliseconds)
primary-primary	$TT_2 + TT_3 + TT_4 + TT_5 + TT_6 + TT_8 + TT_{10} + TT_{12} + TT_{14} + TT_{15} + TT_{16}$
primary-secondary	$TT_2 + TT_3 + TT_4 + TT_5 + TT_6 + TT_9 + TT_{10} + TT_{13} + TT_{14} + TT_{15} + TT_{16}$
secondary-primary	$TT_2 + TT_3 + TT_4 + TT_5 + TT_7 + TT_8 + TT_{11} + TT_{12} + TT_{14} + TT_{15} + TT_{16}$
secondary-secondary	$TT_2 + TT_3 + TT_4 + TT_5 + TT_7 + TT_9 + TT_{11} + TT_{13} + TT_{14} + TT_{15} + TT_{16}$

With the addition of the secondary communications channels the probability of correctly isolating a fault, via either the primary or secondary communications channel, is 0.999849394 with a corresponding TNTP of $1.506 \cdot 10^{-4}$. Even with the failure of both of the primary communications channel there is a 0.9874716 of correctly isolating the fault via the secondary communications channels, with a corresponding TNTP of 0.0125284.

2.5.3 Simple Model Reduction

Existing power and communications systems are large enough that the size of the coincidence matrix will be cumbersome even for simple systems. In order to reduce the coincidence matrix size and facilitate ease of computation simple reduction rules will be applied.

Model reduction is particularly effective in situations where a marking must proceed through several serial processes. For example, in the process of moving data packets from network routers to an optical fiber there are several serial operations such as electrical to optical conversion, dense or coarse wavelength multiplexing, and optical amplification. While each of these operations could be assigned an individual T node, simple model reduction can reduce the group of operations to a single T node.

An example of model reduction is shown in Figure 2.9.

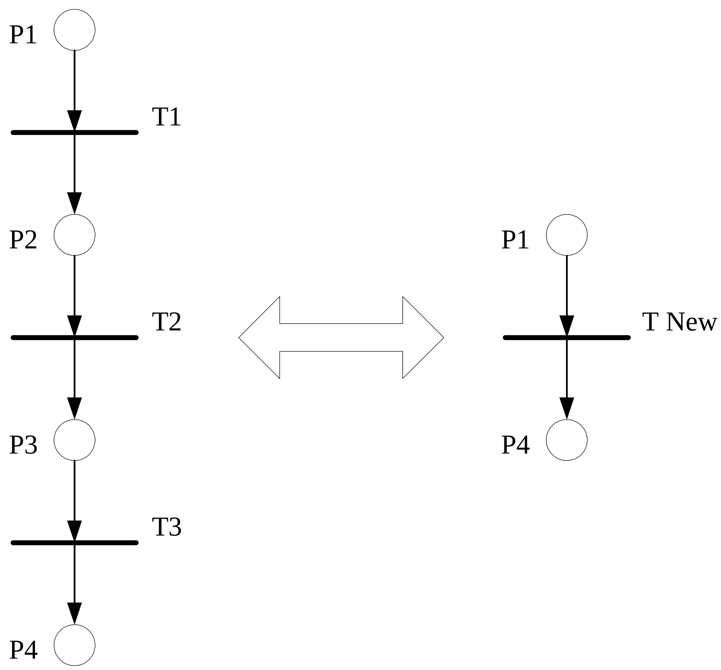

Figure 2.9: Model reduction example

Since the reduction performed in Figure 2.9 is on serial events the translation of TP and TT values follows the simple forms of (2.21) and (2.22).

$$TP_{New} = TP_1 \cdot TP_2 \cdot TP_3 \tag{2.21}$$

$$TT_{New} = TT_1 + TT_2 + TT_3 \tag{2.22}$$

This type of model reduction will be used extensively in Chapter 4 where models of EMSs are considered.

2.6 FIT Rates and MTBF

In order to have meaningful TP values it is convenient to use manufacturer provided data such as FIT Rates or Mean Time Between Failures (MTBF) data. The FIT Rate corresponds to the number of failures per billion hours assuming random failures occurring at a near constant rate. FIT rates and MTBFs are inversely related. Additionally, FIT rates can be translated into percent chance of success, and thus TP, through (2.23).

$$TP = \exp-\left(t * FIT\right) \tag{2.23}$$

The normalized probability of successful operation for a piece of equipment with a given MTBF decreases as its age increases, as shown in Figure 4.20. From Figure 2.10 it can be seen that there is only a 37% chance that there will be no failures after an operating period equal to one MTBF.

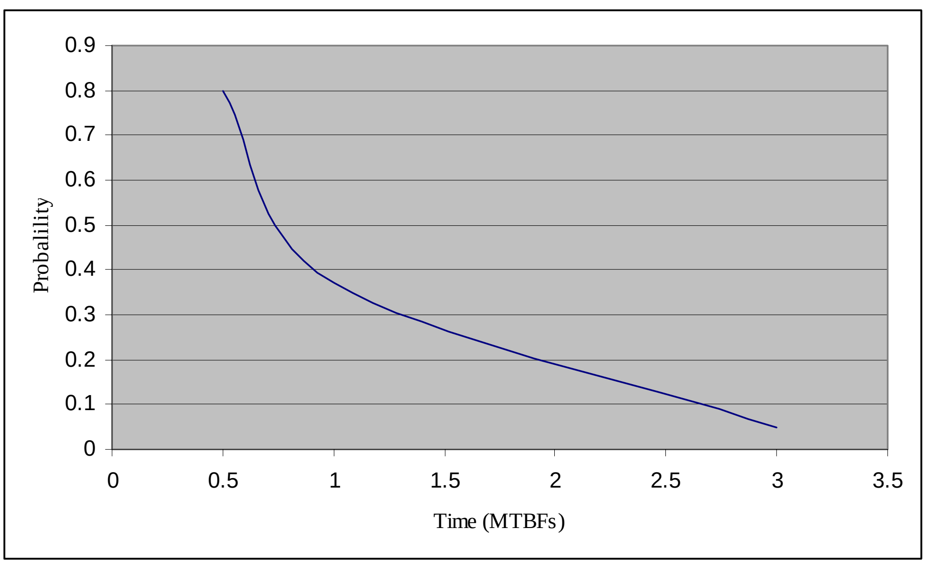

Figure 2.10: MTBF vs. time

What is not shown in Figure 2.10 is the behavior of components early and late in their lifetime. Figure 2.11 shows the well established “bathtub” curve which was originally developed to model mechanical failures but has been used extensively in the semiconductor industry. There are three regions to the bathtub curve: infant mortality, near constant failure rate, and end of life. Infant mortality refers to the initial burn in period when production errors and gross material flaws become evident. Equipment is generally subjected to factory acceptance testing which ensures that all delivered equipment is past the infant mortality region. The near constant failure rate region is the region where Figure 2.10 and equation (2.23) apply. It will be assumed that all equipment is operating in the near constant failure rate region. Once components have aged to the point where they are in the end of life region large numbers of components will begin to fail and the system will soon cease to operate.

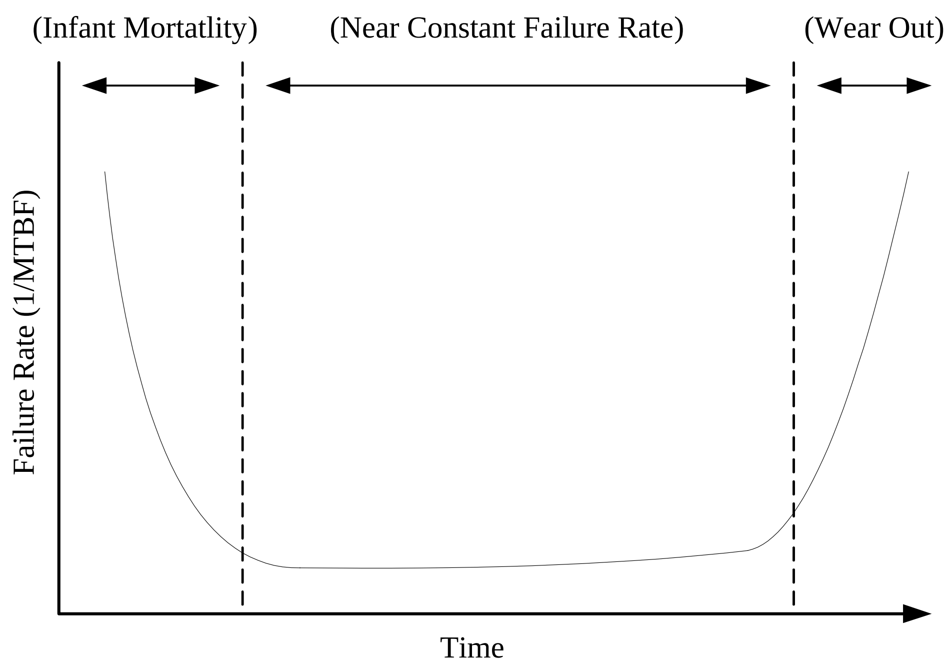

Figure 2.11: Bathtub curve

2.7 Vulnerability Assessment Method

Using the techniques from this chapter, new as well as reviewed, a comprehensive vulnerability assessment method using marked PN models can be outlined. From the previous sections it is clear that the first step is the construction of the marked PN model, which must be accurate in every possible respect or else the information gained from its analysis will be flawed.

The construction of the model for a given system or system function is performed in steps. The first step is to obtain detailed information about every component that will be included in the model. For a typical utility or Independent System Operator (ISO) this would include data about SCADA servers, EMS consoles, and various pieces of field equipment.

Next, the possible states of each of the pieces of equipment must be determined as well as the actions which cause the states to change. The states and their transitions determine the P and T nodes for individual actions in the system. Once the individual P and T nodes are constructed the TP and TT values for the T nodes can be determined from manufacturer data or empirical measurements.

In the final step the individual T and P nodes are combined into a single model spanning the power and telecommunications infrastructures. Within the model each of the T nodes has an associated TP and TT based on the equipment or process represented.

Once the model has been completed and all the data collected the system can be evaluated for infrastructure interactions. The complete methodology for evaluating potential vulnerabilities at the interface of the power and telecommunications infrastructures has three parts.

1) Calculation of the TTP: Calculation of the TTP, and associated TNTP, can be performed assuming all equipment operating in a “normal mode” or with

selected equipment out of service. This allows a system to be evaluated for various contingencies. Additionally, individual or sub-groups of transitions that form interfaces between the power and telecommunications infrastructures can be examined. This is especially important for transitions that are dependant on numerical calculations.

2) Calculation of the TTT: Calculation of the TTT can be performed assuming all equipment operating in a "normal mode" or with selected equipment out of service. This allows systems to be evaluated for various contingencies to determine if system response times stay within allowable limits.

3) Determination of Redundancy: Determining if a lack of redundancy exists can indicate a single point failure mechanism within a system. This is done by examining sub-matrices of the reordered coincidence matrix. The determination of redundancy can be performed for "normal modes" or for contingency analysis.

When performing the assessment of potential vulnerabilities each of the above three parts is applied. Vulnerabilities can take on a number of forms, which is why there are multiple parts. Examination of a particular system or sub-system can lead to the identification of potential vulnerabilities in one, two, or even all three parts of the assessment method.

In each of the three parts it is stated that other than normal modes can be examined. As will be seen in later examples this is an important feature of the proposed method which can allow for contingency analysis. Additionally it can be used to analyze potential system upgrades or changes before the capital investment is made.

The construction of the marked PN model and the subsequent analysis can be performed on any system for which there is sufficient data. In particular, the method is useful for any system which has power and communications components. In addition to being applicable to any electric utilities systems, the method could also be applied to: shipboard marine power systems, satellite power systems, and automotive power systems.

Chapter 3: Vulnerability Analysis of Terrestrial Special Protection Systems

As was seen in section 1.3.1 many SPSs are heavily dependant on the proper operation of a supporting communications system. This chapter will apply the vulnerability assessment method presented in the previous chapter to examine two separate operational SPSs. The first SPS is currently in use by Hydro-Québec and the second by a major European power system. Each of these SPSs will be examined in the context of system failures which have occurred in the past. Based on these examinations the SPSs will be analyzed for potential infrastructure vulnerabilities which could lead to catastrophic blackouts.

3.1 Analysis of Hydro-Québec SPS

One such blackout occurred April 18th 1988 in the Hydro-Québec system and is discussed in section A2.6 and documented in [15]. The following sections will explain in detail the operation of the SPS involved as well as develop and analyze a market PN model of the system. The goal of this analysis will be to identify potential infrastructure vulnerabilities. In particular, it will be shown that the vulnerability which compounded the events of April 18th 1988 could have been identified prior to the blackout. Once the vulnerability had been identified it could have been addressed and the extent of the blackout limited.

3.1.1 Overview

As was discussed in section 1.3.1.1 the transmission lines of the Hydro-Québec system connect significant amounts of remote hydroelectric generation to load centers.

The SPS which protects the 765-kV lines is composed to two functions, load shedding and generation rejection. The load shedding component is intended to restore the systems generation/load balance in order to minimize the severity of transients. The generator rejection element is intended to protect generators from physical damage due to rapid unloading, allowing for a less time consuming restoration process.

When events such as severe weather result in the isolation of a critical transmission line, local relays communicate the change in system topology to the central control center. The central control center then automatically issues load shedding and generation rejection signals based on off-line calculations. When the system operates correctly there is a significant loss of load due to load shedding, but the overall system remains stable preventing a complete system collapse.

3.1.2 Vulnerability Analysis

The first step in analyzing the infrastructure interactions and potential vulnerabilities of the Hydro-Québec SPS is to construct the marked PN model. The complete model is shown in Figure 3.1. There are a number of significant features in the model of Figure 3.1 that must be discussed.

In particular, there are two sets of global P nodes which indicate system level states. P1, P2, and P3 indicate the status of faults with respect to the power system, including if a fault is present on the transmission line but has been isolated from the rest of the power system. P16 and P17 indicate if the system generation is sufficient to supply the existing load plus losses. It is the transition of markings between the global P nodes which indicates that the SPS has operated correctly. A low probability of transition between global P nodes is an indication of a potential vulnerability.

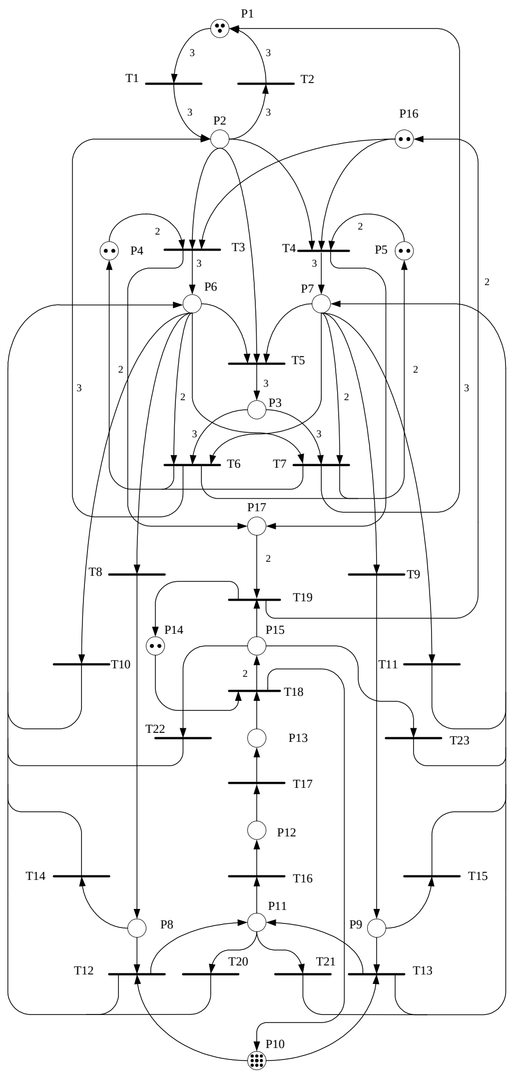

P1- Line and system un-fault
P2- Line and System faulted
P3- Line faulted and system un-faulted
P4- B1 Closed
P5- B2 Closed
P6- B1 open
P7- B2 open
P8- B1 signal in transit to control center
P9- B2 signal in transit to control center
P10- Control center operational
P11- Signal(s) at control center
P12- Signal at control center computer
P13- Signal in transit to load shedding computers
P14- Load shedding computers operational
P15- Signal at load shedding computers
P16- System load+ losses = System Generation
P17- System load+ losses = System Generation

T1- Fault placed on line
T2- Fault removed from line (no operator action)
T3- Open B1
T4- Open B2
T5- Fault removed from system (brk action)
T6- Close B1 and B2 (line fault still present, reclosure)
T7- Fault removed from line and closure of B1 and B2 (operator action post load shedding)
T8- B1 transmit signal to control center
T9- B2 transmit signal to control center
T10- B1 fails to transmit signal to control center
T11- B2 fails to transmit signal to control center
T12- B1 signal received at control center
T13- B2 signal received at control center
T14-B1 signal is not received at control center
T15- B2 signal is not received at control center
T16- Send signal to control center computer
T17- Process signal, determine appropriate action and transmit signal to load shedding computers
T18- Receive signal at load shedding computers
T19- Process signal, shed load, and reset load shedding computers
T20- If redundant signals exist remove
T21- If redundant signals exist remove
T22- Reset markings
T23- Reset markings

Figure 3.1: PN model for Hydro-Québec SPS

Another feature of Figure 3.1 is the presence of a source/sink P node, P_{10}. This node is used to indicate that the overall control center functions are available. This does not preclude the possibility of a fault within the control center, as will be seen. Instead it is used to indicate that there are no major problems with the SCADA or EMS operations.

Section 2.7 showed that the complete analysis is composed of three components: calculation of the TTP, calculation of the TTT, and examination of redundancy. Table 3.1 gives the individual TPs and TTs for the various operations associated with the marked PN model of the Hydro-Québec SPS. The values in Table 3.1 are representative of typical operations but are not based on specific values from Hydro-Québec.

Table 3.1: Transition probabilities and transition times

Operation	TP	TT (msec)
open breaker	.9999999997	15
close breaker	.9999999993	15
transmit breaker open signal to control center	.9999999994	16
receive breaker open signal at control center	.9999999998	3
pass breaker signal to control center computer	.9999999991	2
process breaker open signal and send to load shedding computers	.9999999996	17
receive signal at load shedding computers	.9999999997	3
process signal, shed load, and reset load shedding computers	.9999999999	3

For the system of Figure 3.1, using the values of Table 3.1, the TTP and TTT for the proper shedding of load are calculated as a 99.99999963% of proper operation occurring within 135.5 msec of the initial fault. The TNTP corresponding to this TTP is $3.7 \cdot 10^{-9}$. These values are calculated using the firing matrix of (3.1).

$$U_k^T = [1\ \ 0\ \ 1\ \ 1\ \ 1\ \ 0\ \ 1\ \ 1\ \ 1\ \ 0\ \ 0\ \ 1\ \ 1\ \ 0\ \ 0\ \ 1\ \ 1\ \ 1\ \ 1\ \ 1\ \ 0\ \ 1\ \ 1] \qquad (3.1)$$

In addition to the values for the normal mode of operation, Table 3.2 contains the values for 2 contingency conditions. Contingency condition 1 is the loss of one of the two breaker status transmitters, and contingency condition 2 is the loss of one of the two breaker status receivers at the control center.

Table 3.2: Contingency analysis

Contingency	TTP	TTT (msec)	TNTP	Failures (/10 yrs.)
None	0.9999999963	135.5	$3.7 \cdot 10^{-9}$	10.3
1	0.9999999954	135.5	$4.6 \cdot 10^{-9}$	12.8
2	0.9999999958	135.5	$4.2 \cdot 10^{-9}$	11.7

If either the TTP or the TTT are not within acceptable operating bounds as determined by the individual user, then individual components, sub-systems, or algorithms can be replaced or repaired as necessary. For this particular case there are no evident vulnerabilities. The next step is to check redundancy using the modified coincidence matrix.

The modified coincidence matrix for the marked PN model of Figure 3.1 is given by (3.2). The modified coincidence matrix is divided into four sets of P nodes and four set of T nodes. The first three sub-matrices along the diagonal represent the operations of the three major functional groups of the SPS. Since each of these three functional groups combines operations of the power and telecommunications infrastructures, each contains a telecommunications sub-matrix.

The first two telecommunications sub-matrices to be examined are those associated with the operation of the isolation breakers, $\tilde{C}_{S1-comms}$ and $\tilde{C}_{S2-comms}$ given by (3.3). By observation $\tilde{C}_{S1-comms}$ and $\tilde{C}_{S2-comms}$ are of full rank, indicating that there is no redundancy for the communications system involving the isolation breakers. While the lack of redundancy does constitute a potential vulnerability, the vulnerability is mitigated by the fact that only one of the two breaker signals is necessary to trigger the SPS.

$$
\tilde{C}=
\begin{array}{cc}
 & \begin{array}{cccccccccccccccccc} P_8 & P_4 & P_6 & P_9 & P_5 & P_7 & P_{10} & P_{11} & P_{12} & P_{13} & P_{15} & P_1 & P_2 & P_3 & P_{14} & P_{16} & P_{17} \end{array} \\
\begin{array}{c} T_8 \\ T_{10} \\ T_{12} \\ T_{14} \\ T_3 \\ \\ T_9 \\ T_{11} \\ T_{13} \\ T_{15} \\ T_4 \\ \\ T_{16} \\ T_{17} \\ T_{18} \\ T_6 \\ T_7 \\ T_{20} \\ T_{21} \\ T_{22} \\ T_{23} \\ \\ T_1 \\ T_2 \\ T_5 \\ T_{19} \end{array}
&
\left[\begin{array}{ccc|ccc|ccccc|cccccc}
1 & 0 & -1 & & & & 0 & 0 & 0 & 0 & 0 & 0 & 0 & 0 & 0 & 0 & 0 \\
0 & 0 & -1 & & & & 0 & 0 & 0 & 0 & 0 & 0 & 0 & 0 & 0 & 0 & 0 \\
-1 & 0 & 1 & & 0 & & -1 & 1 & 0 & 0 & 0 & 0 & 0 & 0 & 0 & 0 & 0 \\
-1 & 0 & 0 & & & & 0 & 0 & 0 & 0 & 0 & 0 & 0 & 0 & 0 & 0 & 0 \\
0 & -2 & 3 & & & & 0 & 0 & 0 & 0 & 0 & 0 & -1 & 0 & 0 & -1 & 1 \\
\hline
 & & & 1 & 0 & -1 & 0 & 0 & 0 & 0 & 0 & 0 & 0 & 0 & 0 & 0 & 0 \\
 & & & 0 & 0 & -1 & 0 & 0 & 0 & 0 & 0 & 0 & 0 & 0 & 0 & 0 & 0 \\
 & 0 & & -1 & 0 & 1 & -1 & 1 & 0 & 0 & 0 & 0 & 0 & 0 & 0 & 0 & 0 \\
 & & & -1 & 0 & 0 & 0 & 0 & 0 & 0 & 0 & 0 & 0 & 0 & 0 & 0 & 0 \\
 & & & 0 & -2 & 3 & 0 & 0 & 0 & 0 & 0 & 0 & -1 & 0 & 0 & -1 & 1 \\
\hline
0 & 0 & 0 & 0 & 0 & 0 & 0 & -1 & 1 & 0 & 0 & 0 & 0 & 0 & 0 & 0 & 0 \\
0 & 0 & 0 & 0 & 0 & 0 & 0 & 0 & -1 & 1 & 0 & 0 & 0 & 0 & 0 & 0 & 0 \\
0 & 0 & 0 & 0 & 0 & 0 & 1 & 0 & 0 & -1 & 2 & 0 & 0 & 0 & -1 & 0 & 0 \\
0 & 2 & -2 & 0 & 2 & -2 & 0 & 0 & 0 & 0 & 0 & 0 & 0 & -3 & 0 & 0 & 0 \\
0 & 2 & -2 & 0 & 2 & -2 & 0 & 0 & 0 & 0 & 0 & 0 & 0 & -3 & 0 & 0 & 0 \\
0 & 0 & 1 & 0 & 0 & 0 & 0 & -1 & 0 & 0 & 0 & 0 & 0 & 0 & 0 & 0 & 0 \\
0 & 0 & 0 & 0 & 0 & 1 & 0 & -1 & 0 & 0 & 0 & 0 & 0 & 0 & 0 & 0 & 0 \\
0 & 0 & 1 & 0 & 0 & 0 & 0 & 0 & 0 & 0 & -1 & 0 & 0 & 0 & 0 & 0 & 0 \\
0 & 0 & 0 & 0 & 0 & 1 & 0 & 0 & 0 & 0 & -1 & 0 & 0 & 0 & 0 & 0 & 0 \\
\hline
0 & 0 & 0 & 0 & 0 & 0 & 0 & 0 & 0 & 0 & 0 & -3 & 3 & 0 & 0 & 0 & 0 \\
0 & 0 & 0 & 0 & 0 & 0 & 0 & 0 & 0 & 0 & 0 & 3 & -3 & 0 & 0 & 0 & 0 \\
0 & 0 & -1 & 0 & 0 & -1 & 0 & 0 & 0 & 0 & 0 & 0 & -1 & 3 & 0 & 0 & 0 \\
0 & 0 & 0 & 0 & 0 & 0 & 0 & 0 & 0 & 0 & -1 & 0 & 0 & 0 & -1 & 2 & -2
\end{array}\right]
\end{array}
\qquad (3.2)
$$

$$\tilde{C}^{T}{}_{S1-comms} = \begin{bmatrix} 1 & 0 & -1 & -1 \end{bmatrix}$$

$$\tilde{C}^{T}{}_{S2-comms} = \begin{bmatrix} 1 & 0 & -1 & -1 \end{bmatrix} \tag{3.3}$$

$$\tilde{C}_{S3-comms} = \begin{bmatrix} 0 & -1 & 1 \\ 0 & 0 & -1 \\ 1 & 0 & 0 \end{bmatrix}$$

The third telecommunications sub-matrix to be examined is associated with the operations of the central control center, $\tilde{C}_{S3-comms}$ also given by (3.3). Using singular value decomposition it can be shown that the $\tilde{C}_{S3-comms}$ matrix is of full rank indicating a lack of redundant paths. Unlike the operation of the isolation breakers there are no mitigating factors for the lack of redundancy. This lack of redundancy indicates a potential single point failure which could prevent proper operation of the SPS.

There are three potential solutions for addressing single point failures: the first is to enforce high reliability standards on all components, the second is to redesign the system so that there is redundancy, and the third is a hybrid of the two. Because of the potential social and economic consequences of catastrophic blackouts the hybrid solution is the best engineering practice. Redundant communications paths with the maximum practical reliability should be implemented whenever practical.

The single point failure identified in the SPS is in exactly the same region of the communications system where the problem of April 18th 1988 occurred. Had this issue been identified and correctly addressed the extent of the April 18th blackout would not have been so extensive.

3.2 Analysis of an SPS on a Major European Grid

The second SPS to be examined is an operational system within a Major European Power System. Information was obtained about this case on the condition that the utility would remain unnamed in all documentation, including this dissertation. The particular system utilizes differential current protection on a transmission corridor composed of six parallel lines. While a differential current protection scheme in itself is not a complicated SPS, the fact that there is a substantial supporting communications system makes the differential protection scheme much more complicated than a simple impedance relay scheme. Additionally, the fact that there are six parallel lines indicates that this is a major transmission corridor. For these reasons this system will be examined.

3.2.1 Overview

The second example examines the occurrence of a significant protection system failure in which there was *no* loss of load. Despite this, significant load could have been lost if the initial system conditions had been different. During the time period of interest the system was lightly loaded and as such flows across the transmission corridor were light. While this particular incident did not result in a catastrophic blackout, similar situations in North America have resulted in lost load [3].

Each of the six transmission lines was protected by differential current relays with dedicated channels for communications between adjacent sub-stations. Differential current protection works by comparing current measurements on either side of a transmission line [16]. If the measurements differ by too great an amount then a fault is indicated. There is a certain amount of current mismatch which is allowed because of phenomena such as cable charging. Exactly how much of a mismatch should be allowed varies from system to system. This differential current protection system is similar to the EPE example discussed in section A2.7, but there are key differences.

For the comparison of spatially disparate measurements synchronization using the Global Positioning System (GPS) is the preferred method. This is due to the high reliability and availability of the signal. In the absence of GPS time stamped measurements dedicated communications channels with well established latencies can be used, as done at EPE. With a known latency it is possible to match current measurements that were made at approximately the same time. For this purpose it is necessary to measure the latency as accurately as possible, to ensure proper calculation of the differential current. With an inaccurate value for the latency of the communications channel current measurements could incorrectly compared.

During the time period of interest a single phase to ground fault on one of the six lines resulted in the isolation of the same phase on three of the five parallel lines. The cause of the relay operations on the three parallel non-faulted lines was traced to a communications system error which was the result of maintenance actions. Technicians working on the relay communications system had switched the differential current protection functions to a secondary channel with a significantly higher latency, without notifying the protection engineers. With the longer delay time the comparison of currents from either side of the transmission lines was calculated incorrectly, indicating a fault condition. While this particular communications system failure did not result in a loss of load, if the initial system loading had been higher a catastrophic failure could have been triggered.

3.2.2 Vulnerability Analysis

The first step in analyzing the infrastructure interactions and potential vulnerabilities of the SPS is to construct the marked PN model. The complete marked PN model is shown in Figure 3.2. As in the Hydro-Québec case it is clear that communications links have a significant effect on the operation of the power system.

In the Hydro-Québec case the SPS was examined while operating under a normal mode. For the SPS of the European system there are no problems when it is operating under a normal mode. The TTP and TTT both have values that are acceptable. Additionally, redundancy exists in all key areas.

Instead, the problem arises when the system is operating in an other than normal mode, e.g. the use of the secondary communications channel for differential current measurements.

In this case, the failure of the SPS was due to a lack of coordination between the communications and protection engineers. In particular, differential current relays were not updated with new communications system latency values when the communications was manually switch to the secondary channel. Incorrect latency values caused differential current values to be calculated higher than actual by the relays, resulting in the generation of breaker trip signals. Although four lines were involved in the event only a single line is modeled since each of the four lines had an independent and identical differential current protection system.

As discussed in Chapter 2, T node TPs can be based on the results of numerical calculations. This type of calculation-dependant firing is essential for the analysis of a SPS where isolation breaker trip signals are based on calculated values, as they are in a differential current protection scheme. The calculation of the trip signal is based on three inputs: locally measured current, remotely measured current, and communications latency between the two measurements. The communications latency value is necessary for the correct comparison of spatially disparate non time-stamped measurements when the GPS time stamps are not used.

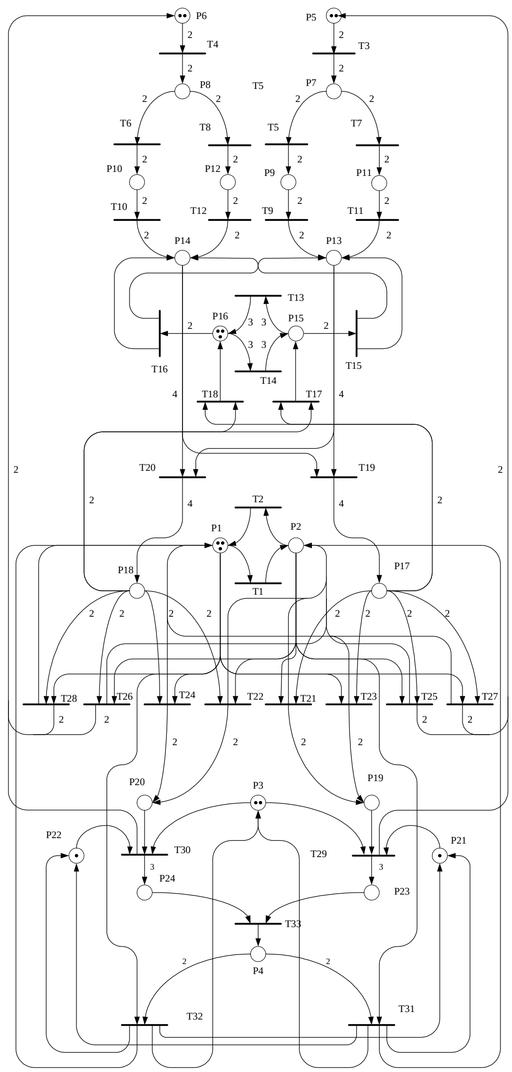

P1- Line un-fault
P2- Line faulted
P3- Line in service
P4- Line isolated
P5- Relay R1 ready
P6- Relay R2 ready
P7- Local current at R1 calculated
P8- Local current at R2 calculated
P9- R1 signal in transit via primary channel
P10- R1 signal in transit via secondary channel
P11- R2 signal in transit via primary channel
P12- R1 signal in transit via secondary channel
P13- Signal at R1
P14- Signal at R2
P15- Secondary channel latency value selected
P16- Primary channel latency value selected
P17- Differential current at R1 calculated
P18- Differential current at R2 calculated
P19- Relay R1 determined a fault condition
P20- Relay R2 determined a fault condition
P21- Breaker B1 closed
P22- Breaker B2 closed
P23- Breaker B1 open
P24- Breaker B2 open

T1- Fault removed from line (no operator action)
T2- Fault placed on line
T3- R1 calculates local current
T4- R2 calculates local current
T5- Transmit local current to remote relay (primary)
T6- Transmit local current to remote relay (primary)
T7- Transmit local current to remote relay (secondary)
T8- Transmit local current to remote relay (secondary)
T9- Signal received at remote relay (primary)
T10- Signal received at remote relay (primary)
T11- Signal received at remote relay (secondary)
T12- Signal received at remote relay (secondary)
T13- Switch from secondary to primary latency value
T14- Switch from primary to secondary latency value
T15- Pass secondary latency value to relays R1 and R2
T16- Pass primary latency value to relays R1 and R2
T17- Complete fault determination w/ sec. latency
T18- Complete fault determination w/ pri. latency
T19- R1 calculates current differential
T20- 21 calculates current differential
T21- R1 determines a fault exists
T22- R2 determines a fault exists
T23- R1 spuriously trips (no fault)
T24- R2 spuriously trips (no fault)
T25- R1 fails to trip (fault condition)
T26- R2 fails to trip (fault condition)
T27- R1 determines no fault exists
T28- R2 determines no fault exists
T29- Open breaker B1
T30- Open breaker B2
T31- Close B1 and B2 (fault not cleared)
T32- Close B1 and B2 (fault not)
T33- Isolate line

Figure 3.2: PN model for European SPS

Since there is a wide range of possible results that the protection relay calculations can produce, they have been separated into four discrete categories.

1) Relay generates a trip signal during a fault condition
2) Relay generates a trip signal during a non-fault condition
3) Relay does not generate a trip signal during a fault condition
4) Relay does not generate a trip signal during a non-fault condition

For each of the above four categories there are associated T nodes whose TP's are determined by relay calculations. Once the relay calculations have been performed the TPs for the T nodes of the associated category are set to 1.0 while the other T nodes are set to 0.0. With the TPs of T nodes in the other three categories set to 0.0, any TTP calculation which they contribute to goes to 0.0.

Under moderate to heavy transmission line loading with the incorrect latency values assumed, the TNTP for operating in condition 2 is $6.5499 \cdot 10^{-12}$ and condition 4 is 1.0. This shows that there is a high probability of improper system operation when the incorrect communications system latency value is assumed.

This is just a single example of the type of contingency analysis that can be applied to these models. Additional contingencies could include complete failure of a communications channel, failure of a single relay, or failure of an isolation breaker to operate. Contingency analysis will be further examined in the next Chapter.

Had this method been previously applied to the European SPS and the correct contingencies selected, this potential problem could have been identified before it ever occurred. Since there are only three variables in the calculation of a differential current it is reasonable to assume that errors in the latency value would be a contingency that is considered.

3.3 Special Protection System Concluding Remarks

Chapter 3 has applied the vulnerability assessment of section 2.7 to two separate SPS. From the results of sections 3.1 and 3.2 it is clear that when there are potential infrastructure vulnerabilities they can be identified in any portion of the three step method. For example, analysis of the Hydro-Québec SPS showed that the TTP and TTT for the normal modes were adequate but the third step showed a lack of redundancy. The European SPS appeared to operate correctly until other than normal operating modes were examined. These two situations show that the full vulnerability analysis of infrastructure vulnerabilities can be very involved.

One area of future collaborative research with industry is the integration of the PN method of section 2.7 with existing methods of reliability analysis. Since many utilities have done limited reliability studies on power system components, and communications components to a lesser extent, it would be useful to integrate this existing work. Studies that have been performed using techniques such as a Reliability Block Diagram (RBD) could be used to generate more accurate TP and TT values for equipment and various processes. If the RBD is performed for a group of process the information could also aid in the reduction of the overall model size. While this type of information will not be incorporated into the work of this Dissertation it is an avenue for future research.

For both of the SPS analyzed in this Chapter the values for individual TPs and TTs had to be assumed. This lack of detail was because of the difficulty of obtaining detailed information about power systems which are currently in operation. Even using assumed values it was possible to perform the vulnerability assessment method of 2.7 and gain insight into the potential vulnerabilities of the SPSs. Chapter 4 will examine a system for which there is ample detailed information for the complete analysis of an EMS system. This detailed information will allow for a more complete analysis as would be done in a utility.

Chapter 4: Vulnerability Analysis of the NEPTUNE Energy Management Systems

The previous chapter examined the vulnerability analysis of infrastructure interactions in SPSs using the method developed in Chapter 2. This chapter will use the same method to examine a single EMS function for potential vulnerabilities. Because of the size and complexity of a modern EMS the various functions will be examined individually.

For this purpose the topology identification component of the NEPTUNE EMS has been chosen for analysis. Topology identification of a power system is necessary for the proper operation of state estimators. When the current system topology is not known, state estimators can generate erroneous outputs which degrade an operator's understanding of system conditions. Incorrect updating of a transmission line status is one of the events that contributed to the August 14^{th} 2003 Eastern Interconnect blackout, as discussed in section A4.5.

Since the NEPTUNE system is still in the design process, some specific details from the systems prototype, the Monterey Accelerated Research System (MARS), will be used. The topology identification scheme was designed specifically for NEPTUNE but the communications system which will be analyzed has been constructed for MARS. The NEPTUNE communications system will be similar to the MARS system. Since MARS is in the final stages of development it will be possible to obtain specific data about individual components. This level of detailed information is necessary to fully exploit the power of the vulnerability assessment method.

4.1 Overview of the NEPTUNE EMS

Supplying power to electrical loads beneath the ocean is currently at a transition point requiring a new operational paradigm [45]. Historically, powering ocean experimentation has been a tradeoff between the power level and duration of the experiment. High power applications that are greater than a few watts generally require a ship-bound tether to supply power. Due to the infeasibility of year round ship deployment, high power oceanographic applications have been severely limited in duration. The NEPTUNE power system will contribute to the change of operational paradigms for ocean exploration and experimentation by providing science users with a continuous and relatively abundant supply of electrical power.

The NEPTUNE power system is a potential gateway to a new generation of power systems that are unlike any currently in operation. Effectively extending the terrestrial power system from the shoreline into an ocean environment requires reexamining issues that have been studied extensively for terrestrial power systems.

4.1.1 Introduction and Background

The NEPTUNE system represents an example of a new form of ocean exploration, cabled observatories. Previous cabled observatories include numerous Japanese observatories used for disaster mitigation as well as various scientific based observatories in the United States [46].

Power systems for both terrestrial and ocean applications such as cabled observatories have been deployed on large scales, but neither application addresses all the requirements of NEPTUNE. Terrestrial power systems are based on inter-connected Alternating Current (AC) networks with parallel loads, while underwater telecommunications systems are Direct Current (DC) point-to-point systems with series loads. The proposed NEPTUNE power system combines elements from each of these designs to create a system that differs significantly from either of the individual designs [45-49].

The proposed system is a highly interconnected DC system with a combination of series and parallel loads interconnected with a 3,000 km cabled under-ocean network powered via two shore landings, intended to supply power at specified locations Figure 4.1.

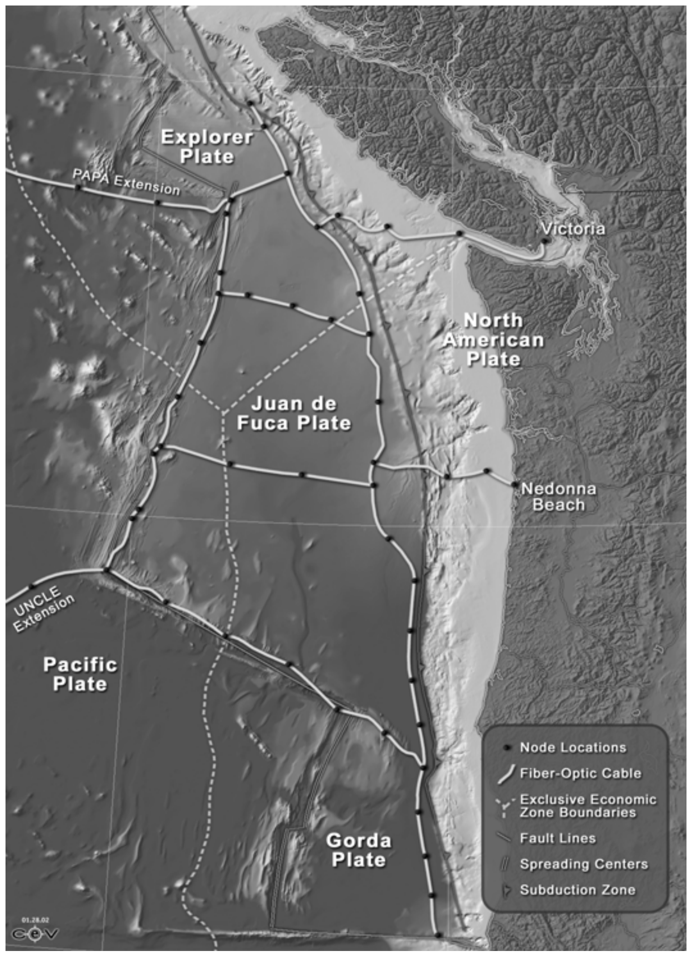

Figure 4.1: Proposed NEPTUNE system

In order to maximize the deliverable power, the back bone system will operate at 10-kV with respect to the ocean. While the nominal 10-kV voltage is well below standard terrestrial transmission and some distribution system voltages, it is the maximum rated voltage for standard under-ocean telecommunications cables that will allow for the required thirty year operational life [45].

Power is supplied to the system at the nominal 10-kV voltage from two Shore Stations (SS), one in the State of Oregon and the other in the Province of British Columbia. The two shore stations will form the interface between the terrestrial power distribution system and the NEPTUNE power system. At the two shore stations the nominal voltage will be maintained through the use of AC-DC converters in conjunction with uninterruptible power supplies.

Each of the forty-six node locations in Figure 4.1 will contain a node Branching Unit (BU), which branches the main cable via a spur. See Figure 4.2. The spur may be up to several kilometers long, depending on the water depth, and will supply power and communications to the science nodes.

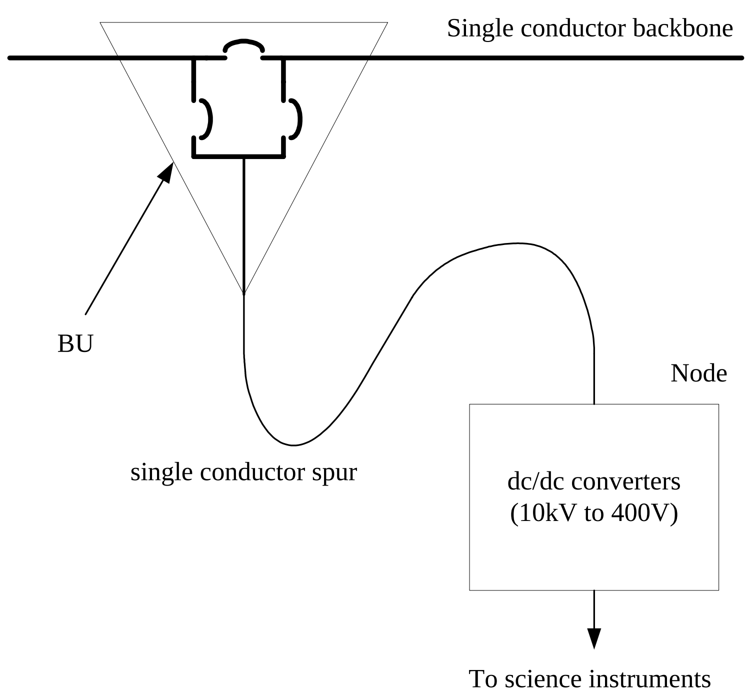

Figure 4.2: Branching Unit to science node connection

Loads at the science node are served by Pulse Width Modulated (PWM) DC-to-DC converters delivering a stable 400V_{DC} and 48 V_{DC} from the incoming BU. Due to the operational characteristics of the converters at the science nodes, the loads at the science node have constant power characteristics. As a result, changes in system voltage do not significantly impact the power consumed by the science node loads. It is at the science node that science users, the end users, are served.

The BU has a series power supply with the simplest feasible implementation for the controls. It has been determined that it is possible to design a system that has only a 50% chance of requiring a service visit to a BU for maintenance or repair once in the thirty year life of NEPTUNE. However, the simplicity of design that is necessary to achieve the required level of reliability results in a design where there is no communications system access to the BUs. Consequently, the voltages, currents and even the status of the switches within a BU are not directly known to the NEPTUNE monitoring system on shore. In order to compensate for the lack of power system data from the BUs, a state estimation algorithm has been developed to determine the voltages at the BUs [51]. The state estimation algorithm allows for the estimation of the BU voltages based on the voltage and current measurements at the science nodes as well as the shore stations in conjunction with the information from the assumed topology of the system.

4.1.2 State Estimation for the NEPTUNE system

In a conventional terrestrial power system, data is collected via the SCADA system and state estimation is performed by the EMS [53-56]. The NEPTUNE equivalent of a SCADA and EMS system is called the Power Monitoring And Control System (PMACS). It is within the PMACS software that the state estimation functions are performed.

The basis of state estimation is the relation of the values measured within the system to the unknown state variables, as shown in (4.1).

$$Z^{meas} = H \cdot x + \varepsilon \tag{4.1}$$

Where:

Z^{meas} : Column vector of measured values
H : Matrix of coefficients relating the known and unknown variables, based on system topology
x : Estimated BU voltages
ε : Measurement errors

Through the use of Kirchhoff's current and voltage laws, it can be shown that the current flowing into a science node and the science node voltage can be expressed in terms of the assumed topology of the system and the unknown BU voltages. Figure 4.3 will be used as an example of how the measurements made at a science node are expressed in terms of the unknown values, BU voltages, and line resistances.

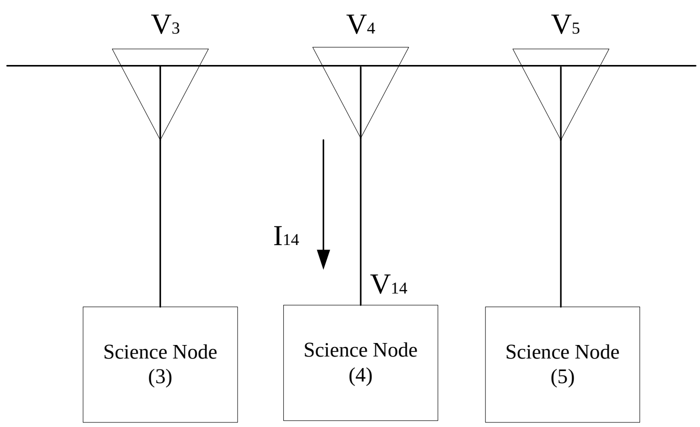

Figure 4.3: Three BU's and three science nodes

Where:

$V_3 - V_5$: Unknown BU voltages
V_{14} : Measured science node voltage
I_{14} : Measured science node current
R_{34} & R_{35} : Backbone resistances
$R_{4(14)}$: Spur resistance

Using equations (4.2) and (4.3) as a framework, the voltage and current measurements at each of the science nodes can be expressed as:

$$I_{14} = \left(\frac{V_4 - V_5}{R_{45}} - \frac{V_3 - V_4}{R_{34}} \right) \tag{4.2}$$

$$V_{14} = V_4 - \left(\frac{V_4 - V_5}{R_{45}} - \frac{V_3 - V_4}{R_{34}} \right) \cdot R_{4(14)} \tag{4.3}$$

While it is possible to express any single BU voltage as a function of only the associated science node, this method does not take advantage of the redundant measurements in the system. In order to account for an over constrained system where there are more measured values than unknown values, it is helpful to construct an expression that gives the maximum likelihood of the unknown values through a Weighted Least Squares (WLS) calculation (4.4).

$$J(x) = \left(Z^{meas} - f\left(x^{est}\right)\right)^T \left(R^{-1}\right)\left(Z^{meas} - f\left(x^{est}\right)\right) \tag{4.4}$$

Where:

$f\left(x^{est}\right)$: estimation of the measured values based on the estimated BU values

R^{-1} : inverse of diagonal matrix of measurement variances

By expanding (4.4) and calculating $\nabla J(x) = 0$, the WLS algorithm is given by (4.5).

$$x^{est} = \left(H^T R^{-1} H\right)^{-1} \left(H^T R^{-1} Z^{meas}\right) \tag{4.5}$$

One advantage of the formulation of (4.5) is that if any single measurement is lost it is still possible to determine the voltages at every BU. Furthermore errors that arise in the measurements are filtered in the WLS calculation. Another advantage of the WLS algorithm for NEPTUNE is that due to the linearity of (4.2) and (4.3) an iterative calculation is not required. While it is possible to obtain multiple or no solutions for a set of linear equations, this has not been an issue for NEPTUNE.

The general formulation of (4.2) and (4.3) is valid for all sections of NEPTUNE since BUs only exist where there is a science node. The equations may change slightly based on the number of adjacent BUs, i.e., number of terms, but the general form of (4.2) and (4.3) remains consistent.

Equation (4.5) gives the WLS approximation of the voltages at the BUs. If the assumed topology of the system is correct and there is no measurement error, then (4.5) will yield the exact voltages at the BUs. When measurements containing a Gaussian error with a nonzero variance are used in conjunction with (4.5) to estimate the BU voltages, the values will not be exact but are more reliable than a single measurement due to the filtering of the WLS fit.

In a system where the topology is known it is possible to approximate the variance of the measurement error using the estimated BU voltages. In order to approximate the variance of the measurement error present in the system, a comparison is made between the measured values and the measured values as calculated from the estimated BU voltages, $f(x)$, the difference is indicated by the mean absolute residual (4.6).

$$\begin{aligned} R_{mar} &= \left(1/n\right) \cdot \sum_{i=1}^{n} \left| z_i - H_i x^{est} \right| \\ &= \left(1/n\right) \cdot \sum_{i=1}^{n} \left| T_i * Z^{meas} \right| \end{aligned} \tag{4.6}$$

Where:

H_i : i[th] row of matrix H

n : number of measured quantities

T : $I - H\left(H^T R^{-1} H\right)^{-1} H^T R^{-1}$

T_i : i[th] row of matrix T

The mean absolute residual, R_{mar} , is the sum of a column vector with each of the elements containing the absolute value of the difference between the measured science node values and those calculated from the estimated BU voltages. When there is no measurement error, zero variance, in the system and the assumed topology is correct; the mean absolute residual will be zero. As the variance of the measurement error is increased from zero, the value of R_{mar} will begin to increase and the estimated BU voltages begin to deviate from the actual values.

If a breaker inside a BU is in a position other than expected, the voltages at the BUs will be estimated incorrectly. With the simultaneous presence of measurement and topological errors, the system operators and PMACS will be supplied with erroneous information. Without the correct information it is possible for PMACS control actions to result in undesired system conditions. For this reason, the topology identification component of PMACS uses the mean absolute residual as a basis for determining the current system topology.

4.1.3 Basis of Topology Identification

For the purposes of this study, there are two distinct classifications of system topology, i.e., the design topology and the operational topology. The design topology is the topology of the system as it is constructed, with all breakers closed and all lines in service. The operational topology is determined by the current status of breakers and combination of lines currently in service. If all breakers are closed and all lines are in service, then the operational topology and the design topology are identical. This section deals with the situation where the operational topology of the system is other than expected due to a breaker status error.

In terrestrial power systems there are redundant sources of information to determine the position of breakers, e.g., breaker auxiliary contacts, current measurements through the breaker, voltage measurements across a breaker, power flow along a line, and visual inspection results. In the absence of direct indications such as auxiliary contacts, conventional methods make use of indirect measurements, such as voltage differences and line flows, to perform the combined function of state estimation and topology identification [57-60]. The lack of comparable indications, direct or indirect, in the NEPTUNE systems requires a new method of topology error identification.

In order to accurately perform the state estimation and topology error identification, it cannot be assumed that the most significant contribution to the mean absolute residual originates with the topology error. There are three sources of error that contribute directly to the mean absolute residual: error from voltage measurements, error from current measurements, and error from topology errors. When the error from one source, e.g., voltage measurement, is much greater than the error source of interest, i.e., topology error, the source of interest is “masked.” If there is no error in the voltage and current measurements, then the topology that gives a zero mean absolute residual would be the correct operational topology. Due to the multiple sources contributing to the mean absolute residual and the associated masking effects, the mean absolute residual at a single operating point will not be sufficient to determine the current operational topology.

In order to examine the system at multiple operating points the system will be perturbed by varying the shore station voltages incrementally within a prescribed band. At each of the increments, data will be collected from the science nodes and the mean absolute residual calculated. The manner in which the mean absolute residual varies with respect to the shore station voltage variations will be the primary indicator of the system topology. By using the variation of the mean absolute residual it will be possible to avoid the problems caused by masking.

When the assumed operational topology is the correct topology, it will initially be assumed that the mean absolute residual will vary in a roughly linear manner in the normal operating region, 8,000-12,000 V_{DC} at all points in the system. Assuming that the variation will be linear, the sensitivity of the mean absolute residual with respect to changes in voltage at a single shore station is calculated by (4.7).

$$\begin{aligned} \frac{\partial R_{mar}}{\partial V_{SS}} &= \left(1/n\right)\cdot \frac{\partial}{\partial V_{SS}}\left(\sum_{i=1}^{n}\left|T_i \cdot Z^{meas}\right|\right) \\ &= \left(1/n\right)\cdot \sum_{i=1}^{n}\left(sign\left(T_i * Z^{meas}\right)\cdot T_i \cdot \frac{\partial Z^{meas}}{\partial V_{SS}}\right) \end{aligned} \quad (4.7)$$

Where:

$\frac{\partial R_{mar}}{\partial V_{SS}}$: sensitivity of the calculated residual

V_{SS} : voltage at the selected shore station

The last term of (4.7), $\frac{\partial Z^{meas}}{\partial V_{SS}}$, requires that the sensitivities of each of the science node and BU voltages with respect to the shore station voltages be calculated. In order to calculate the required sensitivities the power flow equations must be differentiated. The result is given by (4.8).

$$-Y_{i(SS)}\cdot V_i = \left\{\begin{aligned} &\left(Y_{ii}\cdot V_i + \sum_{j=1}^{k+2} Y_{ij}\cdot V_j\right)\frac{\partial V_i}{\partial V_{SS}} + \\ &\left(\sum_{\substack{j=1\\ j\neq i}}^{k} Y_{ij}\cdot V_j \cdot \frac{\partial V_j}{\partial V_{SS}}\right) \end{aligned}\right\} \quad (4.8)$$

Where:

Y_{ii} : ii^{th} element of the bus admittance matrix

V_i : voltage at the i^{th} bus

k : total number of science nodes and BU's in the system

Equation (4.8) is calculated with i ranging from 1 to the number of science nodes, k, while setting SS equal to the node number of the shore station that is being varied. When i is varied from 1 to the number of science nodes, the voltage at each of the science nodes, as well as each of the BUs, with respect to the voltage at the shore stations can be calculated using (4.9). Equation (4.9) must be calculated at each operating point for each operational shore station. For the system in Figure 4.1 there are maximally two shore stations in operation at any given time.

$$\partial = A^{-1} \cdot B \cdot V \tag{4.9}$$

Where:

$$\partial = \begin{bmatrix} \dfrac{\partial V_1}{\partial V_{SS}} \\ \vdots \\ \vdots \\ \dfrac{\partial V_k}{\partial V_{SS}} \end{bmatrix} \qquad A = \begin{bmatrix} Y_{1(1)}V_1 + \sum_{j=1}^{k+2} Y_{1(j)}V_j & Y_{1(2)}V_1 & \cdots & Y_{1(k)}V_1 \\ Y_{2(1)}V_2 & Y_{2(2)}V_2 + \sum_{j=1}^{k+2} Y_{2(j)}V_j & \cdots & Y_{2(k)}V_2 \\ \vdots & \vdots & \ddots & \vdots \\ Y_{k(1)}V_k & Y_{k(2)}V_k & \cdots & Y_{k(k)}V_k + \sum_{j=1}^{k+2} Y_{k(j)}V_j \end{bmatrix}$$

$$B = \begin{bmatrix} -Y_{1(SS)} & 0 & \cdots & 0 \\ 0 & -Y_{2(SS)} & \cdots & 0 \\ \vdots & \vdots & \ddots & \vdots \\ 0 & 0 & \cdots & -Y_{k(SS)} \end{bmatrix} \qquad V = \begin{bmatrix} V_1 \\ \vdots \\ \vdots \\ V_k \end{bmatrix}$$

Once the sensitivities of each of the science node and BU voltages are available, each of the elements of (4.7) can be calculated. Equation (4.7) gives the sensitivity of the mean absolute residual with respect to the shore station voltage for a system composed of only linear components. The next step is to determine if any of the power system devices used in NEPTUNE introduces non-linearities into (4.7) and, if they do, determine their non-linear characteristics. Three particular elements will be examined: the voltage measurement devices, current measurement devices, and DC-to-DC converters.

4.1.3.1 Voltage Measurements Device Characteristics

The power system devices that will be examined first are those used to measure the voltage in the science nodes. These devices are connected as a voltage divider, as shown in Figure 4.4.

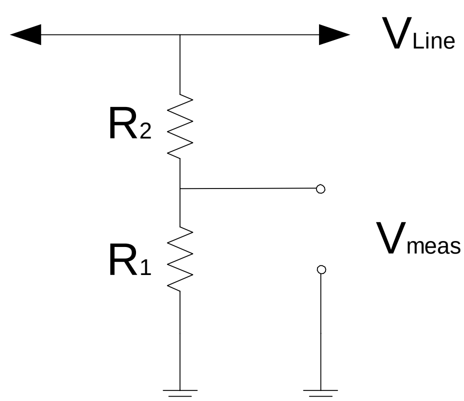

Figure 4.4: Voltage measurement schematic

For a voltage divider with ideal resistors, i.e., exact values, the measured voltage, V_{meas}, is given by (4.10).

$$V_{meas} = \frac{R_1}{R_1 + R_2} V_{Line} \tag{4.10}$$

Since it is not possible to obtain ideal resistors, it is necessary to introduce error into the values of resistance, (4.11).

$$\tilde{R}_1 = R_1 + \varepsilon_1 R_1 = R_1 (1 + \varepsilon_1) \tag{4.11}$$

$$\tilde{R}_2 = R_2 + \varepsilon_2 R_2 = R_2(1 + \varepsilon_2)$$

Where:

ε_1 : fractional error of resistor R_1

ε_2 : fractional error of resistor R_2

Substituting (4.11) into (4.10) yields (4.12).

$$V_{meas} = \frac{(1 + \varepsilon_1)}{(1 + \varepsilon_1) + \frac{R_2}{R_1}(1 + \varepsilon_2)} V_{Line} \tag{4.12}$$

In order to reduce the measured voltages, V_{meas}, to usable control levels, the ratio of resistor values is set so that $\frac{R_2}{R_1} = 999$. The result is a V_{meas} of between 8 and 12 V_{DC} as V_{Line} varies from 8,000 to 12,000 V_{DC}, i.e., the nominal operating range for the NEPTUNE power system.

For any sufficiently short interval of time, minutes to hours, the error of the resistor values can be considered constant. With the resistor error constant, the error in the measured voltage, V_{meas}, is reduced to a constant, multiplied by the line voltage, V_{Line}, which yields a linear relationship between line voltage and the measured voltage, shown in Figure 4.5.

Figure 4.5 shows a plot of the measurement error as the line voltage is increased from 0 to 15,000 V_{DC} for an isolated voltage measurement device. The solid line represents V_{meas} when the values of R_1 and R_2 are exact. The two dashed lines represent V_{meas} when R_1 and R_2 contain errors of ±2%. The key observation to be gained from examination of Figure 4.5 is that as the line voltage is increased, the *magnitude* of the measured voltage error is also increased in a linear manner. A linear increase in the magnitude of line voltage will increase the magnitude of the mean absolute residual linearly. The result is that the voltage measurement devices do not introduce any non-linear characteristics to (4.7).

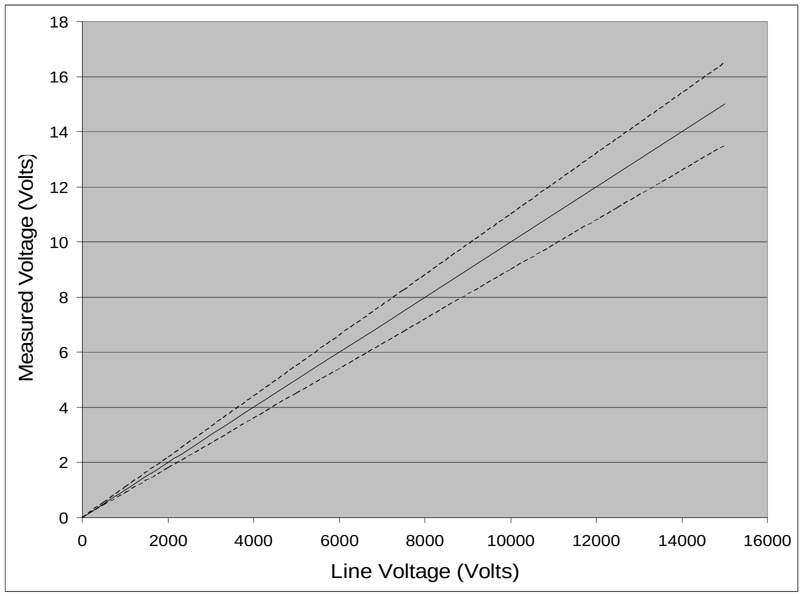

Figure 4.5: Voltage error variation with line voltage

4.1.3.2 Current Measurement Device Characteristics

The second set of power system devices to be examined includes those used to measure the current flowing into the science nodes. These devices are of a shunt design, as shown in Figure 4.6.

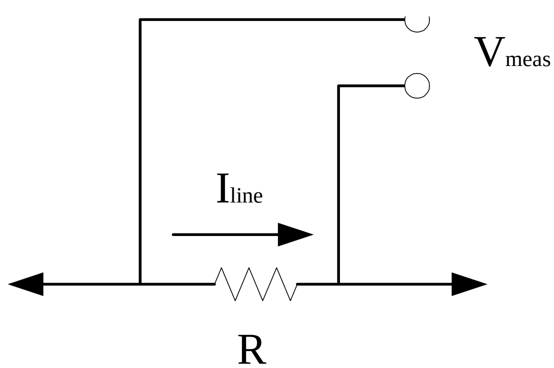

Figure 4.6: Current measurement schematic

Assuming that the resistive element, R, will have an error, (4.13) and (4.14) provide the calculated values of V_{meas} and the line current.

$$V_{meas} = I_{Line(actual)} \cdot R(1+\varepsilon) \tag{4.13}$$

$$I_{Line(calculated)} = (1+\varepsilon) \cdot I_{Line(actual)} \tag{4.14}$$

Equations (4.13) and (4.14) show that as the line current increases linearly, the *magnitude* of the measurement error and the corresponding mean absolute residual will also increase linearly. The result is that the current measurement devices do not introduce non-linear characteristics to (4.7).

4.1.3.3 Converter Characteristics

The third and final set of power system devices that will be examined is the DC-to-DC converters used at the science nodes. The converters step down the 10-kV nominal backbone voltage to a constant 400V for the end users. Since the output voltage is independent of the input voltage, the loads exhibit a constant power characteristic.

When the total system load is zero, the converters characteristics do not affect the system, resulting in a purely resistive and linear system. A zero system load, however, is not practical since the voltage and current measurements consume power in order to record and transmit their information to PMACS.

In order to examine the characteristics of a converter, the current vs. voltage profile for a single isolated converter will be examined. See Figure 4.7. As the load on the converter is increased from zero to the maximum value, non-linear characteristics become more pronounced due to the hyperbolic relation between current and voltage for a constant power device. Figure 4.7 shows the current vs. voltage profile for three different power levels for a single isolated converter connected to an ideal voltage source.

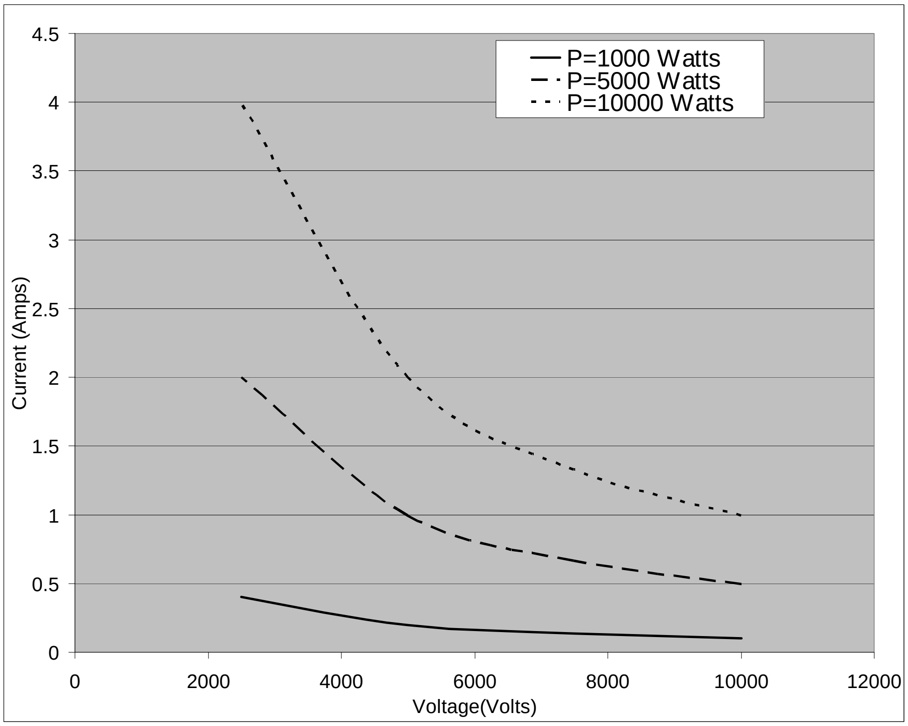

Figure 4.7: Non-linear converter characteristics

Due to the slight non-linear variations that arise from the converter dynamics, the ability of (4.7) to predict the variation of the mean absolute residual will depend on the loading of the various converters in the system. The result is that the converters have a non-linear contribution to (4.7). The maximum non-linear converter contribution is determined by the maximum system load. Thus, the maximum load scenario sets an upper bound for the converters' contribution to non-linearity for a given operational topology.

4.1.4 Sensitivity Analysis Method of Topology Identification

With the correct topology assumed, the only non-linear effects on the mean absolute residual are due to the converter dynamics. In order to take the converter dynamics into account a maximum bound must be set on the non-linear effects of the converter. The bounds correspond to the worst case non-linear effect that converters can contribute to the mean absolute residual for a given operational topology.

Once the deviation from linearity is determined for the maximum system load, all load combinations of a lower level will cause less deviation. For the system of Figure 4.1 the maximum variation from a linear approximation is .847%. Therefore, the assumed topology, for which the mean absolute residual varies by less than .847% from linearity as shore station voltages are varied, indicates the correct system topology. All topologies that yield a variation higher than .847% correspond to incorrect assumed operational topologies.

The flow chart in Figure 4.8 shows the procedure for determining the correct current operational topology of the NEPTUNE system when using the sensitivity based method.

The complete procedure to detect the existence of a topology error and thereby determine the current operational topology is to first vary the voltage at SS 1 from 8,500V_{DC} to 11,000V_{DC} while calculating the mean absolute residual at 500V_{DC} intervals. The voltage at SS 1 is then returned to nominal and the same procedure is repeated with the voltage at SS 2. The mean absolute residuals are determined with the assumed topology. The following criteria applied:

1) The maximum variation of the mean absolute residual must be less than the value that is bounded by the characteristics of the converters at maximum system load.
2) The variation of the mean absolute residual must maintain a positive slope throughout the voltage range.

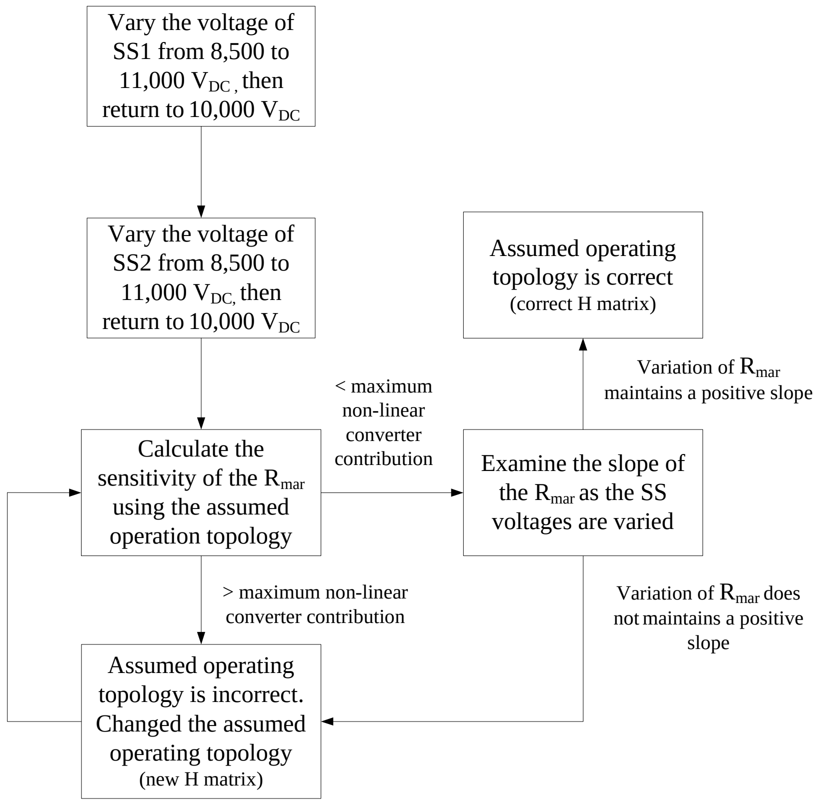

Figure 4.8: Topology identification procedure

If either of the above two criteria is not met, a topology error is indicated. In order to determine the current operational topology the mean absolute residuals are recalculated with different assumed operational topologies, H matrices, until the H matrix that satisfies the two criteria is found. The H matrix that satisfies the two requirements represents the correct operational topology. When the mean absolute residuals are recalculated for each possible operational topology, it is not necessary to vary the shore station voltages again; the same measurements data can be used that was collected for the initial test.

As discussed earlier, masking is a condition that can result in an incorrect operational topology. By examining the mean absolute residual at multiple operating points, the proposed method ensures that masking does not interfere with topology identification. When the mean absolute residual is examined at a single operating point based on the magnitude criteria, masking occurs when multiple sources contribute to the magnitude. The proposed method examines a characteristic, i.e., sensitivity of the mean absolute residual, which only has two sources of contribution: topology errors and converter dynamics. The maximum contribution of the converter dynamics is calculated for a given operational topology and this value determines the upper bounds for the converter contribution. With the contribution from the only other source bounded, sensitivity effects from topology errors can be identified.

The masking of the mean absolute residual at a single operating point will be evident in cases where the second criterion is not met. When the variation of the mean absolute residual has a negative slope, it is an indication that measurement errors and topology errors are masking each other. While masking is a problem for some methods of topology identification, the sensitivity based method uses the presence of masking to identify topology errors.

In order for the proposed method of topology identification to be applicable to any potential design topology, it is necessary to show that changes in the design topology do not introduce nonlinearities into the sensitivity of the mean absolute residual. To this end, (4.7) will be examined with respect to changes in the design topology. This is accomplished by operating only in the normal voltage range and with the system at no load. Operation in the normal voltage range ensures the $sign\left(T_i * Z^{meas}\right)$ term of (4.7) can be simplified as the term is a column vector of ones. Operation at no load allows for the nonlinear characteristics of the converters to be ignored. With the effects of the converters ignored the system becomes a connection of purely resistive elements and the $\frac{\partial Z^{meas}}{\partial V_{SS}}$ term of (4.7) is a constant, as shown in (4.9). Under these conditions (4.7) is a summation of constants, resulting in a constant slope. For various design topologies, the elements of the associated Y matrix will affect the $\frac{\partial Z^{meas}}{\partial V_{SS}}$ term of (4.7). As a result, a summation of different constants for different design topologies yields different slopes. The result is that changes in the design topology do not introduce nonlinearities into the sensitivity of the mean absolute residual, and, as such, the method shown in Figure 4.8 is valid for all potential design topologies.

4.1.4.1 Case 1: Single Topology Error

Figure 4.9 shows the variation of the mean absolute residual, as calculated by (4.7), when there is a single topology error. Following the flow chart of Figure 4.8, it is clear that the assumed operational topology is not correct since the variation of the mean absolute residual does not satisfy either of the two criteria detailed in section 4.5. Furthermore, the negative slope of the mean absolute residual indicates that there is masking of the mean absolute residual at certain individual operating points. As discussed in section 4.5, the masking of individual operating points manifests itself as a negative slope and indicates the presence of a topology error

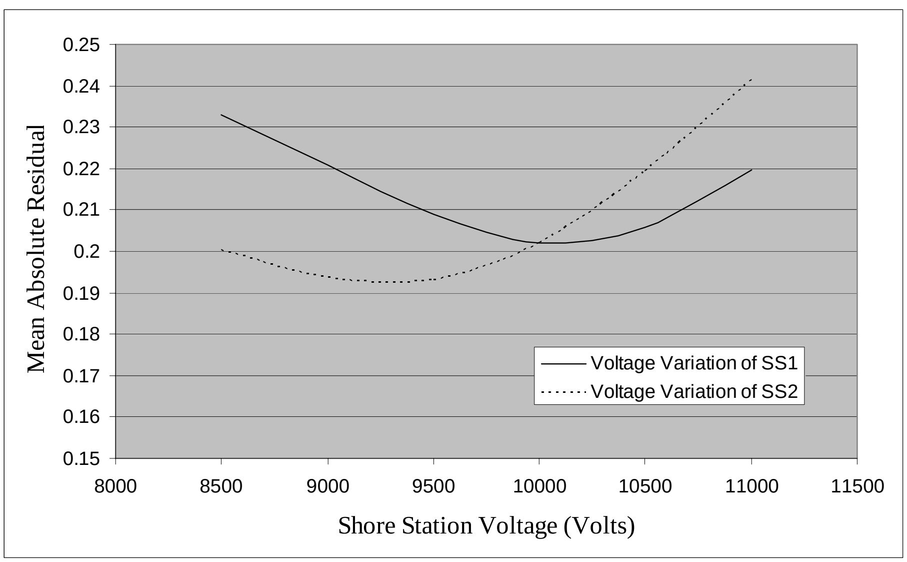

Figure 4.9: Single topology error with incorrectly assumed operational topology

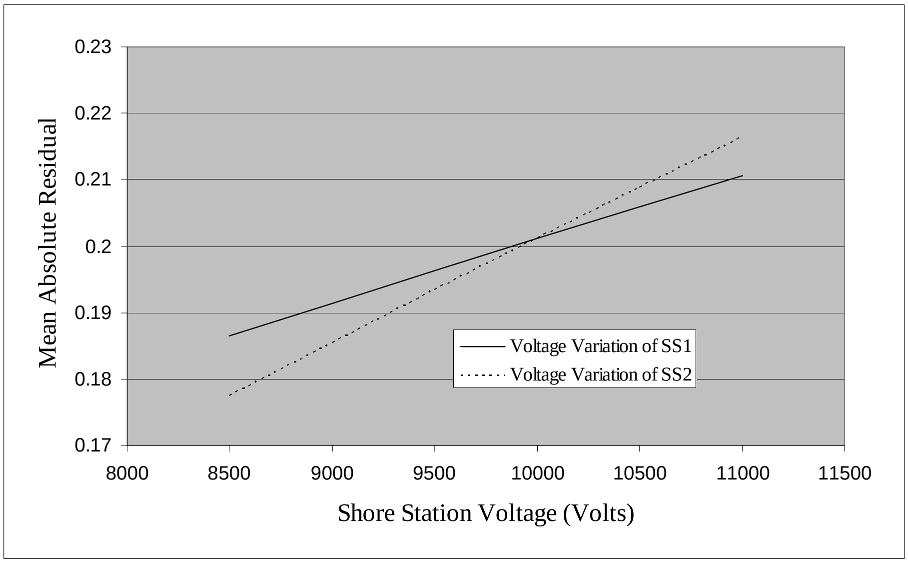

Figure 4.10: Single topology error with correctly assumed operational topology

When the H matrix associated with the correct operational topology is used in calculating (4.7), the mean absolute residual varies as shown in Figure 4.10. The error between the variation shown in Figure 4.10 and a linear variation as calculated by (4.7) is approximately .70% over the given voltage range, less than the maximum converter contribution of .85%. Additionally, the variation of the mean absolute residual maintains a positive slope over the entire voltage range. Following the flow chart of Figure 4.8, these two conditions indicate a correctly assumed operational topology.

The inclusion of the single gross measurement error of 30% does not affect the linear characteristics of the mean absolute residual. The effect of gross measurement errors is to increase the magnitude of the mean absolute residual, in effect shifting the curve upward. The location of the gross measurement errors can be identified by examining the individual elements of the mean absolute residual. A gross measurement error presents itself as a value associated with an individual measurement that is much larger than the statistical average. Additionally, a Chi Squared test can be applied to the individual elements of the mean absolute residual to aid in the identification of gross measurement errors.

4.1.4.2 Case 2: Double Topology Errors

Figure 4.11 shows the variation of the mean absolute residual, as calculated by (4.7), when there are two topology errors. Following the flow chart of Figure 4.8 it is clear that the assumed operational topology is not correct since the variation of the mean absolute residual does not satisfy either of the two criteria detailed in section 4.5

As with the case 1, the mean absolute residual is shown with the correctly assumed operational topology, see Figure 4.12. Following the flow chart of Figure 4.8 these two conditions indicate a correctly assumed operational topology.

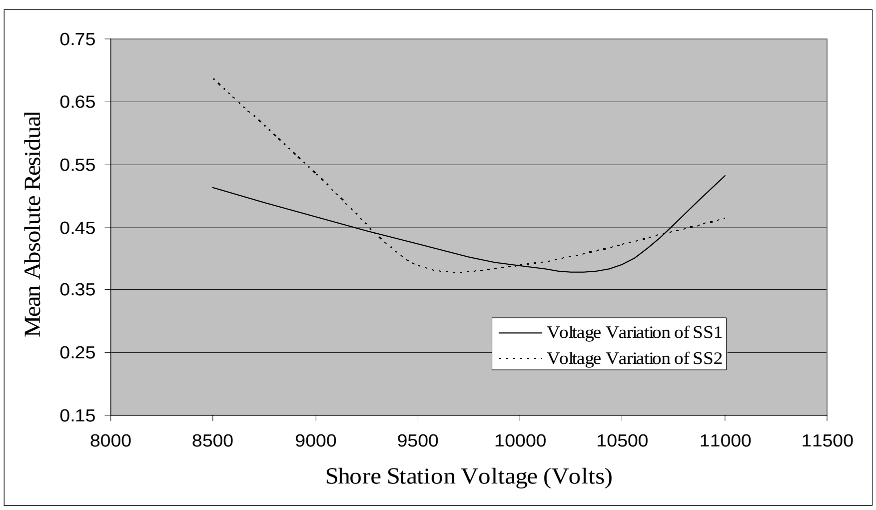

Figure 4.11: Dual topology error with incorrectly assumed operational topology

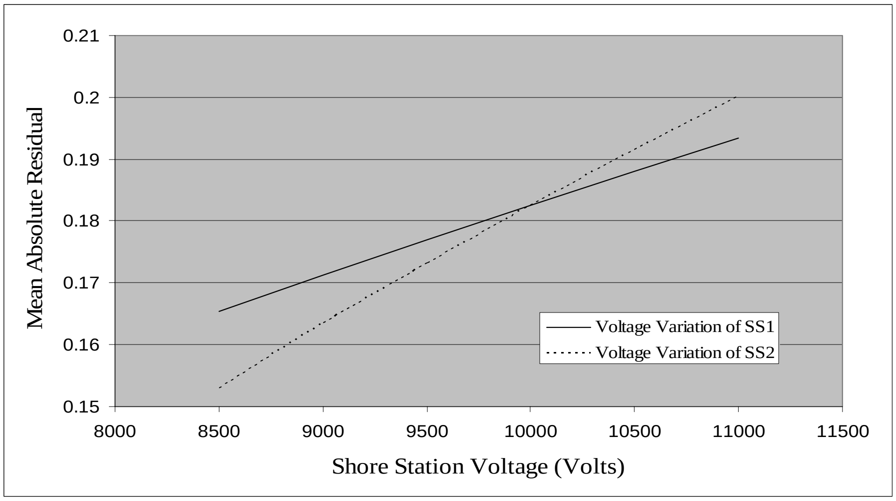

Figure 4.12: Dual topology error with correctly assumed operational topology

In order to find the actual operational topology in the presence of topology errors, each of the possible topologies must be examined. This requires, at most, the calculation of (4.7) for each possible operational topology involving a single topology error. For the system of Figure 4.1 this requires calculating (4.7) thirty seven times for a single topology error, and 37^2 times for double topology errors. While complete enumeration may be necessary, it is possible to reduce the search space by neglecting radial links. Radial links can be omitted from the search space since topology errors in these links have other gross indications, e.g., loss of science node information. For the system of Figure 4.1 this reduces the number of calculations of (4.7) to twenty four and 24^2, for single and double topology errors respectively. For triple topology errors and higher, the number of required calculations becomes prohibitive. These events will be extremely rare, however, for the NEPTUNE system.

4.1.5 Neural Network Method of Topology Identification

As was discuses in section 4.1.4 the topology of the system is determined by applying a dual criteria method to the equation of (4.7). Since (4.7) is a sensitivity calculation it requires that the voltage at the shore stations be varied and the various science node voltages and currents be measured. Both varying the shore station voltages and collecting the system data are tasks which require extensive use of the communications system. In an attempt to minimize system perturbations and reliance on the communications system an Artificial Neural Network (ANN) can be applied to the topology identification task [67].

4.1.5.1 Neural Network Structure and Training

Artificial neural networks are structured, in a fashion, after elements of the human nervous system [68]. The advantage to this structure is that it allows for the calculation of large non-linear problems with relatively simple algebraic computations, once the network has been trained. The major structural elements of an artificial neural network are the neurons and their interconnecting weights, Figure 4.13.

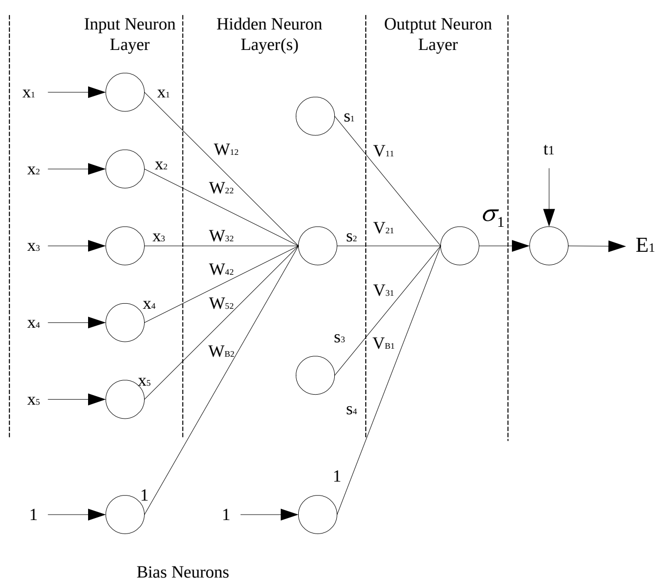

Figure 4.13: Three layer neural network structure

The ANN of Figure 4.13 is governed by equation (4.15)-(4.18).

$$S_i = \frac{1}{1+e^{-\lambda(net_i)}} \tag{4.15}$$

$$net_i = \sum_{j=1}^{5}\left(W_{ij}X_j\right)+W_{i6} \tag{4.16}$$

$$\sigma_1 = \sum_{j=1}^{3}\left(V_{ij}S_j\right)+S_4 \tag{4.17}$$

$$E = \frac{1}{2}\left(t_1-\sigma_1\right)^2 \tag{4.18}$$

Where:

λ : Gain that determines non-linearity of the sigmoid
t : The output associated with the inputs from the training data

The method used to train the ANN for this work is the well established method of back error propagation, where the weights of the k+1 iteration are calculated based on the value of the kth iteration (4.19) and (4.20).

$$V_{ij}^{(k+1)} = V_{ij}^{(k)} - \eta\frac{\partial E^K}{\partial V_{ij}^{(k)}} \tag{4.19}$$

$$W_{ij}^{(k+1)} = W_{ij}^{(k)} - \eta\frac{\partial E^K}{\partial W_{ij}^{(k)}} \tag{4.20}$$

Where:

$V_{ij}^{(k)}$: Weight between hidden neuron i and output neuron j
$W_{ij}^{(k)}$: Weight between input neuron i and hidden neuron j
$\eta^{(k)}$: Step size of the iteration
$E^{(k)}$: Difference between the output neuron value and the output value of the training data

The sensitivity of the error $E^{(k)}$ with respect to the weights, $V_{ij}^{(k)}$ and $W_{ij}^{(k)}$, is calculated at each iteration of the training processes. The general forms are found through the use of the chain rule:

$$V_{ij}^{(k+1)} = V_{ij}^{(k)} - \eta\left(-\left(t_1 - \sigma_1\right)S_j\right) \tag{4.21}$$

$$W_{ij}^{(k+1)} = W_{ij}^{(k)} - \eta\left(\left(\sum_{k=1}^{p}\left(t_1 - \sigma_1\right)V_{ki}\right)\left(S_i\lambda\left(1 - S_i\right)\right)\left(X_j\right)\right) \tag{4.22}$$

As the number of iterations, epochs, increases, the RMS error, $E^{(k)}$, should converge. Once the error has converged to a satisfactory value, as determined by the desired level of accuracy, the system can then be considered trained.

4.1.5.2 Training Data

For topology identification of the system shown in Figure 4.1, training data will be generated using a Newton-Raphson power flow scheme. A power flow algorithm has been designed that will allow for the non-linear zener diodes that are in the lines of the system to be taken into account. In addition, a Gaussian error of .1% will be introduced into the voltage and currents calculated by the power flow in order to simulate measurement error. A Gaussian error of 0.1% will also be introduced into the load values to reflect unknown/unexpected system loads.

The inputs of the ANN will be the forty six voltages and forty six currents measured at the science nodes in addition to the loads at the forty six nodes. The output will be the position of sixty four breakers, which will determine the topology of the system. The outputs will be binary with 1 indicating a closed breaker and 0 indicating an open breaker. From Figure 4.1 there are three classifications that each of the cable sections fall under:

1) Radial, connected to shore

2) Radial, not connected to shore
3) Networked

A topology error can easily be identified if it is in a cable section that falls within the first two classifications. In the first case a simple adjustment of the shore station voltage will only affect the science nodes between the topology error and the shore station. In the second case all of the science nodes down stream of the topology error will be disconnected from the system. It is only topology errors within the networked portion of the system that will be identified using the ANN.

Within the networked portion of the system there are thirty seven cable sections that could potentially become disconnected. Including the case where all of the breakers are closed, there are thirty eight potential topologies that must be examined for a complete *single contingency* analysis. For each of the thirty eight potential topologies two hundred power flow calculations are performed with varying system loads and random measurements errors in order to create the training data. The order in which the training data is presented to the ANN was randomized in order to prevent the possibility of the ANN memorizing the data instead of training properly.

4.1.5.3 Results of ANN Topology Identification

The ANN that was used to obtain the results of Table 4.1 consisted of one hundred thirty eight input neurons, twenty hidden neurons in a single layer, and sixty four output neurons. Initially the network was trained with the previously mentioned 7,600 test patterns for 1,000 epochs with a single line out of service. The out of service line is represented by the open state of breakers 44 and 45, while all other breakers are in the closed state. The raw results of the ANN are shown in Table 4.1.

From Table 4.1 it is clear that the output values are not always the ideal binary values, 0 and 1, but instead vary can by some small amount. Fortunately the variation from the ideal values is small enough that the breaker positions can be determined by using threshold values. An example set of threshold values is given in (4.23).

Table 4.1: Typical ANN outputs (1-64), for 1000 epochs

Output	Value	Output	Value	Output	Value
1	1.00000	23	1.00000	45	0.000435
2	1.00000	24	1.00000	46	0.996269
3	1.00000	25	0.999999	47	0.999738
4	1.00000	26	1.00000	48	0.999996
5	1.00000	27	1.00000	49	1.00000
6	1.00000	28	1.00000	50	1.00000
7	0.999986	29	1.00000	51	0.999966
8	1.00000	30	1.00000	52	1.00000
9	1.00000	31	1.00000	53	1.00000
10	1.00000	32	1.00000	54	1.00000
11	1.00000	33	0.999974	55	1.00000
12	1.00000	34	1.00000	56	0.999473
13	1.00000	35	1.00000	57	1.00000
14	1.00000	36	1.00000	58	1.00000
15	1.00000	37	1.00000	59	1.00000
16	1.00000	38	1.00000	60	1.00000
17	1.00000	39	1.00000	61	1.00000
18	0.994556	40	0.999257	62	1.00000
19	0.999561	41	0.997703	63	1.00000
20	0.999976	42	1.00000	64	1.00000
21	1.00000	43	0.999964		
22	0.999998	44	0.008322		

$$\begin{aligned} &value > .99 \Rightarrow \text{ Breaker is closed} \\ &value < .01 \Rightarrow \text{ Breaker is open} \end{aligned} \tag{4.23}$$

Using the threshold values of (4.23) allows for clear discrimination between the two possible breaker positions, open or closed. Table 4.2 shows the data from Table 4.1 after the threshold values have been applied in post processing. The open state of breaker 44 and 45, output 44 and 45 of the ANN, are clearly distinguished from the closed state of the rest of the system breakers. The identification of the improper position of the two breakers gives the operation a clear indication of the topology error.

The values in Table 4.1 and 4.2 are typical of the values that the ANN gives for a number of different load and topology configurations, as such the threshold values of (4.23) are valid for all possible single contingency topology errors for the system of Figure 4.1. Double topology errors are not considered for the ANN method of topology identification.

Table 4.2: ANN outputs after threshold values are applied

Output	Value	Output	Value	Output	Value
1	closed	23	closed	45	open
2	closed	24	closed	46	closed
3	closed	25	closed	47	closed
4	closed	26	closed	48	closed
5	closed	27	closed	49	closed
6	closed	28	closed	50	closed
7	closed	29	closed	51	closed
8	closed	30	closed	52	closed
9	closed	31	closed	53	closed
10	closed	32	closed	54	closed
11	closed	33	closed	55	closed
12	closed	34	closed	56	closed
13	closed	35	closed	57	closed
14	closed	36	closed	58	closed
15	closed	37	closed	59	closed
16	closed	38	closed	60	closed
17	closed	39	closed	61	closed
18	closed	40	closed	62	closed
19	closed	41	closed	63	closed
20	closed	42	closed	64	closed
21	closed	43	closed		
22	closed	44	open		

It is also possible to train the system for more than 1,000 epochs in order to gain greater discrimination between the two possible breaker states. The need for further discrimination is not necessary for the system in Figure 4.1 but may be necessary for other more complicated systems. For this reason the training results beyond 1,000 epochs will be examined.

As can be seen from Figure 4.14 the ANN output value for breaker 44, an open breaker, continues to asymptotically approach 0 as the ANN is trained for a greater number of epochs. Conversely, Figure 4.15 shows that the ANN output value for breaker 41, a closed breaker, continues to asymptotically approach 1 as the ANN is trained for a greater number of epochs. Some ANN outputs such as 42, from Table 4.1, converge to their correct value, 1 in the case of output 42, after only a few hundred epochs.

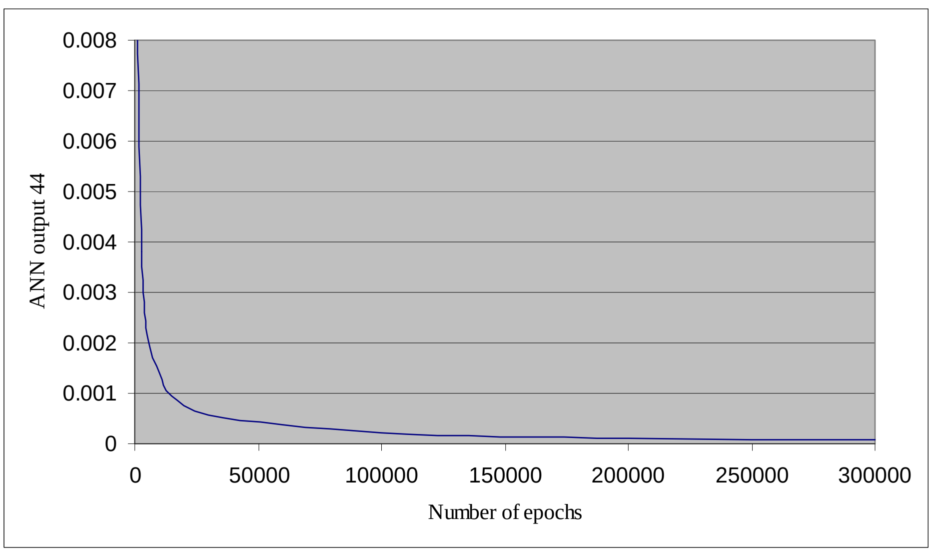

Figure 4.14: Training results up to 300000 epochs, open status

The level of training required is dependent on the desired level of discrimination between the two breaker states. If the training is allowed to continue for too long there is the possibility of the ANN memorizing the data instead of training [64]. This was prevented from occurring in the data presented in Figure 4.14 and Figure 4.15 by randomly varying the order of the test patterns in the training process as well as verifying the results against patterns not included in the 7,600 training patterns.

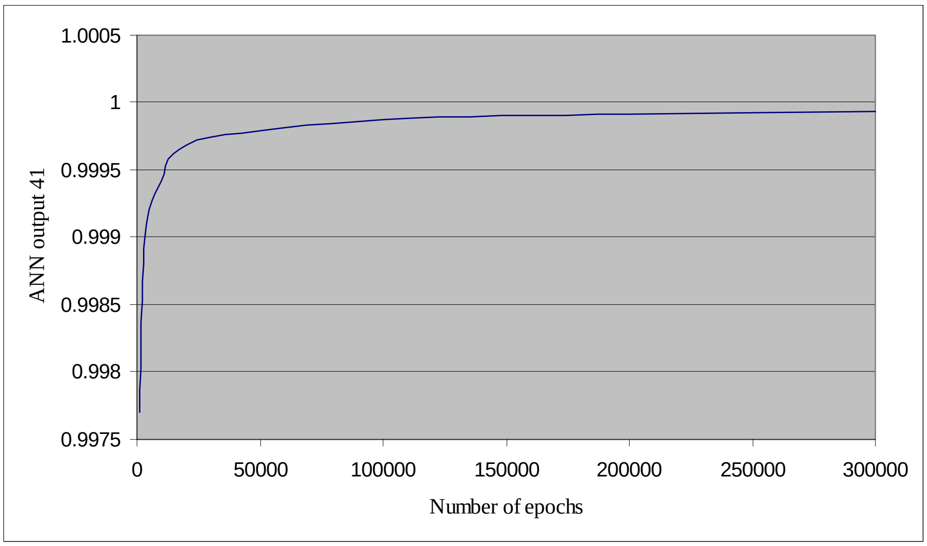

Figure 4.15: Training results up to 300000 epochs, closed status

The results show that for the system of Figure 4.1, an ANN is able to determine single contingency topology errors with a high degree of accuracy. This is accomplished in the absence of any direct indication of the breaker position or any indirect indications such as current through the breaker, one of which is required for any of the conventional topology identification methods.

The primary advantage of the ANN method is that it allows for the voltage residual relationship of (4.7) to be exploited without having to directly calculate (4.7). After the time required performing the initial training of the network, the actual calculation time required to determine the topology of the system is much lower than if (4.7) had been directly calculated for each potential topology.

4.1.6 NEPTUNE Communications System

The NEPTUNE EMS functions are heavily dependant on the supporting communications system. Therefore in order to fully examine the interface interactions which occur during topology identification it is necessary to have detailed information about the communications system. The communications system that will be examined in this section was originally designed for MARS but its functionality will be extended to the larger NEPTUNE system. MARS was developed as a proof of concept test bed for NEPTUNE where new technologies could be tested and proved before the full NEPTUNE system was deployed, this included the communications system.

4.1.6.1 Monterey Accelerated Research System (MARS)

The goal of MARS is to test the high power and high bandwidth ocean technologies that are proposed for NEPTUNE. In order to test these technologies it was determined that a single shore station located at the Monterey Bay Aquarium and Research Institute (MBARI) serving a single science node would be adequate. Since there is only a single science node and no BU, topology identification is accomplished via direct observation of telemetered system data. Despite a relative lack of complexity MARS does incorporate a rudimentary PMACS. The MARS PMACS architecture is similar to that which will be used on the NEPTUNE system. As such this rudimentary system will be useful as a basis for analysis of the two NEPTUNE topology identification methods.

The MARS communications system is a redundant, full duplex, Dense Wavelength Division Multiplexed (DWDM) optical system. Figure 4.16 shows an overview of the primary in-band MARS communications system, including the PMACS components.

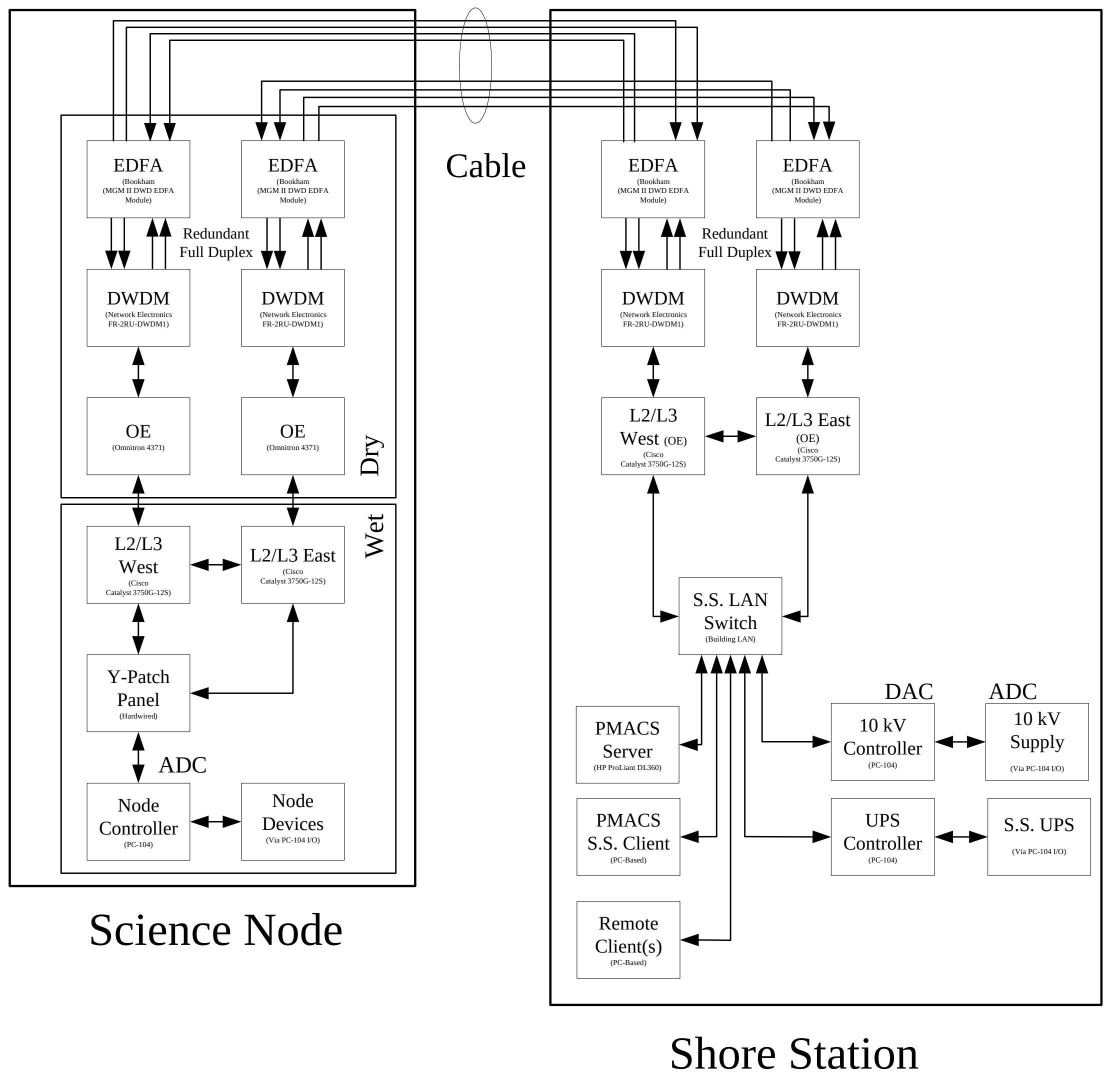

Figure 4.16: MARS communications system

4.1.6.1.1 PMACS Architecture

This section discusses the components which comprise the MARS PMACS. PMACS can be divided into two distinct components; the PMACS client and the

PMACS server. The client contains the Graphical User Interface (GUI) where the operator controls the system as well as the EMS functions. Commands from the PMACS client are routed through the shore station Local Area Network (LAN) switch to a PMACS server. At the server the commands from the client are converted from engineering units to digital values. Once the conversion is completed the commands are sent to the L2/L3 communications switches via the shore station LAN.

When information is sent to the shore station from the science node it enters the shore station LAN via the L2/L3 communications switches. From there the information is sent to the PMACS server via the shore station LAN. At the server the digital information from the science node is converted to engineering units using tables of calibrations coefficients. Once the conversions are completed the information is passed to the PMACS client via the shore station LAN. The primary PMACS client is located at the shore station but it would be possible to have a secondary PMACS client at a remote location, e.g., the University of Washington Applied Physics Lab (APL). This ability allows the system to be operated anywhere an internet connection is available, provided the correct user authority is verified. Between the shore station LAN and the public networks there are several layers of network security.

Power system information such as science node voltage and current are collected at the science node once a second and transmitted to the PMACS server. The information is then accessed by the PMACS client via server polling protocols. When the server is polled the most recent data is made available to the client, older data is not readily available to the client but can be accessed through a data archive. The server archives all data to an external hard drive which is accessible for off-line analysis.

4.1.6.1.2 Communications Architecture

The MARS communications system begins at the two shore station L2/L3 switches, the “east” and “west” switch. There are two L2/L3 switches since a science node typically has two sets of cable connections. Since MARS only has a single science node both of the cables are routed to the shore station. This configuration allows for higher system reliability as well as facilitating the connection of a potential second science node at a future date. This would be accomplished by disconnecting the “west” cable and connecting it to a second science node. The second cable from the second science node could then be routed to shore or connected to a third science node.

At the L2/L3 switches the gigabit Ethernet signals are converted to optical signals which are passed to the DWDM. At the DWDM the optical signal is multiplexed into four wavelengths: 1558.98 nm, 1555.75 nm, 1552.52 nm, and 1549.32 nm. Beginning at the DWDM the system becomes a redundant full duplex system. Redundancy is ensured by duplicating the signals onto two separate fibers. Full duplex means that there are separate fibers for transmitting and receiving signals which allows for continuous uninterrupted transmission and reception. The result is that starting at the DWDM the system utilizes four fibers, two for transmission and two for reception, each carrying four wavelengths.

In order to transmit optical signals over long distances while ensuring sufficient signal strength a push pull amplification scheme is used. Directly after the DWDM the signals pass through an Erbium Doped Fiber Amplifier (EDFA) and the signals are “pushed” on the cable leading to the science node. At the science node the signal passes through another EDFA completing the push pull amplification scheme. From the EDFA the fibers are routed to a DWDM and the signals are combined back to a single fiber. At the science node the conversion from Optical to Electrical (OE), and vice versa (EO), is not performed in the L2/L3 switches as is done at the shore station.

Instead, OE and EO conversion is performed in a separate unit. The reason for the additional equipment in the science node is that the L2/L3 switches are operated in a section filled with fluorinert FC-77. When fluorinert penetrates into a connection between two fibers significant signal attenuation and/or distortion can occur. For this reason OE and EO conversion is performed in the dry side and the signal sent to the science node L2/L3 switches via gigabit Ethernet.

As was mentioned in section 4.1 the 10-kV nominal backbone voltage is stepped down to 400 V for use at the science node. Although the converters that perform this task are >95% efficient there is still a substantial amount of waste heat. In order to move the waste heat away from the power electronics and to the science node housing, the science node is split into two sections. The section containing the converter is filled with fluorinert FC-77. While fluorinert is effective at conducting heat to the pressure housing it can have undesired effects on fiber optic connections.

Once at the L2/L3 switches the signal can either be routed to the science node controller or passed to the other L2/L3 switch for transmission to the next node in the system, if there is more than one. The science node controller is a PC-104 stack with a Power PC processor. The science node controller is the gateway back into the power system for commands that originate at the PMACS client. Conversely it is the portal through which science node power data enters the communications system as it moves to the PMACS client.

4.1.6.2 Extrapolated NEPTUNE Communications System

Since the MARS design only calls for a single science node the second cable connection is routed back to the shore station. NEPTUNE will contain tens of science nodes so that the second cable connection on each science node will be connected to the adjacent node. This section will expand the MARS communications system presented in the previous section.

NEPTUNE will also contain BUs but these will not be included in this analysis of the infrastructure interactions. This is a reasonable simplification because of the extensive experience that industry has had with existing BU designs, i.e., they are extremely high reliability devices. Additionally there will be little or no equipment within the BUs. As such failures in the BUs will not be specifically addressed. Figure 4.17 shows a small portion of the communications system which will be used for analysis.

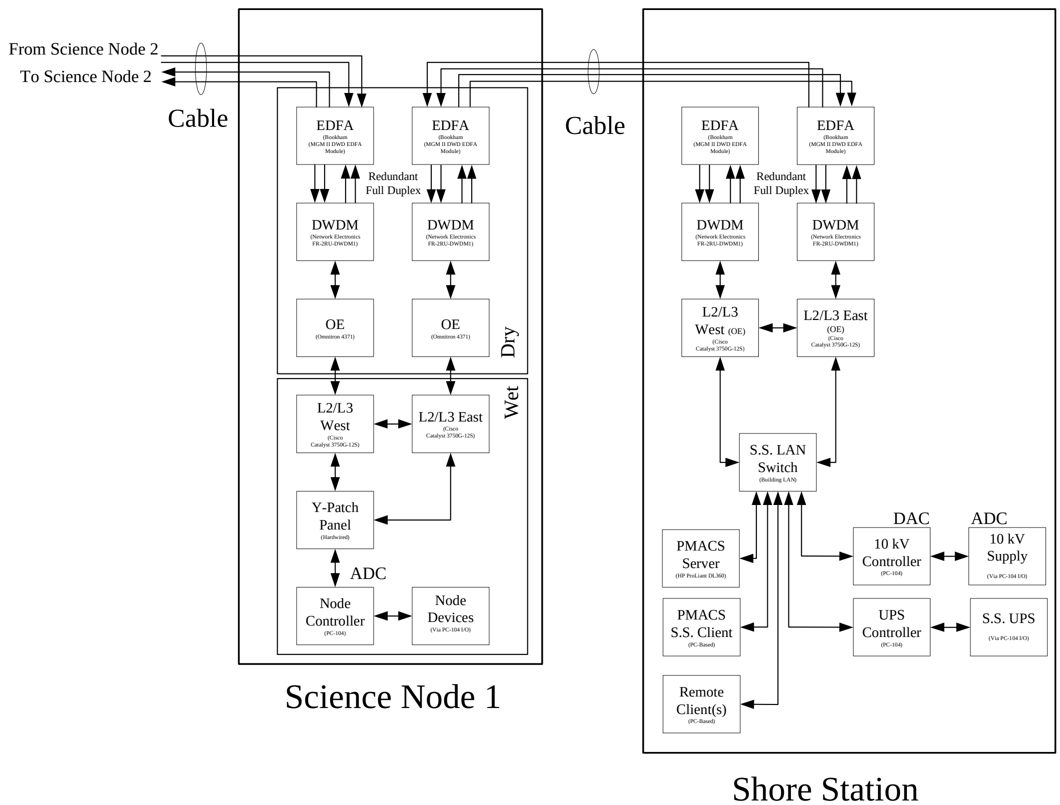

Figure 4.17: Portion of potential NEPTUNE communications system

The principal difference between the systems of Figure 4.16 and 4.17 is the potential for the connection of multiple science nodes. Instead of routing the “west” communications fibers back to the shore station they are routed to the next science node. This allows for the connection of as many science nodes as desired. Additional hard wired connections will also be available so that the system can be networked as shown in Figure 4.1. The additional connection will be no different than the communications hardware in a science node; only the routing table software will be different. Information is sent to the PMACS server once a second where it is available for use by the PMACS client; just as with the MARS power system. Command functions are sent to the science node asynchronously.

4.2 Vulnerability Analysis of NEPTUNE Topology Identification

In section 4.1 the two methods of topology identification for the NEPTUNE power system were discussed. In each of the two methods the power and communications system interact to varying degrees. The following sections will apply the method of section 2.7 to evaluate the potential infrastructure interface vulnerabilities of the two topology identification methods. The results of this analysis will determine if one of the two methods is more robust than the other with respect to infrastructure interactions.

Because of the complexity of the communications system used for NEPTUNE it will be necessary to make extensive use of the model reduction methods discussed in section 2.5.3.

4.2.1 Reduction of the Communications Model

From Figure 4.1 it can be seen that the communications system for NEPTUNE will be a meshed system identical in topology to the power system. When a measurement is taken at a science node the information will be broadcast on all available communications paths to the adjacent nodes. This “flood broadcasting” can be seen in the PN model of Figure 4.18 which shows two science nodes and is based on the MARS communications architecture described in section 4.2.4. Signals which originate within a science node enter the L2/L3 switches via a Y-patch. The function of the Y-patch is to pass information from the science node controller to the two L2/L3 switches within the science node. From the L2/L3 switches the signal is sent to both EO converters for transmission on "out going" fibers. Signals which do not originate within the science node enter the L2/L3 switches from the "in coming" OE converter. The L2/L3 switch then passes the signal to the opposite out going EO converter for eventual transmission.

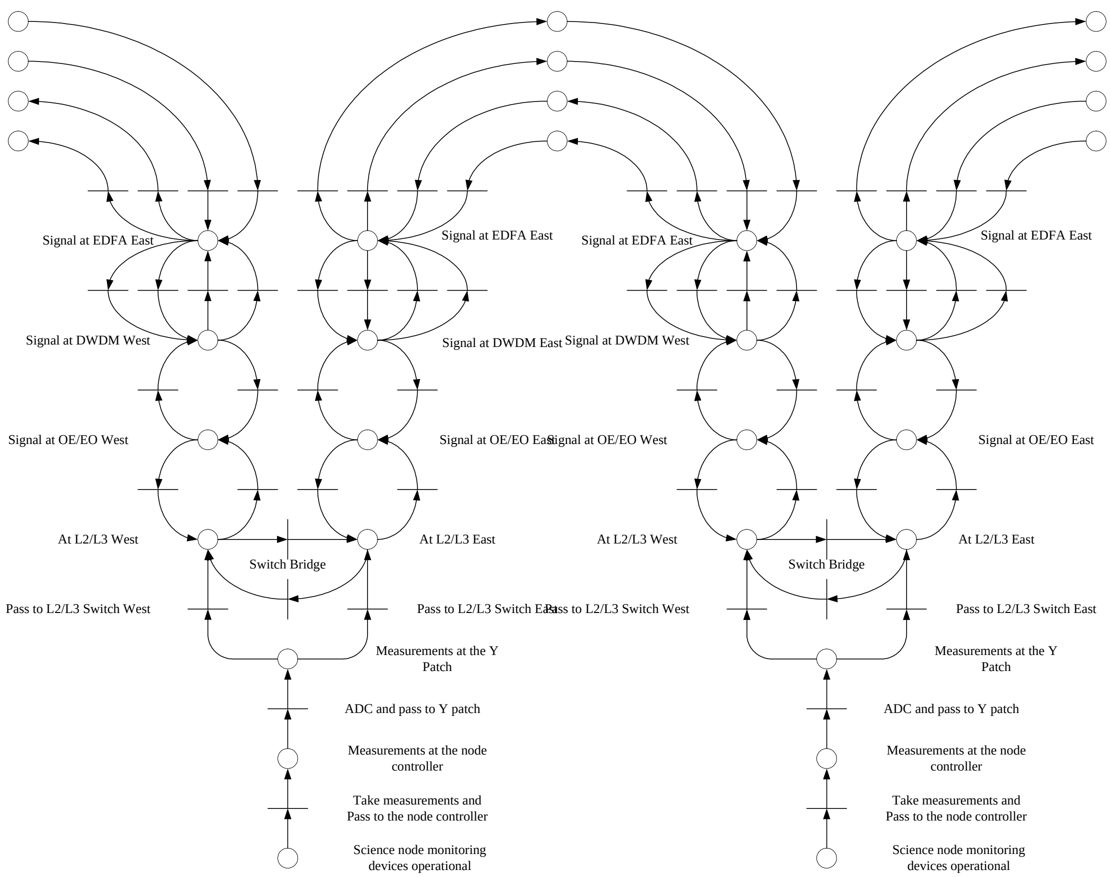

Figure 4.18: Portion of NEPTUNE communications model

When the signal reaches a branch it will again be broadcast on all available paths. As the signals propagate through the system they will eventually arrive at one of the shore stations. From the shore stations the information is passed to clients who have polled the shore station, e.g. the PMACS client.

It is the job of the routing table software in the L2/L3 switches to delete signals as they age, thus preventing signals from traveling indefinitely in a loop consuming bandwidth. Since the optimization of routing protocols is not central to the work of this dissertation the entire communications system will be modeled as a single science node broadcasting directly to each of the shore stations as shown in Figure 4.19.

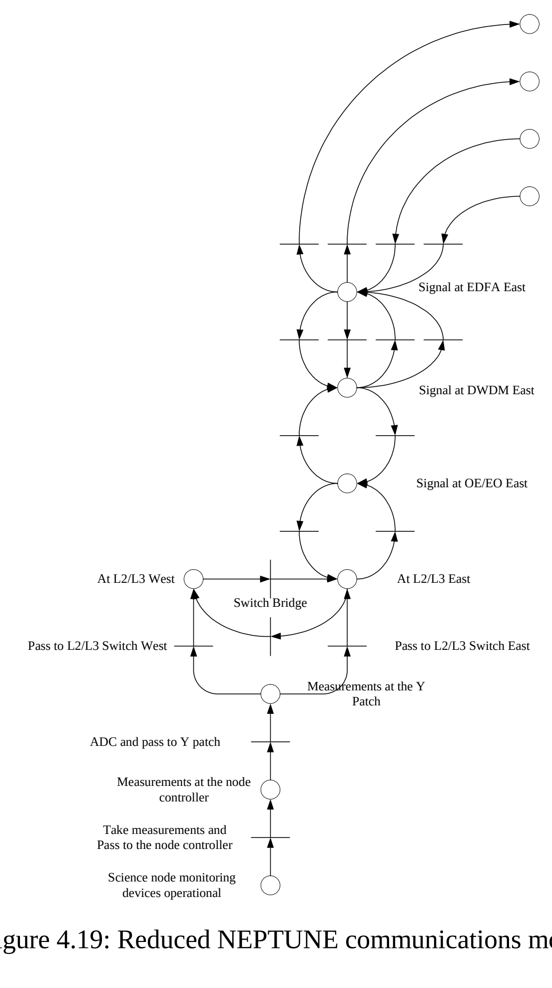

Figure 4.19: Reduced NEPTUNE communications model

The individual TPs and TTs will be adjusted to reflect that each transition is in fact a representation of multiple identical transitions, similar to what was done in section 2.5.3. The PN model shown in Figure 4.19 will be the reduced model for the NEPTUNE communications network leading to one of the two shore stations. A signal which propagates from the science node P node to the shore station will represent data from a single science node arriving at the shore station. Additionally, each of the individual T nodes will represent the actions from multiple science nodes. Therefore, it will be necessary for the T nodes to fire multiple times in order to represent information being colleted from all the science nodes.

These simplifications will result in a model which is significantly less complicated to deal with while losing little relevant technical detail. What will be lost is some information pertaining to redundancy of communications paths. This is addressed by allowing the information to be received at either of the shore stations.

4.2.2 PN Analysis of Topology Identification (Sensitivity Calculation)

Figure 4.20 shows the PN model for the sensitivity based topology identification scheme detailed in the flow chart of Figure 4.8. Due to the size and complexity of the model the coincidence matrix will not be presented in full. Instead, portions of the reordered coincidence matrix will be presented as necessary for analysis, e.g. telecommunications sub-matrices.

Additionally, due to the number of P and T nodes in the model of Figure 4.20, the tables detailing their information and the various equations are contained in Appendix 4. Table A4.1 is a list that shows what each P and T node physically represents and Table A4.2 gives detailed information for each of the T nodes in the model of Figure 4.20. Individual TPs are calculated from FIT rates using (2.23) and individual TTs are calculated from hardware bandwidths and data packet sizes.

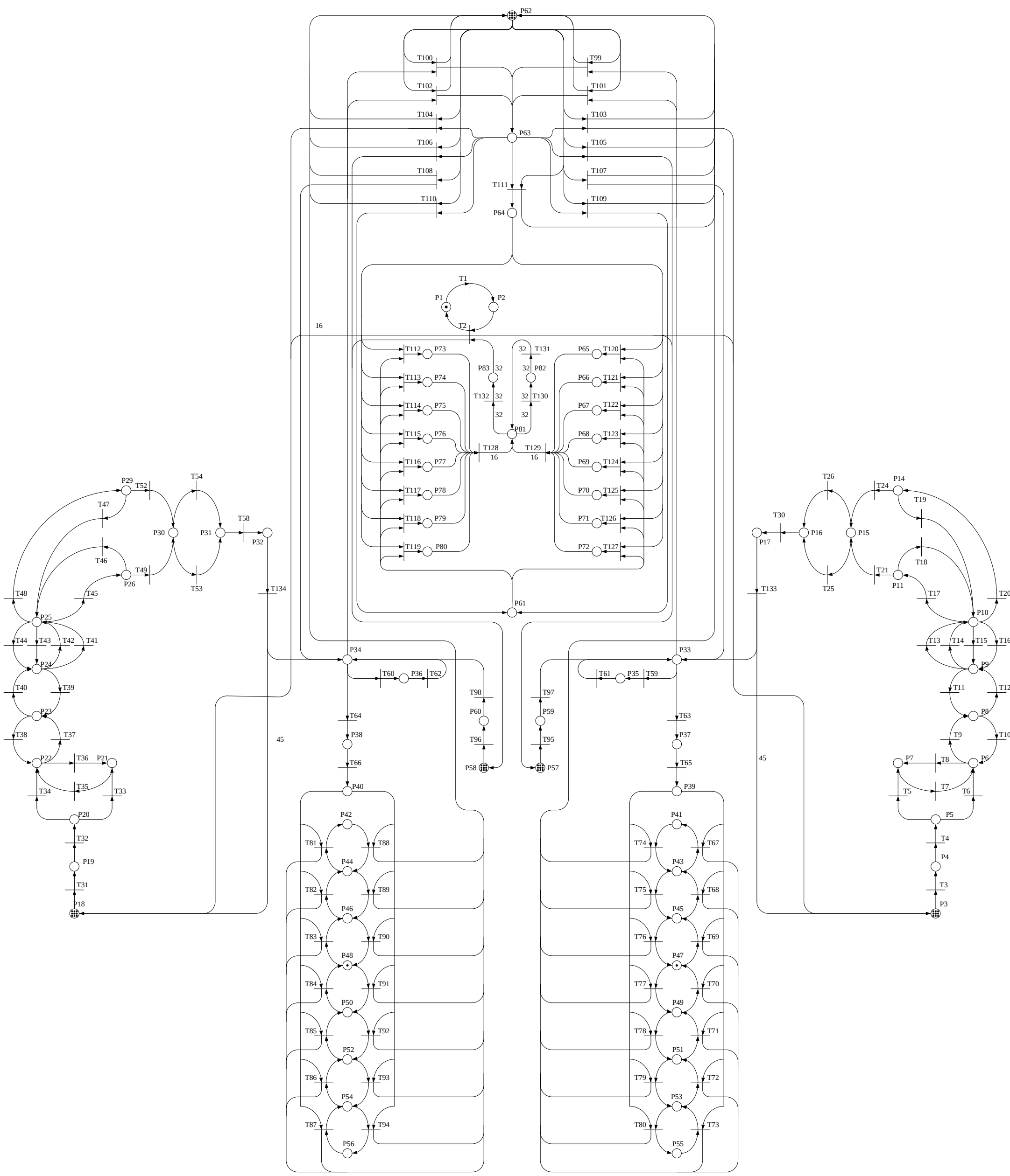

Figure 4.20 NEPTUNE sensitivity based topology identification PN model

4.2.3.1 Calculation of the TTP

The normal mode of operation for the sensitivity based topology identification process is the complete identification of the current operational topology based on the procedures detailed in section 4.1. This includes the variation of shore station voltages and the subsequent collection of data from each of the science nodes. This information is then used at the PMACS client to determine the current operation topology.

In order to calculate the TTP and TTT for the normal mode of operation, the model of Figure 4.20 will be divided into three sections. By making this division the TTP and TTT for the three sections can be calculated and then combined into a single TTP and TTT. With three separate sections it will be possible to clarify assumptions which are made and to fully examine the modeling of the sensitivity based topology identification EMS function. These sections are not the same as the sub matrices of the modified coincidence matrix, but they are similar. The three sections are:

1) Communications via the shore stations: this section includes the T and P nodes between P3/18 and T133/134. This accounts for the collection of data at the science node and its transmission to the shore station LAN.

2) Adjustment of shore station power supplies: this section includes the T and P nodes between T63/64 and P62. This accounts for the transmission of control signals to the shore station power supplies as well as the subsequent collection of data, i.e. shore station voltage and current.

3) PMACS Operations: this section includes the T and P nodes not included in the two previous sections. This sections accounts for all of the operations that occur within the PMACS server and client.

4.2.3.1.1 Communications TP

Data is collected at each of the science nodes and transmitted to the shore stations once a second. The information is flood broadcasted so that it can reach either or both of the shore stations. From the shore station the signal is sent to the PMACS server as described in section 4.1. The data packets contain sufficient header information to prevent redundant information from being processed by PMACS.

In the model of Figure 4.20 there is only a single communications route from a science node to a shore station. This simplification is made to ensure that the model size is manageable. Otherwise it would be necessary to model multiple communications paths from each of the forty six science nodes. This model would be especially large since some signals are relayed by up to twenty science nodes before the signal reaches a shore station.

To simplify this problem, while still maintaining model validity, science node data which originates at P3/18 in the model of Figure 4.20 will need to be collected 46 times, once for each science node. Additionally, markings will progress to P11/14 or P26/29 and then back to P6/22 a number of times to represent the relaying of data from one science node to the next. The number of times that a signal must be relayed for each of the science nodes is shown in Table 4.4; the number of science nodes the signal must be relayed through to reach shores station 1 and shore station 2. Therefore, a marking must travel from P11/14 or P26/29 and then back to P6/22 a number of times equal to the shore station 1 or 2 entry in Table 4.3 before it can transition to P16/31. The markings will collect at the shore station L2/L3 switch node until a complete data set is collected. The data cannot transition from this point until a full data set has been collected.

Since the signals will only need to reach one of the two shore stations it will be necessary to calculate the TTP for both so that a cumulative TTP can be determined.

Table 4.3: Number of science nodes between a science node and shore stations

Node	SS 1	SS 2	Node	SS 1	SS 2	Node	SS 1	SS 2
1	20	13	17	12	5	33	13	8
2	19	12	18	11	4	34	6	5
3	18	11	19	10	3	35	5	6
4	17	10	20	11	4	36	4	7
5	16	9	21	12	5	37	5	8
6	17	10	22	13	6	38	6	9
7	18	11	23	14	7	39	6	10
8	19	12	24	15	8	40	7	9
9	20	13	25	9	2	41	10	1
10	19	12	26	8	3	42	11	0
11	18	11	27	7	4	43	3	8
12	17	10	28	8	5	44	2	9
13	16	9	29	9	6	45	1	10
14	15	8	30	10	7	46	0	11
15	14	7	31	11	8			
16	13	6	32	12	9			

The TP for data moving from a science node to either of the two shore stations, including relaying across other science nodes is given by (A4.1). This assumes that the communications path on the left hand side of the model is to SS 1 and that the right hand side is to SS 2. For both paths the number of relay operations that must be performed is considered. Because of the size and complexity of the equations they are presented in Appendix 4. The equation of (A4.1) is based on the probability axiom of (2.19) for parallel events. Calculating (A4.1) gives a $TP_{Section1}$ of 0.9999999999999590 for the collection of data at the science nodes as well as its transportation to the shore stations via the NEPTUNE communications system. This is the probability that data will be received by at least one of the two shore stations. Expressed as a NTP the value is $4.10 \cdot 10^{-14}$. This assumes that there are forty six science nodes in the system and that fifteen sets of unique data are collected. As was discussed in section 4.1 a full data set must be obtained while the shore stations vary their output over a predefined range. This range is nominally from 8,500 V_{DC} to

12,000 V_{DC} in 500 V_{DC} increments, which yields fifteen independent data sets.

4.2.3.1.2 Shore Station Power Supply TP

Calculation of the TP for adjustments of shore station voltage is significantly less complicated than for the communications system. This is due in part to having only two shore stations, but also because the signals do not use the NEPTUNE communications system. Therefore it is not necessary to calculate transitions through numerous science nodes.

The calculations for this section begin once the signal has left the shore station LAN and is on route to the PMACS server. At the server the control signal is processed and sent to the shore station power supply controller via the shore station LAN. Once the voltage has been adjusted voltage and current measurements are made and the values are sent back to the shore station LAN. From the LAN the measurements are sent to the PMACS server for conversion into engineering units. Once this conversion has been performed the values are sent to the PMACS client for display and use in EMS calculation. Using the data from Table A4.2 it is possible to calculate the TP for this section (A4.2).

The calculation of (A4.3) includes the adjustment of both shore stations from their nominal operating voltage of 10,000 V_{DC} over the complete range discussed in section 4.1. This includes returning both shore stations to their nominal operating voltage after the calculations. Calculating (A4.2) gives a $TP_{Section2}$ of 0.999999950094850 for the adjustment of shore station values and subsequent measurements as described in section 4.1.4. Expressed as a NTP the value is $4.99 \cdot 10^{-8}$.

4.2.3.1.3 PMACS Operations TP

Calculating the TP for the operations of PMACS involves the transitions which were not addressed in the two previous sections. This includes the application of conversion factors at the PMACS servers for the science node data, but not the shore station data. Just as with the shore station data the conversion factors convert the raw data into engineering units. After the conversion to engineering units the data is transferred from the shore station LANs to the PMACS LAN via Internet. Once the data has reached the PMACS client it will be assumed that the topology identification software and the client hardware are working properly. Therefore, many of the individual TPs will be set to 1.0. The purpose of this section is to check that all the necessary data is received by the PMACS client so that the topology identification process can be performed. Using the information from Table 4.3 it is possible to calculate the TP for this section (A4.3).

Assuming that all necessary information is available at both of the shore stations the calculation of (A4.3) yields 0.999999999988333. Expressed as a NTP the value is $1.17 \cdot 10^{-11}$.

4.2.3.1.4 Complete TTP

In this section the results from the previous three sections will be combined to give a complete TTP for the NEPTUNE sensitivity based topology identification process. Because of the complexity of the system it is not possible to use simple superposition. For example, the $TP_{Section3}$ value assumed that all information was available at both of the shore station LANs. As was shown by the $TP_{Section1}$ calculations, it is possible for data to arrive at one shore station but not the other. By correctly accounting for these issues the complete TTP can be calculated using (A4.4).

From (A4.4) the complete TTP for performing the sensitivity based topology identification process described in section 4.1.4 is 0.9999999619629130, with a corresponding TNTP of $3.80 \cdot 10^{-8}$. The TNTP is sufficiently low that there are no apparent vulnerabilities in the system. This result is a direct outcome of a design which made extensive use of high reliability components and redundancy.

4.2.3.2 Calculation of the TTT

The calculation of the TTP and the TNTP were achieved by calculating sub values and then combining them into the complete TTP and TNTP. While the same process can be used with the TTT, for this particular system more insight can be gained by looking at the sub values. The reason for this is the large difference in time scales between the different sections. For example, the communications system works on the order of tens to hundreds of milliseconds while the adjustment of power supplies is on the order of seconds to tens of seconds. The longer time associated with adjustments of a shore station power supply is due to the finite converter slew rates and settling times for system transients. These longer times associated with the power supplies can mask events in the communications section if the two values are combined into a single TTT. The second reason for examining the sub values in lieu of the complete TTT is that the topology identification process is not as time critical as the protection functions examine in Chapter 3. The following four sections will calculate the TTs for the three sub sections as well as the complete TTT, just as was done for the TTP.

4.2.3.2.1 Communications TT

The calculation for the TP of the communications section (A4.1) gave a value which reflected the probability of a signal arriving at either of the two shore stations. When considering the TT only the shorter of the two times will be used. The PMACS client will take the first set of data that it receives and then ignore any further data with the same IP header; this data will simply be discarded.

The first step in calculating the TTs is to determine which T nodes are involved in transmitting data to the shore station and how many times each must fire. From (A4.1) the T nodes involved in moving a single data set from the science nodes to each of the shore stations can be determined (A4.5) and (A4.6). While (A4.5) and (A4.6) give the TPs they do not reflect that many of the transitions are occurring simultaneously.

From Table 4.3 it can be seen that the most remote science node requires that data be relayed through twenty science nodes to reach SS 1 and thirteen to SS 2. The TT for the transmission of data from the most remote science node to SS 1 and 2 is given by (A4.7) and (A4.8) respectively with n_{SS1}=20 and n_{SS2}=13. Since there are two possible paths it is necessary to calculate a TT for each.

Calculating (A4.7) and (A4.8) gives 460 msec and 348 msec respectively. This assumes that there is no competition for bandwidth and that the measurement data has a high priority in the queue. Additionally, it is assumed that the measurements reach the shore stations via the shortest path. Other potential paths could be considered in a contingency analysis.

Examining the TTs of (A4.7) and (A4.8) indicates that the calculation starts with the physical measurements and their analog to digital (A/D) conversion, which takes 100 msec. The remaining time is spent relaying data from one science node to the next. While none of these values represent system vulnerabilities the times could be decreased by the addition of communications bandwidth. This would be a large change in the system and could only be performed before the initial system deployment. Nothing shown in this work would indicate the need for such a large change.

4.2.3.2.2 Shore Station Power Supply TT

While the communications section of the system operates on the order of hundred of milliseconds, the shore station power supplies operate on the order of seconds. As was mentioned before, this is due to the finite power supply slew rates and settling times for system transients. As with the previous section it will be necessary to calculate two TTs since there are two shore stations in the system of Figure 4.1. For a single shore station adjustment of ± 500V_{DC} (A4.9) and (A4.10) give the TTs.

Solving for (A4.9) and (A4.10) yields 1.16 seconds for both, since they are identical processes; this could change in the future as hardware at the two shore stations is upgraded over time. The majority of the 1.16 seconds is the physical adjustment of the shore station power supply which takes 1.00 second. The actual slew rate of the converters is 500 V_{DC}/s. but an additional 500 ms. is allowed before measurements are taken in order for the system transients to settle. Since fourteen adjustments must be made to vary the voltage over the complete range and return it to the nominal operating voltage, the minimum complete operating time is 16.24 seconds.

4.2.3.2.3 PMACS Operations TT

The time requirements for PMACS are dictated by the time necessary to gather the data at the PMACS client. The actual time required to perform the topology identification is minor in comparison when dealing with single or double topology error contingencies in a system the size of that shown in Figure 4.1. The TT for PMACS operations is calculated using (A4.11).

Solving for (A4.11) gives a time of 631.5 ms assuming that the initial assumed operational topology is correct. For each additional assumed topology that must be checked an additional 0.5 ms will be added to the time. Assuming a dual topology error in the assumed operational topology this will add an additional 684.5 msec. at most. The time of 631.5 milliseconds may vary based on the performance of the internet connections which move data from the two shore station LANs to the PMACS LAN. For these calculations a conservative figure has been used.

4.2.3.2.4 Complete TTT

Because of the difference in time frames of the three sections a complete TTT is not as useful as it was in Chapter 3. The longer time frame of the shore station converter adjustments could mask any potential vulnerability associated with TTs of the communications system. Additionally, the difference between signals arriving at shore station 1 and 2 are also masked since the difference is at most only 112 milliseconds. For these reason the complete TTT will be calculated assuming the science node data arrives at shore station 2, shown in (A4.12).

The complete TTT for the NEPTUNE topology identification process, assuming that the science node data arrives at shore station 2, is 17.3315 seconds. Based on the individual as well as the complete TTT the NEPTUNE topology identification procedure has no apparent vulnerabilities.

4.2.3.3 Determination of Redundancy

For some of the operations in the NEPTUNE sensitivity based topology identification process the determination of redundancy is not necessary. For example, since there are two shore stations it is clear that there are redundant paths for communications from the science nodes to the shore. For other process the issue is not so obvious. Based on the procedure used for the decomposition of the coincidence matrix presented in section 2.5.1 it is possible to establish the form of the reduced coincidence matrix for the NEPTUNE topology identification process. As was stated previously the entire coincidence matrix will not be presented. Instead only the sub-matrices of interest will be presented. The five sub-matrices are shown in (4.24), which has the same form as (2.12).

$$\tilde{C}^T = \left[\begin{array}{c:c:c:c:c} C_{S1} & & & & \\ \hdashline & C_{S2} & & & \\ \hdashline & & C_{S3} & & \\ \hdashline & & & C_{S4} & \\ \hdashline & & & & C_{S5} \end{array}\right] \tag{4.24}$$

Where:

$\tilde{C}_{S1}$: Sub-matrix of $\tilde{C}^T$, involving PMACS operations
$\tilde{C}_{S2}$: Sub-matrix of $\tilde{C}^T$, involving SS2 operations
$\tilde{C}_{S3}$: Sub-matrix of $\tilde{C}^T$, involving SS1 operations
$\tilde{C}_{S4}$: Sub-matrix of $\tilde{C}^T$, involving science node data transfer to SS2
$\tilde{C}_{S5}$: Sub-matrix of $\tilde{C}^T$, involving science node data transfer to SS1

Of the five sub-matrices shown in (4.24), only one will be examined for redundancy. The PMACS operations will not be examined since the majority of the $\tilde{C}_{S1}$ sub-matrix involves software operations. Additionally, since the operations of the shore stations are identical it is only necessary to examine $\tilde{C}_{S2}$ or $\tilde{C}_{S3}$. The system of

Figure 4.1 is clearly a meshed structure which ensures that there are redundant communications paths, therefore $\tilde{C}_{S4}$ and $\tilde{C}_{S5}$ will not be examined. Equation (4.25) shows the $\tilde{C}_{S2}$ sub-matrix which contains the entries for the P and T nodes associated with the adjustment of shore station 1.

$$\tilde{C}_{S2} = \begin{array}{cc} & \begin{array}{cccccccccccccc} P_{33} & P_{35} & P_{37} & P_{39} & P_{57} & P_{59} & P_{41} & P_{43} & P_{45} & P_{47} & P_{49} & P_{51} & P_{53} & P_{55} \end{array} \\ \begin{array}{c} T_{59} \\ T_{61} \\ T_{63} \\ T_{65} \\ T_{95} \\ T_{97} \\ T_{67} \\ T_{68} \\ T_{69} \\ T_{70} \\ T_{71} \\ T_{72} \\ T_{73} \\ T_{74} \\ T_{75} \\ T_{76} \\ T_{77} \\ T_{78} \\ T_{79} \\ T_{90} \end{array} & \begin{bmatrix} -1 & 1 & 0 & 0 & 0 & 0 & 0 & 0 & 0 & 0 & 0 & 0 & 0 & 0 \\ 1 & -1 & 0 & 0 & 0 & 0 & 0 & 0 & 0 & 0 & 0 & 0 & 0 & 0 \\ -1 & 0 & 1 & 0 & 0 & 0 & 0 & 0 & 0 & 0 & 0 & 0 & 0 & 0 \\ 0 & 0 & -1 & 1 & 0 & 0 & 0 & 0 & 0 & 0 & 0 & 0 & 0 & 0 \\ 0 & 0 & 0 & 0 & -1 & 1 & 0 & 0 & 0 & 0 & 0 & 0 & 0 & 0 \\ 1 & 0 & 0 & 0 & 0 & -1 & 0 & 0 & 0 & 0 & 0 & 0 & 0 & 0 \\ 0 & 0 & 0 & 0 & 0 & 0 & 1 & -1 & 0 & 0 & 0 & 0 & 0 & 0 \\ 0 & 0 & 0 & 0 & 0 & 0 & 0 & 1 & -1 & 0 & 0 & 0 & 0 & 0 \\ 0 & 0 & 0 & 0 & 0 & 0 & 0 & 0 & 1 & -1 & 0 & 0 & 0 & 0 \\ 0 & 0 & 0 & 0 & 0 & 0 & 0 & 0 & 0 & 1 & -1 & 0 & 0 & 0 \\ 0 & 0 & 0 & 0 & 0 & 0 & 0 & 0 & 0 & 0 & 1 & -1 & 0 & 0 \\ 0 & 0 & 0 & 0 & 0 & 0 & 0 & 0 & 0 & 0 & 0 & 1 & -1 & 0 \\ 0 & 0 & 0 & 0 & 0 & 0 & 0 & 0 & 0 & 0 & 0 & 0 & 1 & -1 \\ 0 & 0 & 0 & 0 & 0 & 0 & -1 & 1 & 0 & 0 & 0 & 0 & 0 & 0 \\ 0 & 0 & 0 & 0 & 0 & 0 & 0 & -1 & 1 & 0 & 0 & 0 & 0 & 0 \\ 0 & 0 & 0 & 0 & 0 & 0 & 0 & 0 & -1 & 1 & 0 & 0 & 0 & 0 \\ 0 & 0 & 0 & 0 & 0 & 0 & 0 & 0 & 0 & -1 & 1 & 0 & 0 & 0 \\ 0 & 0 & 0 & 0 & 0 & 0 & 0 & 0 & 0 & 0 & -1 & 1 & 0 & 0 \\ 0 & 0 & 0 & 0 & 0 & 0 & 0 & 0 & 0 & 0 & 0 & -1 & 1 & 0 \\ 0 & 0 & 0 & 0 & 0 & 0 & 0 & 0 & 0 & 0 & 0 & 0 & -1 & 1 \end{bmatrix} \end{array} \qquad (4.25)$$

The telecommunications sub-matrix associated with $\tilde{C}_{S2}$ is shown in (4.26). This sub-matrix shows the propagation of the control signal thought the PMACS server located at the shore station and its arrival at the shore station power supply controller.

$$\tilde{C}_{S2-comms} = \begin{bmatrix} -1 & 1 & 0 \\ 1 & -1 & 0 \\ -1 & 0 & 1 \\ 0 & 0 & -1 \end{bmatrix} \tag{4.26}$$

By performing a SVD it is found that (4.26) is of full rank, indicating only a single marking path. Therefore the PMACS servers located at the shore stations represent a potential single point failure mechanism in the communications system which could disable the sensitivity based topology identifications component of the NEPTUNE EMS. With the addition of parallel servers this vulnerability could be eliminated. Even though the failure of the sensitivity based topology identification process could not directly cause a blackout in the NEPTUNE system, it could be a contributory cause just as occurred with the East Coast blackout of 2003.

The addition of parallel servers is a relatively easy operation and would not require a redesign of the system; it is therefore recommended.

4.2.3.4 Contingency Analysis

The vulnerability assessment method of section 2.7 allows for the analysis of various contingencies. This section will analyze the TTP and TNTP calculations with respect to various failed and degraded components. Table 4.4 shows the TTP, TNTP, and TTT calculations for various contingencies for the sensitivity based topology identification. Additionally, the TTP and TNTP values are converted and expressed as failures per 10 years. This allows for a more meaningful comparison of contingencies.

The values from Table 4.4 are calculated using (A4.4) with values changed based on the nature of the contingency.

Table 4.4: Contingency analysis (sensitivity)

Contingency	TTP	TNTP	Failures (per 10 yrs.)	TTT (msec)
1) None	0.9999999619	$3.80 \cdot 10^{-8}$	.7	17.3
2) Loss of SS1 comms. with science nodes	0.9999995018	$4.98 \cdot 10^{-7}$	9.1	17.3
3) Loss of SS2 comms. with science nodes	0.9999997671	$2.33 \cdot 10^{-7}$	4.2	17.3
4) Aged DWDMs (i.e. FIT·2)	0.99999996196	$3.80 \cdot 10^{-8}$	.7	17.3
5) Loss of SS1 power supply controller	0.0	1.0	N/A	17.3

4.2.4 PN Analysis of Topology Identification (ANN)

As was discussed in section 4.1.5 an ANN was applied to the topology identification method of section 4.1.4 in an attempt to minimize system perturbations. This was done by training an ANN to detect the current operational topology of the system based on a complete set of measurements taken at a single shore station voltage setting. With a properly trained ANN the current operational topology can be determined without adjusting the shore station voltages or having to directly calculate (4.7).

The analysis of the ANN topology identification method is similar to that discussed in section 4.2.3. With the exception of the shore station power supplies the ANN method uses the same equipment as the sensitivity method. Since the voltages at the shore stations are held constant only a single set of measurements needs to be taken, reducing the reliance on the NEPTUNE communications system. In order to evaluate potential infrastructure vulnerabilities a modified version of the model in

Figure 4.20 will be used. The modified model is shown in Figure 4.21, with the remaining P and T nodes labeled as shown in Figure 4.20 and described in Table A4.1.

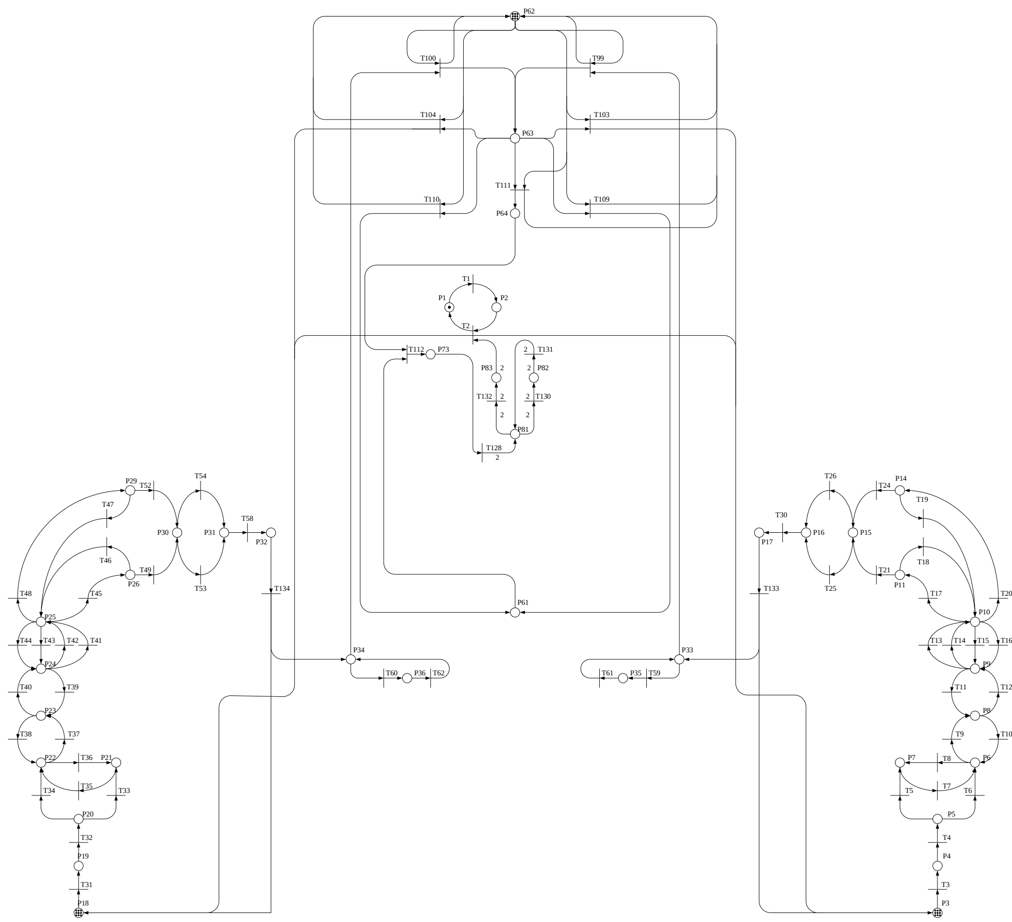

Figure 4.21: NEPTUNE ANN based topology identification PN model

The model of Figure 4.21 does not contain nodes or arcs that are not present in the model of Figure 4.20. The model of Figure 4.21 was constructed by removing portions of the previous model, i.e. P and T nodes as well as their arcs which related to the shore station converters and the collection of multiple data sets. The TTP and TTT for the model of Figure 4.21 are given by (A4.13) and (A4.14).

In addition to the calculation of the normal mode TTP and TTT of (A4.13) and

(A4.14), the same contingencies of Table 4.4 have been presented in Table 4.5, including the failure rates per 10 years.

Table 4.5: Contingency analysis (ANN)

Contingency	TTP	TNTP	Failures (per 10 yrs.)	TTT (msec)
1) None	0.99999999999954	$4.51 \cdot 10^{-13}$	.0002	979.5
2) Loss of SS1 comms. with science nodes	0.99999998462851	$1.54 \cdot 10^{-8}$	4.9	979.5
3) Loss of SS2 comms. with science nodes	0.99999998802195	$1.20 \cdot 10^{-8}$	3.9	979.5
4) Aged DWDMs (i.e. FIT·2)	0.99999999999955	$4.52 \cdot 10^{-13}$	.0002	979.5
5) Loss of SS1 power supply controller	0.99999999999955	$4.52 \cdot 10^{-13}$	.0002	979.5

4.3 NEPTUNE EMS Concluding Remarks

The previous sections have shown how the power and telecommunications infrastructures of NEPTUNE need to interact in order to determine the power system operational topology. From the analysis it was shown that the sensitivity based method contained a single potential infrastructure vulnerability, a lack of redundancy in the PMACS servers. This potential vulnerability also existed in the ANN method. In fact, the entire shore station voltage adjustment procedure is the weakest link in the topology identification process as seen by the results of Table 4.4 and Table 4.5. This is partially due to the difference in time frames over which the equipment operates. Each individual component of the telecommunications infrastructure only has to be in use for a matter of milliseconds as opposed to the multiple seconds required for the shore station power supplies. For this reason the ANN method is superior in reliability.

Additionally, the training of the ANN can be altered so that the shore station measurements are not required to determine the current operational topology, thus removing the potential single point failure mechanism associated with the PMACS servers.

The assessment of the topology identification component of the NEPTUNE EMS indicates that the ANN method is superior to the sensitivity based method with regard to infrastructure interface vulnerabilities. Furthermore, the ANN method is resistant to some failures in the shore station power supply equipment that would cripple the sensitivity based method, as shown in Table 4.4 and Table 4.5. The result of analysis the analysis of Chapter 4 is that redundancy should be added for the PMACS server and the ANN method of topology identification used as the primary method. These actions will help to reduce the vulnerabilities at the infrastructure interface.

Future analysis of the NEPTUNE EMS will be necessary since the system must be designed and deployed in stages. There will be two major parallel efforts to deploy the system, NEPTUNE U.S. and NEPTUNE Canada. As of November 2005 NEPTUNE Canada is proceeding with the selection of vendors for the construction and deployment of the Northern part of the system, while at the same time work on the U.S. section is awaiting the completion of MARS and funding from Congress.

These parallel efforts may lead to differences in the design of the two portions of the system, resulting in two distinctly different systems which are connected together to form the entire NEPTUNE system. If this does occur the final design can analyzed for infrastructure interactions using the procedure of section 2.7. The only element of the analysis that will change is the structure of the models shown in Figures 4.20 and 4.21. These models will have to change to reflect the final design of the system that is physically deployed as well as any changes to the topology identification methods. Since the analysis method of section 2.7 is not system specific it will be a useful tool for the analysis of infrastructure interactions regardless of the final NEPTUNE design.

Chapter 5: Concluding Remarks

The evolving complexity of modern power systems has introduced vulnerabilities which have previously never been considered. Foremost among these new vulnerabilities are those associated with the extensive integration of communications systems into the power infrastructure. The full scale integration of power and telecommunications infrastructures began in response to the Northeastern blackout of 1965. Initial applications of telecommunications to power system operations were successful because of their relative simplicity. As communications systems have penetrated deeper into power systems and increased in complexity they have themselves begun to contribute to blackouts.

As the level of penetration and complexity increased the interactions of the two infrastructures have become more closely related. As a result, the telecommunications infrastructure is now an integral part of the day-to-day operation of the power infrastructure. So much so that failures within it can significantly contribute to or even trigger catastrophic blackouts. Two areas where this can be seen are in the designs of SPSs and EMSs.

This dissertation has developed a method for the analysis of potential vulnerabilities which affect the interface of the power and telecommunications infrastructures. Using this analysis method, vulnerabilities which contribute to catastrophic blackouts can be identified. This method has been implemented using two existing SPSs as well as an existing EMS.

While it is not possible to prevent the occurrence of catastrophic blackouts, the method of identifying potential vulnerabilities between the power and telecommunications infrastructures presented in this dissertation can help to minimize their occurrence and severity. This work will become of even greater importance with the emergence of new technologies such as Wide Area Measurement Systems (WAMSs) which use highly integrated communications systems to coordinate power system operations. Analyzing the infrastructure interactions of these new systems as they are integrated into existing control centers will help to minimize the occurrence of catastrophic blackouts in the future.

Bibliography

[1] President's Commission on Critical Infrastructure Protection, "Critical Foundations: Protecting America's Infrastructures", 1997, available: www.tsa.gov/public/interweb/assetlibrary/Infrastructure.pdf

[2] S. M. Rinaldi, J. P. Peerenboom, and T. K. Kelly, "Identifying, Understanding, and Analyzing Critical Infrastructure Interdependencies", *IEEE Control Systems Magazine*, Vol. 21 , Issue 6 , December 2001 pp. 11-25.

[3] North American Electric Reliability Council (NERC) Disturbance Analysis Working Group (DAWG) database, available: http://www.nerc.com/~dawg/

[4] Final Report on the August 14th, 2003 Blackout in the United States and Canada: Causes and Recommendations.

[5] J. W Evans, "Energy Management System Survey of Architectures", *IEEE Computer Applications in Power*, Vol. 2, Issue 1, January 1989 pp. 11-16.

[6] U.S. Department of Energy Incident and Disturbance Reporting Requirements, available: http://www.nerc.com/~dawg/append-a.html

[7] Report to the President by the Federal Power Commission on the Power Failure in the Northeastern United States and the Province of Ontario on November 9-10, 1965.

[8] Federal Power Commission, "Prevention of Power Failures, Volume I: Report of the Commission to the President", Washington D.C., July 1967.

[9] Federal Power Commission, "Prevention of Power Failure Volume II: Advisory Committee Report, Reliability of Electric Bulk Power Supply", Washington D.C., June 1967.

[10] Federal Power Commission, "Prevention of Power Failures, Volume III: Studies of the Task Groups on the Northeast Power Interruption", Washington D.C., June 1967.

[11] G. S. Vassell "Northeast Blackout of 1965", *IEEE Power Engineering Review*, January 1991, pp. 4-7.

[12] United States Department of Energy Federal Energy Regulatory Commission (FERC), "The Con Edison Power Failure of July 13th and 14th 1977".

[13] C. W. Taylor and D. C. Erickson, "Recording and Analyzing the July 2 Cascading Outage", *IEEE Computer Applications in Power*, Vol. 10, Issue 1, January 1997, pp. 26-30.

[14] Western System Coordinating Council Disturbance Report for the Power Outage that Occurred on the Western Interconnection August 10th, 1996 15:48 PST.

[15] Hydro-Québec Executive Summary, "Analysis of the Hydro-Québec System Blackout on April 18th 1988".

[16] J. L. Blackburn, "Protective Relaying Principles and Applications Second Edition", Marcel Dekker Inc., 1998.

[17] P. M. Anderson and B. K. LeReverend, "Industry Experience with Special Protection Schemes", *IEEE Transactions on Power Systems*, Vol. 11, Issue 3, August 1996, pp. 1166-1179.

[18] E. K. Nielsen, M. E. Coultes, D. L. Gold, and J. R. Taylor, "An Operations View of Special Protection Systems", *IEEE Transactions on Power Systems*, Vol. 3, Issue 3, August 1988, pp. 1078-1083.

[19] J. D. McCalley and F. Weihui, "Reliability of Special Protection Systems", *IEEE Transactions on Power Systems*, Vol. 14, Issue 4, November 1999, pp. 1400-1406.

[20] G. Trudel, S. Bernard, and G. Scott, "Hydro-Québec's Defense Plan Against Extreme Contingencies", *IEEE Transactions on Power Systems*, Vol.14 , Issue 3, August 1999, pp. 958-966.

[21] G. Trudel, J. P. Gingras, and J.R. Pierre, "Designing a Reliable Power System: Hydro-Québec's Integrated Approach", *Proceedings of the IEEE*, Vol. 93, Issue 5, May 2005, pp. 907-917.

[22] V. X .Filho, L. A. S. Pilotto, N. Martins, A. R. C. Carvalho, and A. Bianco, "Brazilian Defense Plan Against Extreme Contingencies", *Power Engineering Society Summer Meeting*, Vol. 2, July 2001, pp. 834-839.

[23] O. Faucon, and L. Dousset, "Coordinated Defense Plan Protects Against Transient Instabilities", *IEEE Computer Applications in Power*, Vol. 10, Issue

3, July 1997, pp. 22-26.

[24] E. M. Martinez and J. J. L. Márquez, “Applications of Phasor Measurement Units in the Adaptive Protection of Interconnected Systems” *Latin American Symposium on Protection of Electrical Power Systems*, Monterrey Mexico, November 12-17, 2000.

[25] A. Moshref, C. Henville, R. Curtis, K. Morison, L. Albassam, M. Owayedh, O. El Said, and M. Ashiq, “Design of a Special Protection System to Maintain System Security at High Import”, *IEEE Power Engineering Society General Meeting*, Vol. 1, July 2003, pp. 311-319.

[26] G. P Azevedo and A. L Oliveira Filho, “Control Centers with Open Architectures [Power System EMS] ”, *IEEE Computer Applications in Power*, Vol. 14 , Issue 4 , October 2001, pp. 27-32.

[27] G. P. Azevedo, B. Feijo, and M. Costa, “Control Centers Evolve with Agent Technology”, *IEEE Computer Applications in Power*, Vol. 13 , Issue 3 , July 2000, pp.48-53.

[28] S. M. Rinaldi, J. P. Peerenboom, and T. K. Kelly, “Identifying, Understanding, and Analyzing Critical Infrastructure Interdependencies”, *IEEE Control Systems Magazine*, Vol. 21, Issue 6, December 2001, pp. 11-25.

[29] S. M. Rinaldi, “Modeling and Simulating Critical Infrastructures and Their Interdependencies”, *Proceedings of the 37th Annual Hawaii International Conference on System Sciences*, January 2004, pp. 54-61.

[30] O. Gursesli and A. A. Desrochers, “Modeling Infrastructure Interdependencies Using Petri Nets”, *IEEE International Conference on Systems, Man and Cybernetics*, Vol. 2, October 2003, pp. 1506-1512.

[31] Q. Liu, J. Hwang, and C. C. Liu, “Communications Infrastructure for Wide Area Protection of Power Systems”, *CRIS International Institute for Critical Infrastructures*, Beijing, Peoples Republic of China, September 2002.

[32] S. Cherian and R. Ambrosio, “Towards Realizing the GridWise^{TM} Vision: Integrating the Operations and Behavior of Dispersed Energy Devices, Consumers and Markets”, *Proceedings IEEE PES Power System Conference and Exposition*, Vol. 1, October 2004, pp. 1-6.

[33] C. H. Hauser, D. E. Bakken, and A. Bose, “A Failure to Communicate: Next Generation Communication Requirements, Technologies, and Architecture for the Electric Power Grid”, *IEEE Power & Energy Magazine*, Vol. 3, No. 2, March/April 2005, pp. 47-55.

[34] Eastern Interconnect Phasor Project information available: http://phasors.pnl.gov/

[35] Personal conversation with Mike Hoffman of the Bonneville Power Administration.

[36] W. Fu, S. Zhao, J. D. McCalley, V. Vittal, and N. Abi-Samra, “Risk Assessment for Special Protection Systems”, *IEEE Transactions on Power Systems*, Vol. 17 , Issue 1 , February 2002, pp. 63-72.

[37] C. A. Petri, “Communications with Automata”, New York: Griffiss Air Force Base Technical Rep. RADC-TR-65-377, Vol. 1, Suppl. 1, 1966.

[38] T. Murata, “Petri Nets: Properties, Analysis and Applications”, *Proceedings of the IEEE*, Vol. 77, Issue 4, April 1989, pp. 541-580.

[39] T. Murata, “State Equation, Controllability, and Maximal Matchings of Petri Nets”, *IEEE Transactions on Automatic Control*, Vol. 22, Issue 3, June 1977, pp. 412-416.

[40] M. K. Molloy, “Performance Analysis Using Stochastic Petri-Nets”, *IEEE Transaction on Computers*, Vol. C-31, No. 9, September 1982, pp. 913-917.

[41] R. Zurawski and M. Zhoui, “Petri Nets and Industrial Applications: A Tutorial”, *IEEE Transactions on Industrial Electronics*, Vol. 41, No. 6, December 1994, pp. 567-583.

[42] S. M. Rinaldi, “Modeling and Simulating Critical Infrastructures and Their Interdependencies”, *Proceedings of the 37th Annual Hawaii International Conference on System Sciences*, January 2004, pp. 54-61.

[43] O. Gursesli and A. A. Desrochers, “Modeling Infrastructure Interdependencies Using Petri Nets”, *IEEE International Conference on Systems, Man and Cybernetics*, Vol. 2, October 2003, pp. 1506-1512.

[44] Phone conversation with Mark Quez of El Paso Electric.

[45] NEPTUNE Phase 1 Partners, (University of Washington, Woods Hole

Oceanographic Institute, Jet Propulsion Laboratory, Pacific Marine Environmental Laboratory), “Real Time, Long-term Ocean and Earth Studies at the Scale of a Tectonic Plate: NEPTUNE Feasibility Study”, (prepared for the National Oceanographic Partnership Program), University of Washington, Seattle, 2000.

[46] “The 3rd International Workshop on Scientific Uses of Submarine Cables and Related Technologies”, Komaba Campus, The University of Tokyo, Tokyo, Japan, June 25-27, 2003.

[47] J. Delaney, G. R. Heath, A. Chave, H. Kirkham, B. Howe, W. Wilcock, P. Beauchamp, and A. Maffei, “NEPTUNE Real-Time, Long-Term Ocean and Earth Studies at the Scale of a Tectonic Plate”, *Proceedings 2001 MTS/IEEE Oceans Conference and Exhibition*, Vol. 3, pp. 1366-1373.

[48] B. Howe, H. Kirkham, and V. Vorperian, “Power System Considerations for Undersea Observatories”, *IEEE Transactions on Oceans Engineering*, Vol. 27, No. 2, April 2002, pp. 267-274.

[49] B. Howe, H. Kirkham, V. Vorperian, and P. Bowerman, “The Design of the NEPTUNE Power System”, *Proceedings 2001 MTS/IEEE Oceans Conference and Exhibition*, Vol. 3, pp. 1374-1380.

[50] K. Schneider, C. C. Liu, T. McGinnis, B. Howe, and H. Kirkham, “Real-Time Control and Protection of the NEPTUNE Power System”, *Proceedings 2002 MTS/IEEE Oceans Conference and Exhibition*, Vol. 2, pp. 1799-1805.

[51] C. C. Liu, K. Schneider, B. Howe, H. Kirkham, “State Estimation for the NEPTUNE Power System”, *Proceedings IEEE Transmission and Distribution Conference*, Vol. 2, pp. 748-754.

[52] E. Handschin, F. C. Schweppe, J. Kohlas, and A. Fiechter, “Bad Data Analysis for Power System State Estimation”, *IEEE Transactions on Power Apparatus and Systems*, Vol. PAS-89, No. 1, January 1970.

[53] M. B. D. C. Filho, A. M. L. da Silva, and D. M. Falcao, “Bibliography on Power System State Estimation (1968-1989)”, *IEEE Transactions on Power Systems*, Vol. 5, Issue 3, August 1990, pp.950-961.

[54] A. Monticelli, C. A. F. Murari, and F. F. Wu, “A Hybrid State Estimator: Solving Normal Equations by Orthogonal Transformations”, *IEEE Transactions on Power Apparatus and Systems*, Vol. PAS-104, No. 12, December 1985, pp.

3460-3468.

[55] A. Abur and A. G. Expósito, “Power System State Estimation Theory and Implementation”, Marcel Dekker, Inc., 2004.

[56] L. Mili, G. Steeno, F. Dobraca, and D. French, “A Robust Estimation Method for Topology Error Identification”, *IEEE Transactions on Power Systems*, Vol. 14, Issue 4, November 1999 pp. 1469-1476.

[57] F. F. Wu and W. H. Liu, “Detection of Topological Errors by State Estimation”, *IEEE Winter Meeting*, 1988, Paper no.216-4.

[58] K. A. Clements and P. W. Davis, “Detection and Identification of Topology Errors in Electric Power Systems”, *IEEE Transactions on Power Systems*, Vol. 3, No. 4, November 1988, pp. 176-183.

[59] I. S. Costa and J. A. Leao, “Identification of Topology Errors in Power System State Estimation”, *IEEE Transactions on Power Systems*, Vol. 8, No. 4, November 1993, pp. 1531-1538.

[60] A. Abur and M. K. Celik, “Topology Error Identification by Least Absolute Value State Estimation”, *Proceedings 7th Electrotechnical Conference,* 1994, Vol.3, pp. 972-975.

[61] P. R. Bevington and D. K. Robinson, “Data Reduction and Error Analysis for the Physical Sciences”, WCB/McGraw-Hill, 1992.

[62] C. C. Liu, J. Jung, G. T. Heydt, V. Vittal, and A. G. Phadke, “Conceptual Design of the Strategic Power Infrastructure Defense (SPID) System”, *IEEE Control System Magazine*, Vol. 20, Issue 4, August 2000, pp. 40-52.

[63] M. J. Damborg, M. Kim, J. Huang, S. S. Venkata, and A. G. Phadke, “Adaptive Protection as Preventive and Emergency Control”, *Power Engineering Society Summer Meeting,* July 2000, Vol. 2, pp. 1208-1212.

[64] A. A. El Desouky, M. M. Elkateb, "Hybrid Adaptive Techniques for Electric-load Forecast using ANN and ARIMA", *IEE Proceeding Generation Transmission and Distribution*, Vol. 147, Issue 4, July 2000, pp.213-217.

[65] Y. Zhang, O. P. Malik, G. S. Hope, G. P. Chen, "Application of an Inverse Input/Output Mapped ANN as a Power System Stabilizer", *IEEE Transactions on Energy Conversion* ,Vol. 9, Issue 3 , September 1994, pp. 433-441.

[66] A. S. Farag, "Estimation of Polluted Insulators Flashover Time Using Artificial Neural Networks", *Industrial and Commercial Power Systems Technical Conference*, 1997 Conference Record, Papers Presented at the 1997 Annual Meeting , May 1997, pp.184-192

[67] K. Schneider and C. C. Liu, “Topology Error Identification for the NEPTUNE Power System Using an Artificial Neural Network”, *Proceedings IEEE PES Power System Conference and Exposition*, Vol. 1, October 2004, pp. 60-65.

[68] S. Haykin, "Neural Networks a Comprehensive Foundation", 1999, Prentice-Hall, Inc.

[69] J. De La Ree, Y. Liu, L. Mili, A. G. Phadke, and L. DaSilva, “Catastrophic Failures in Power Systems: Causes, Analysis, and Countermeasures”, Proceedings of the IEEE, Vol. 93, Issue 5, May 2005, pp. 956-964.

Appendix 1: List of Acronyms

AC: Alternating Current

AEP: American Electric Power

ANN: Artificial Neural Network

APL: Applied Physics Lab

BPA: Bonneville Power Administration

BU: Branching Unit

CFE: Comisión Federal de Elecricidad

DAWG: Disturbance Analysis Working Group

DC: Direct Current

DOE: Department Of Energy

DWDM: Dense Wavelength Division Multiplexed

SEC-ERB: Eastern Region Branch of the Saudi Electric Company

EDF: Electricité de France

EDFA: Erbium Doped Fiber Amplifier

EIPP: Eastern Interconnect Phasor Project

EO: Electrical to Optical

EMS: Energy Management System

EPE: El Paso Electric

ERO: Electric Reliability Organization

FE: First Energy

FIT: Failures In Time

FPC: Florida Power Company

GPS: Global Positioning System

GUI: Graphical User Interface

HVDC: High Voltage Direct Current

ISO: Independent System Operator

LAN: Local Area Network

MARS: Monterey Accelerated Research System

MBARI: Monterey Bay Aquarium and Research Institute

MISO: Mid-West Independent System Operator

MTBF: Mean Time Between Failures

NEPTUNE: North East Pacific Times-series Underwater Networked Experiment

NERC: North American Reliability Council

NIS: National Interconnected System

NPCC: Northeast Power Coordinating Pool

NSM: Network Security Matrix

NYPA: New York Power Authority

NYPP: New York Power Pool

O&M: Operation and Maintenance

OE: Optical to Electrical

PG&E: Pacific Gas and Electric

PJM: Pennsylvania New Jersey Maryland

PLC: Programmable Logic Controller

PMACS: Power Monitoring And Control System

PMU: Phasor Measurement Unit

PN: Petri Net

POTT: Permissive Over-reaching Transfer Trip

PS: Peninsular System

PWM: Pulse Width Modulated

QoS: Quality of Service

RBD: Reliability Block Diagram

RTE: Réseau de Transport d`Eletricité

SCADA: Supervisory Control And Data Acquisition

SEC-CRB: Central Branch Region of the Saudi Electric Company

SPS: Special Protection System

SS: Shore Station

SVD: Singular Value Decomposition

TNTP: Total Non Transition Probability

TP: Transition Probability

TT: Transition Time

TTP: Total Transition Probability

TTT: Total Transition Time

WECC: Western Electricity Coordinating Council

WLS: Weighted Least Squares

Appendix 2: Power System Blackouts

This appendix is provided as summary of blackout analyses that have been performed in the past by government agencies and power companies. This allows the reader to view selected blackouts in their historical context without having to read the full length official reports [6-15].

A2.1 Northeast Blackout- November 9th, 1965

The Northeast blackout of 1965 was an event that took the power industry, as a whole, by surprise. Until the afternoon of November 9th the prevailing belief in the power industry was that a catastrophic cascading failure of the modern interconnected power system was not possible. These preconceptions were shattered when one of the five 230-kV transmission lines supplying power to Ontario from the Sir Adam Beck No. 2 hydroelectric plant tripped due to an incorrect relay setting [7-11]. While the relay had been correctly set to reflect the power flows seen in 1963, the settings did not reflect the operating conditions of 1965. The following is a summary of the reports of [7-11].

When the 230-kV line was tripped the power that it had been carrying was redistributed to four parallel 230-kV lines. The increase in load on the four parallel lines resulted in the actuation of protective relays on the remaining lines. With the loss of the five 230-kV lines which had been sending power into Ontario, 1,500 MW of power began to surge into the Northeastern Power system. Immediately generators at the Beck and Niagara generating facilities begin to speed up due to the rapid unloading caused by the sudden inrush of power. The generators at both Beck and Niagara were soon out of phase with the rest of the system due to the large amount of energy they had absorbed. At this point the system had become unstable and there was little that could have been done to prevent the ensuing blackout.

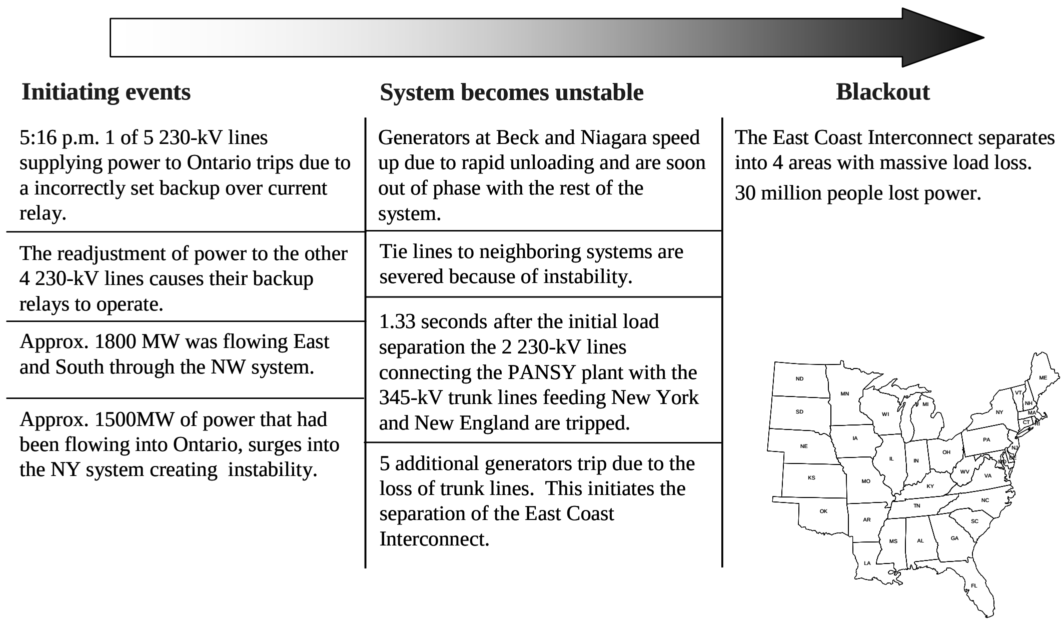

Figure A2.1: 1965 Northeast blackout time line

Soon after the loss of generation at Beck and Niagara, tie lines to neighboring systems tripped due to large system oscillations. From the time the first 345-kV line was lost until the loss of the tie lines was only 1.33 seconds. With the loss of the tie lines additional generators tripped, resulting in the separation of the Northeastern Power system. Service was interrupted to 30 million customers.

As a result of the 1965 blackout NERC was formed in 1968. NERC is a voluntary organization with the goal to ensure that the bulk transmission system in North America is secure and reliable. NERC divided the United States into ten reliability regions [4]. The formation of NERC was the most significant result of the 1965 blackout.

A2.2 New York Blackout- July 13th, 1977

The New York blackout of 1977 while smaller in scale than the 1965 blackout had a much larger cultural impact on the general populous. While the bulk electric power system had benefited from the lessons learned in 1965 there were other non-technical issues that had not been of consequence twelve years earlier. The following is a summary of the reports of [12].

At 9:19:11 p.m. a 345-kV line from Niagara tripped due to a phase B to ground fault, most likely caused by sagging conductors contacting a tree. The W80 and W81 lines from Niagara had been supplying 1,202 MW of power to the Consolidated Edison (Con Ed) system. Several seconds later at 9:19:53 a 345-kV/138-kV transformer at the Pleasant Valley sub-station tripped on overload isolating a further 415 MW of capacity. The loss of the transformer resulted in the remaining three interconnections carrying load in excess of their short-time emergency ratings.

Initiating events	**System becomes unstable**	**Blackout**
8:37:17 p.m. initial lighting strikes remove the W97 and W98 345-kV lines from service, additionally this isolated the Indian point no. 3 Nuclear Plant.	9:29:41 The Consolidated Edison system becomes isolated from the rest of the Eastern Interconnect.	With the loss of the Ravenswood No.3 Generator, and its 844 MW of output, the entire Con Edison system collapsed. 9 million people lost power.
8:55:53 p.m. additional lighting strikes remove the W93/W79 and W99/W64 345-kV lines from service.	At the time of separation the total Con Edison load was 5,981MW while generation was only 4,282 MW, a deficiency of 1,680 MW.	
9:19:11 p.m. due to overloading the 345-kV line 92 from Niagara sags and contacts a tree isolating 1,202 MW of generation.	Immediate load shedding and generation increase was needed.	
9:19:53-9:29:41 a series of equipment malfunctions and operator errors lead to the isolation of the Consolidated Edison system.	Under frequency load shedders operated automatically at three levels; 59.3, 58.8, and 58.3 Hz. This shed 2,230.6 MW of load.	
	Once the load was shed, voltage rapidly increased due to extensive underground 138-kV and 345-kV lines resulting in the tripping of the Ravenswood No. 3 Generator.	

Figure A2.2: 1977 New York blackout time line

At 9:22:11 p.m. with the approval of the New York Power Pool (NYPP) control center one of the three remaining interconnections was opened by the Long Island Lighting Co. system operator because the meters on the line were reading off scale.

This action resulted in the loss of an additional 520 MW to the Con Ed system.

At 9:29:41 p.m. a tap-changing mechanism on one of the two remaining interconnections failed due to excessive overloading. The loss of an additional 1,150 MW overloaded the last interconnection and the Con Ed system was completely isolated from all external systems. At this point there was 5,981 MW of load and only 4,282 MW of generation in the Con Ed system, a 28.4% deficiency. This quickly resulted in the collapse of the Con Ed system.

While the details of the individual component failures and overall system responses were of value to engineers, it was the conduct of the citizens of New York City that captured the news headlines. With the breakdown of basic services such as trains, elevators, and lighting the city devolved into the dark ages. There were wide spread cases of looting and other criminal acts, the city officials were not able to immediately establish order. The New York blackout of 1977 remains a testament to the potential social consequences of failures of critical infrastructures.

A2.3 WECC Blackout - July 2nd, 1996

On July 2nd 1996 a blackout occurred in the Western Electricity Coordinating Council (WECC) that, while not rivaling the impact of the 1977 blackout, was unprecedented in the scale of the geographic area affected. The events of July 2nd 1996 were the third major disturbance to impact the WECC, the first being the 1994 Northridge earthquake in California and the second being a disturbance occurring December of 1994. As of July 2nd 1996 this was the largest disturbance the WECC had ever experienced. The following is a summary of the reports of [13].

At 2:24 p.m. the 345-kV Jim Bridger-Kingport line tripped due to sagging conductors. The sagging conductors were a result of high local temperatures, 38°C, and high transmission line power flows. Incorrect operation of an analog ground unit relay on the parallel Jim Bridger-Goshen 345-kV line resulted in its simultaneous isolation. The isolation of two of the three lines connecting the Jim Bridger power plant in Wyoming resulted in the correct tripping of two of the four Jim Bridger units, 1,000 MW of capacity, via a special protection system. The tripping of the two Jim Bridger units should have returned the WECC to a stable operating condition but the untimely operation of other system equipment prevented this. The result was a significant voltage depression in Southern Idaho.

Initiating events

8:37:17 p.m. initial lighting strikes remove the W97 and W98 345-kV lines from service, additionally this isolated the Indian point no. 3 Nuclear Plant.

8:55:53 p.m. additional lighting strikes remove the W93/W79 and W99/W64 345-kV lines from service.

9:19:11 p.m. due to overloading the 345-kV line 92 from Niagara sags and contacts a tree isolating 1,202 MW of generation.

9:19:53-9:29:41 a series of equipment malfunctions and operator errors lead to the isolation of the Consolidated Edison system.

System becomes unstable

9:29:41 The Consolidated Edison system becomes isolated from the rest of the Eastern Interconnect.

At the time of separation the total Con Edison load was 5,981MW while generation was only 4,282 MW, a deficiency of 1,680 MW.

Immediate load shedding and generation increase was needed.

Under frequency load shedders operated automatically at three levels; 59.3, 58.8, and 58.3 Hz. This shed 2,230.6 MW of load.

Once the load was shed, voltage rapidly increased due to extensive underground 138-kV and 345-kV lines resulting in the tripping of the Ravenswood No. 3 Generator.

Blackout

With the loss of the Ravenswood No.3 Generator, and its 844 MW of output, the entire Con Edison system collapsed.

9 million people lost power.

Figure A2.3: July 2nd 1996 WECC blackout time line

Approximately twenty four seconds after the initial tripping of the Jim Bridger-Kingport line the Anaconda-Amps-Antelope 230-kV line tripped in response to a faulty zone 3 impedance relay which detected a minor overload with a concurrent minor voltage depression. Had the zone 3 relay been operating correctly the minor overload in conjunction with a minor voltage depression would not have generated a trip signal and the blackout would not have propagated any further. As a result of the incorrect operation of a single zone 3 relay power delivery was interrupted to 2 million people.

A2.4 WECC Blackout - August 10th, 1996

Shortly after the blackout of July 2nd 1996 similar events were repeated in the WECC. On August 10th 1996 the WECC was operating in conditions similar to those of July 2nd when the Keeler-Alliston 500-kV line contacted a tree due to inadequate right-of-way maintenance [14]. The parallel Pearl-Keeler 500-kV line was not in operation due to an out of service 500-kV/230-kV transformer. The absence of the two 500-kV lines significantly reduced the reactive power reserves for the system. As a result the system began to experience overloads as well as low voltage conditions.

Initiating events	**System becomes unstable**	**Blackout**
2:24 p.m. Jim Bridger-Kinport 345-kV line is tripped due to sag. Due to a faulty relay the parallel Jim Bridger-Goshen also trips.	Mill Creek-Antelope 230-kV line trips due to a faulty Zone 3 relay.	Within 8 seconds of the initial event, 5 asynchronous islands had been formed. 2 million people lost power.
2 of the 4 generators at the Jim Bridger disconnected by a Remedial Action Scheme.	Voltage in the Boise Idaho area as well as voltage on the COI began to rapidly collapse.	
The loss of 2 parallel lines was considered a single contingency event, and as such the system was able to handle the loss of 2 345-kV lines and the associated loss of generation.	Due to collapsing voltages 4 230-kV lines between Boise and the Brownlee substation tripped.	
	Further, protective devices at the Malin and Captain Jack substations in southern Oregon automatically disconnected the COI.	
For approx. 23 seconds the system seems to handle the events properly despite minor voltage fluctuations. Then a faulty relay destabilized the system.	Disconnecting the COI interrupted 4,000 MW of power flow and separated the WECC.	

Figure A2.4: August 10th 1996 WECC blackout time line

This condition was exacerbated by the loss of the McNary power house which had been supply 494 MVAR of reactive power. With the loss of the McNary power house the system began to experience mild oscillations at 0.224 Hz, a known natural frequency of the system. Shunt capacitors were inserted for reactive power support and damping but the oscillations persisted. Soon 1,000 MW oscillations with 60-kV peak-to-peak values were seen on the Pacific Intertie and special protection schemes began to operate. The WECC broke into four asynchronous islands and power delivery was interrupted to 7.5 million people.

A2.5 Eastern Interconnect Blackout -August 14th, 2003

On August 14th 2003 the United States and Canada suffered the largest blackout in the history of North America [4]. Unlike many of the early blackouts experienced in North America there was no single triggering event, instead it was the result of complex interactions which spanned both the power and telecommunications infrastructure.

The final report detailing the events of the blackout sub-divided the individual events into four phases [4].

- Phase 1: A Normal afternoon degrades (12:15-14:14)
- Phase 2: First Energy's computer failures (14:14-15:59)
- Phase 3: First Energy's 345-kV line failures (15:05-15:57)
- Phase 4: Collapse of the 138-kV system (15:39-16:08)
-

One of the first contributing events in Phase 1 occurred at 1:07 p.m. when First Energy (FE) turned off their state estimator in response to erroneous output data. With the state estimator off-line the source of the problem was identified as an incorrectly updated line status attributed to a faulty communications link. Once the communications link was repaired the state estimator operated correctly. The state estimator was restarted but due to operator error it was not returned to operation; thus the control room operators were not receiving the data.

Initiating events

15:48 p.m. Keeler-Allston 500-kV line contacts a tree due to inadequate right-of-way maintenance. Additionally the Pearl-Keeler line is forced out of service due to the Keeler 500/230-Kv transformer being OOS.

With the loss of these 2 lines, 5 lines are now out of service, removing hundreds of MVAR.

Lines throughout the system begin to experience overloads as well as low voltage conditions. Additional lines trip due to sagging.

15:47:40-15:48:57 p.m. Generators at the McNary power house supplying 494 MVAR trip. The system begins to experience “mild oscillations”.

System becomes unstable

Mild .224 Hz oscillations were seen throughout the system and began to appear on of the PDCI.

Shunt capacitor banks were switched in to raise the voltage but the oscillations were not being damped.

15:48:51 p.m. Oscillations on the POI reached 1000MW and 60-kV peak-to-peak.

PDCI Remedial Action Schemes (RAS) began to actuate. Shunt and series capacitors were inserted.

Blackout

The WECC broke into 4 asynchronous islands with heavy loss of load.

7.5 million people lost power.

Figure A2.5: 2003 Eastern Interconnect blackout time line

At 1:31 p.m. the Eastlake 5 generation unit tipped off line and was shut down, significantly reducing the available reactive power in the region. Approximately half an hour later at 2:02 p.m. the Stuart-Atlanta 345-kV line made contact with a tree and tripped the isolation breakers. The only significant effect the loss of the Stuart-Atlanta 345-kV line had was on the Mid-West Independent System Operator (MISO) state estimator, which was significant.

The second phase was characterized by a series of failures within FE’s computer systems. Between 2:00 p.m. and 3:00 p.m. a number of energy management consoles in sub-stations failed to operate. Additionally, both the primary and secondary alarm servers failed. The simultaneous loss of both alarm servers significantly affected the EMS computers and greatly decreased the control center data refresh rate. Instead of updating data every one to three seconds, latencies of up to fifty nine seconds were occurring. These events had a detrimental effect on the situational awareness of the FE operators and prevented them from having a clear picture of the system they were operating.

The third phase was characterized by the loss of three key 345-kV transmission lines in the FE control area. Each of the three lines tripped while transferring power well below their emergency or even the normal set points. The operation of the protection relays was attributed to line sag due to thermal effects coupled with inadequate transmission right-of-way maintenance. The result was that each of the three lines sagged and made contact with trees.

Indications that 345-kV lines were out of service were not immediately apparent to FE operators because of continuing problems with their EMS. Adjacent system operators from American Electric Power (AEP), Pennsylvania New Jersey Maryland (PJM), and their reliability coordinator, MISO were attempting to inform FE of the lost 345-kV lines. During the third phase it was determined that the FE operators took no significant actions to arrest what was quickly becoming an unstable situation [4].

The fourth and final phase was the collapse of the 138-kV system. As the various 345-kV lines tripped and were removed from service power flows were slowly transferred to the lower 138-kV system. This eventually led to the loss of sixteen 138-kV lines. The significant losses in the 138-kV system resulted in the overloading and isolation of the Sammis-Star 345-kV line. Once the Sammis-Star 345-kV was lost the system became unstable and a catastrophic blackout occurred, affecting over 50 million people.

A2.6 Hydro-Québec Blackout- April 18th, 1988

The topology of the Hydro-Québec system is notable for a number of reasons. One of the most significant characteristics is that there are no synchronous connections to external power systems. While this isolates the system from external disruptions it also prevents Hydro-Québec from relying on the benefits of synchronous interconnections. The system topology is characterized by three large central hydroelectric complexes connected to distant load centers via an extensive

765-kV transmission network. The three hydroelectric generation complexes are: James Bay Complex 15,000 MW, Manic-Outardes Complex 8,100 MW, and Church Falls Complex 5,600 MW. The major load centers served by these three complexes are the Montreal and Québec areas located several hundred kilometers to the south.

The follow discussion of the events of April 18th 1988 is taken from [15]. On April 18 1988 at 8:08 p.m., a series of flashovers caused by accumulated wet snow and freezing rain on the insulators affected all three phases at the Arnaud sub-station. As a result, all of the sub-stations 765-kV transmission lines tripped; this completely isolated the Churchill Falls complex. Following the isolation of the Churchill Falls complex a signal to activate a remote load shedding and generation rejection system was generated.

The automatic remote load-shedding system failed to operate. As a result, 1.7 seconds later one line section on the James Bay transmission network tripped, followed by the remaining parallel lines. This separated the La Grande network from the rest of the system. Shortly after the separation of the La Grande network three transformer units at La Grande 4 also failed.

Fifteen seconds later, the Manicouagan-Montreal transmission network collapsed. This led to the loss of all DC interconnections as well as the tripping of eight units at the Beauharnois generating station, which had been isolated from the Hydro-Québec system in order to supply the New York Power Authority (NYPA) system. The imbalance in generation and load resulted in the interruption of 18,500 MW of load.

When the Churchill Falls network separated, a remote load-shedding signal was sent to the system control center. A faulty contact in the control center communications equipment prevented this signal from reaching the computers dedicated to remote load shedding. This defect was repaired within hours of the catastrophic blackout. Had this system worked properly, it would have prevented the system blackout and the loss of interconnections.

Initiating events

8:08 p.m. Wet snow and freezing rain cause flash over on all three phases at the Arnaud substation

8:08 p.m. 3200 MW of generation from the Church Falls generation complex is isolated due to isolation of transmission lines

8:08 p.m. In response to the loss of the Church Fall generation station, a signal to initiate load shedding is sent to the central control center

The load shedding signal was not received at the central control center due to a faulty contact in the communications system

System become unstable

1.7 seconds after the failure of the load shedding system the first of the James bay transmission lines tripped, followed by the other two

With the loss of the James bay transmission lines the Le Grand network was separated from the rest of the system. Shortly afterward three transformers at Le Grand 4 failed

15 seconds later the Manicouagan-Montréal transmission system collapsed. This lead to the loss of all DC interconnections as well as 8 generators at the Beauharnois generating station which had been isolated to serve the Ney York Power Authority (NPA)

Blackout

18,500 MW of load was lost because 3,200 MW of automatic load shedding failed to occur

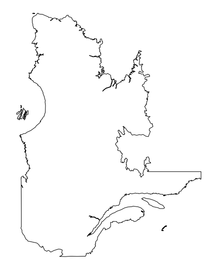

Figure A2.6: Hydro-Québec blackout time line

The following day, April 19 at 8:35 a.m., another series of short circuits at the Arnaud sub-station once again triggered the separation of the Churchill Falls network. The automatic load-shedding system, which had been repaired overnight, enabled the system to shed 3,200 MW of load across Québec and thus remain stable.

A2.7 El Paso Electric Blackout-January 31st 2001

The following information was obtained from the initial incident report to NERC [3], as well as phone conversations with Mark Quez a protection engineer with El Paso Electric (EPE) [43]. A disturbance occurred on the EPE system at 09:13 Mountain Standard Time on January 31, 2001. A jumper burned off a 115-kV line causing an intermittent fault that lasted approximately forty cycles. This line and a 345-kV line opened at about the same time. System protection removed the 345-kV line from service incorrectly due to a communications channel error. The fault spread to a second 115-kV line, which was under-built on the same support structures, and system protection then removed the line from service. Because an autotransformer at a 345-kV sub-station was not in service, a second 345-kV was not in service.

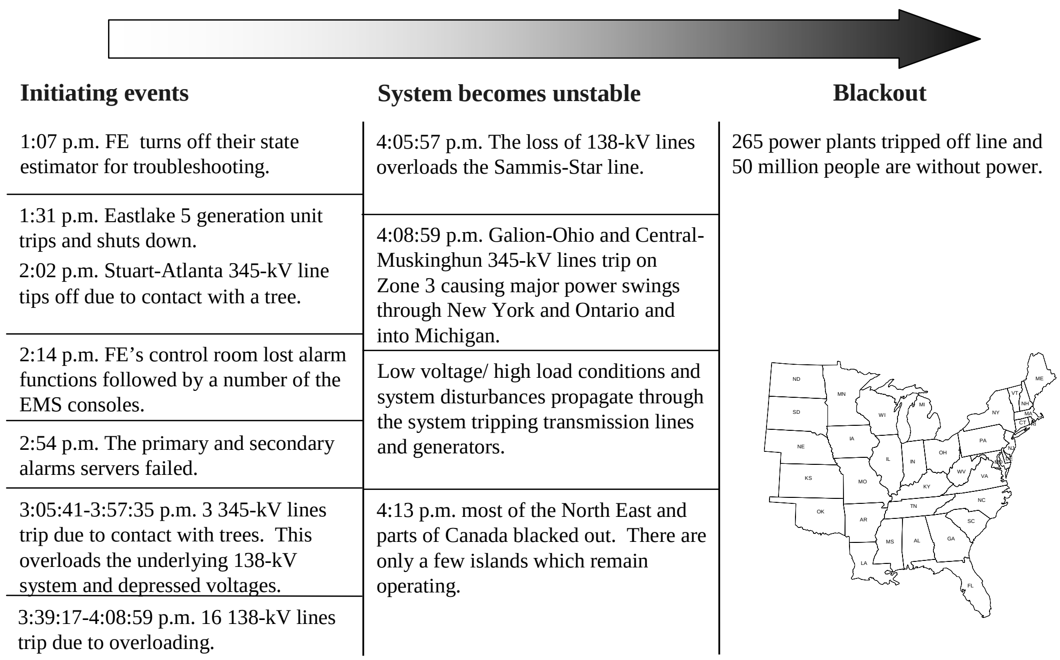

Figure A2.7: 2001 El Paso Electric blackout time line

When the first 345-kV line was removed from service, the entire fault contribution from the 345-kV system went through a third 345-kV line. This line had a hybrid <u>P</u>ermissive <u>O</u>ver-reaching <u>T</u>ransfer <u>T</u>rip (POTT) scheme that was part of a voting scheme. Because the fault was so far from this line, the blocking part of the hybrid scheme did not identify the fault correct1y and system protection on the third 345-kV line operated independently, opening the line.

Due to the loss of these lines, power flows on the EPE 115-kV transmission system increased, resulting in voltage swings and decreased voltage across the system.

The EPE under voltage protection scheme worked as designed and automatically disconnected 116 MW of load at various predetermined sub-stations throughout the EPE system.

The disconnecting of the initial 345-kV line was due to a fault in the communications system that was used by the phase angle comparison relays. The power flowing across the line was calculated by comparing the phase angle difference at the two ends of the line compensated for the latency of communication. At some unknown time a fault in the primary command path had occurred and the communications system had automatically rerouted the signal to a secondary path. This secondary path had a greater communications latency than the primary path, but this information was never communicated to the power system or any of its operators. As a result, the phase comparison relays were receiving data with a latency which was larger than the constant pre-programmed into the relays. This condition alone was not enough to cause a relay actuation, but it did result in a hidden failure. When the first 115-kV line failed the load on the 345-kV line increased to a level well below the operating limit, but well above the limit as calculated by the phase comparison relays, at which time the relays determined that a fault was present on the line.

El Paso Electric has worked with their communications engineers to ensure that this type of event does not occur again. Additionally, the Hybrid POTT has been replaced with a standard POTT relay scheme.

Appendix 3: Special Protection Systems

A3.1 Hydro-Québec Defense Plan

In 1990 Hydro-Québec initiated a program with the goals of increasing reliability, improving service quality, and conforming to criteria of the Northeast Power Coordinating Pool (NPCC) [20] and [21]. The final design had the further criteria that it must not operate during normal contingencies while at the same time ensuring that catastrophic blackouts do not occur. The final design was specifically tailored to the unique physical arrangement of the Hydro-Québec system which was discussed in section 1.2.6. The final system is designed to operate in three levels.

The first level of operation utilizes limited generation rejections and 735-kV shunt capacitors to ensure system stability without affecting service continuity. The level of generation rejection is limited to about 1,400 MW to ensure that maximum continuity of service is maintained. The first level of operation is not designed to defend against extreme contingencies.

Extreme contingencies are first addressed in the second level of protection which utilizes 735-kV shunt reactors, under voltage load shedding, and underfrequency load shedding. The underfrequency load shedding system is dispersed among one hundred and fifty 25-kV distribution sub-stations. The under voltage load shedding is still under study and has not been fully implemented. Due to the extensive scale of the underfrequency load shedding component it is expected that a moderate loss of load will occur when the second level of protection is actuated.

The third and final level of the system utilizes massive generation rejection and load shedding in the event of an extreme contingency. When the third level of protection is actuated it is expected that there will be a severe loss of load. The severe loss of load is considered an acceptable tradeoff for saving a portion of the system. With a portion of the system operating the restoration time for the affected portions of the system will be lessened. During the blackout discussed in section 1.2.6 it was the third level of protection which encountered the failure at the infrastructure interface.

A3.2 Brazilian Defense Plan

In many respect the Brazilian power system is similar to that of Hydro-Québec. The system has a total installed capacity of 65,000 MW of which 94% is hydroelectric. The Itaipu power plant which is the world second largest hydroelectric plant constitutes 18% of the installed capacity in Brazil. Just as with the Hydro-Québec system the hydroelectric plants and load centers are separated by significant distances. Interconnections between generators and load centers are made via 345-kV, 440-kV, and 750-kV transmission lines as well as HVDC links.

On March 11th 1999 the Brazilian power company ELETROBRÁS experienced the most severe blackout in its history [22]. The blackout resulted in the interruption of 24,731 MW of load which affected 75 million people. As a result of the severity of the blackout the Brazilian Ministry of Energy instructed ELETROBRÁS to convene a joint working group to investigate methods of improving reliability of the power system.

The joint working group formed seven task forces, each with its own area of interest. The seven working groups generated a color coded Network Security Matrix (NSM) which classified sub-stations into risk categories based on intrinsic reliability of a sub-station and its impact on the network security. Remedial measures were then developed for high risk sub-stations in an attempt to move them to lower risk categories. Finally, existing SPSs were evaluated and a new Programmable Logic Controller (PLC) based SPS was designed.

The new PLC based SPS divided the central and southern section of the system into independent security zones. Within each security zone slave PLCs were placed at various sub-stations for acquiring local system information. The information from the various sub-stations is then communicated to a master PLC. Commands such as generator tripping and load shedding are generated at the master PLCs and dispatched to the slave PLCs. Each of the security zones contains its own master PLC with the slaves communicating in a star configuration. When information needs to be communicated between security zones it is via the master PLCs. In order to increase the reliability of the system the master PLCs and all their equipment is duplicated and operated in a hot standby mode. Operation of the master PLCs is monitored by the National Supervisory Center which can block or unblock signals as necessary. The communications system necessary for proper operation of the new SPS is extensive and the consequences of communications failures have not been fully evaluated.

A3.3 French Coordinated Defense Plan

Electricité de France (EDF), now Réseau de Transport d`Eletricité (RTE), developed a coordinated defense plan to protect against transient stability in the late 1990's [23]. The plan was based on the observation that blackout restoration times increase as the geographic extent of a blackout increases. Therefore, if the size of a blackout can be minimized then restoration times can also be minimized. Prolonged restoration times can have a significant social impact as was seen in the New York blackout of 1977.

The French power system has approximately twenty regions which respond similarly to large system transients. The existence of these regions formed the foundation for a defense plan which seeks to isolate instabilities to a single region before they can propagate throughout the system.

Measurements are made at various points in the system using Phasor Measurement Units (PMUs) and the information is transmitted to the central control center in Paris. The information is sent via redundant communications paths, one satellite and one microwave. At the control center the data is collected and analyzed to determine if an instability condition exists anywhere in the system. If an instability condition exists the control center generates two signal types, line tripping and load shedding. Line tripping signals are used to isolate any area where an instability condition exists. The load shedding signals are sent to remote regions to prevent potential instability which could occur due to a load/generation mismatch caused by the change in system topology. In order for the system to operate properly no more than 1.3 seconds can pass from initial detection of the instability to the time when action is taken.

Currently RTE is not using the coordinated defense plan because of Operation and Maintenance (O&M) costs. It was not deemed fiscally responsible to spend the significant sums of money necessary to maintain the system for events that may never happen.

A3.4 Mexican Adaptive Protection System

The Comisión Federal de Elecricidad (CFE) of Mexico is composed of the National Interconnected System (NIS) and the Peninsular System (PS). Within the CFE there are fifteen PMUs which have previously been used to validate system models and more recently have be used as the foundation for an adaptive protection system [24].

Historically power has flowed from the NIS to the PS which was a generation deficient area. Similar to the coordinated defense plant of the EDF, the CFE viewed coordinated islanding as a viable solution to the problem of transient instability. In particular, CFE protection scheme 81/32 calls for the separation of the NIS and PS during a transient instability condition caused by a loss of generation in the Villahermosa sub-area. The separation is achieved by the opening of two parallel 230-kV lines.

These conditions changed with the installation of the 490 MW combined cycle

Central Mérida plant within the PS. With the Central Mérida plant operating at maximum rated output power flows from the PS to the NIS, the opposite of historical trends. This change in operating conditions presented potential problems and as such it was determined that the existing SPS needed to be modified to reflect the new generation source. Three operating conditions for the Central Mérida plant were defined and studied: shutdown (0 MW), mid-range output (235 MW), and maximum output (490 MW).

In the case where the Central Mérida plant is shutdown the existing 81/32 protection system operates as it was originally designed. The Villahermosa sub-area is separated from the NIS but remains connected to the PS. Additionally, the frequency drops significantly due to the loss of generation and the connection between the NIS and PS is severed via the interconnecting 230-kV lines.

In the second case where the Central Mérida plant has a mid-range output the 81/32 protection system should still operate for faults that isolate the Villahermosa sub-area but not for faults or losses of generation within the PS. During the studies it was noted that system angles within the PS were determined more by the output of the Central Mérida plant than by the amount of power being imported.

The third case studied was with the Central Mérida plant at maximum rated output. With such a large amount of generation in the PS power flowed from the PS into the NIS. Under these conditions faults occurring in either the NIS or the PS initiated tripping of the 81/32 protection system, which was undesirable.

An adaptive relay scheme based on PMU measurements was seen as the solution to these problems. The phase angle difference between the NIS and PS was used to determine the power transfer between the two areas and this was used as the basis for arming/disarming the 81/32 protection system. The 81/32 protection scheme remains armed until the output of the Central Mérida plant is high enough to start reversing power flows between the two systems, at which time it is disarmed.

A3.5 Saudi Arabian Special Protection System

Installing SPSs can be a relatively low cost method of increasing the power transfer capability for a transmission system. This is especially true when compared to the cost of installing additional transmission lines. One such economically based installation of an SPS occurred in the Saudi Arabian Electric Company [25].

The Central Branch Region of the Saudi Electric Company (SEC-CRB) is connected to the Eastern Region Branch (SEC-ERB) via three transmission paths. Two of the paths are double circuit 380-kV lines and the third is a double circuit 230-kV line. The previous method of operating the system was to limit the import of power into the SEC-CRB to 1,800 MW if the local load exceeds 4,500 MW or to 40% of system load if local load is below 4,500 MW. The goal of the new SPS was to increase the import of power into the SEC-CRB above the existing limits. In particular it was intended for the system to maintain stability during the loss of a double circuit 380-kV line. Loss of transmission lines is determined by local logic devices and undervoltage relays. Additionally, the SPS must be armed via a signal from the EMS system at the central control center. When armed automatic load shedding will be initiated if two of the four 380-kV lines are removed from service and there is a simultaneous low voltage condition.

Analysis was done to ensure voltage stability, small signal stability, and transient stability during the operation of the SPS. As such the system is armed when the import of power into the SEC-CRB is above the capability of the system to remain stable during the loss of two out of four 380-kV lines. Since the system is secure for the worst contingency, loss of two out of four 380-kV lines, the transfer limits into the SEC-CRB were able to be raised and still maintain a safety margin.

The new SPS utilizes the existing communications system which was a meshed digital fiber optic network with linear extension. To the extent practical, load shedding locations were selected so that they were not on a linear extension of the fiber optic network. The result is that the majority of the components in the SPS have at least two paths of digital fiber optic communications.

Appendix 4: Equations and Tables

Table A4.1: T and P node representation

Node	Representation
P1	Topology correctly assumed
P2	Topology incorrectly assumed
P3	Science node monitoring devices operational
P4	Measurements at the node controller
P5	Measurements at the Y Patch
P6	Signal at L2/L3 West
P7	Signal at L2/L3 East
P8	Signal at OE/EO East
P9	Signal at DWDM East
P10	Signal at EDFA East
P11	Signal on fiber 1
P14	Signal on fiber 2
P15	Signal at shore station 2 EDFA
P16	Signal at shores station 2 DWDM
P17	Signal at shore station 2 L2/L3 switch
P18	Science node monitoring devices operational
P19	Measurements at the node controller
P20	Measurements at the Y Patch
P21	Signal at L2/L3 West
P22	Signal at L2/L3 East
P23	Signal at OE/EO East
P24	Signal at DWDM East
P25	Signal at EDFA East
P26	Signal on fiber 1
P27	Not Used
P28	Not Used
P29	Signal on fiber 2
P30	Signal at shore station 1 EDFA
P31	Signal at shores station 1 DWDM
P32	Signal at shore station 1 L2/L3 switch
P33	Signal at shore station 2 LAN
P34	Signal at shore station 1 LAN
P35	Signal at shore station 2 PMACS server
P36	Signal at shore station 1 PMACS server
P37	Signal at shore station 2 10 kV Controller
P38	Signal at shore station 1 10 kV Controller
P39	Signal at shore station 2 10 kV Supply

Table A4.1 (Continued)

P40	Signal at shore station 1 10 kV Supply
P41	Shore station 2 voltage =8,500V
P42	Shore station 1 voltage =8,500V
P43	Shore station 2 voltage =9,000V
P44	Shore station 1 voltage =9,000V
P45	Shore station 2 voltage =9,500V
P46	Shore station 1 voltage =9,500V
P47	Shore station 2 voltage =10,000V
P48	Shore station 1 voltage =10,000V
P49	Shore station 2 voltage =10,500V
P50	Shore station 1 voltage =10,500V
P51	Shore station 2 voltage =11,000V
P52	Shore station 1 voltage =11,000V
P53	Shore station 2 voltage =11,500V
P54	Shore station 1 voltage =11,500V
P55	Shore station 2 voltage =12,000V
P56	Shore station 1 voltage =12,000V
P57	Shore station 2 measurement devices operational
P58	Shore station 1 measurement devices operational
P59	Measurements at the shore station 2 power supply controller
P60	Measurements at the shore station 1 power supply controller
P61	Signal available to PMACS client (shore station voltage)
P62	PMACS client operational
P63	Signal available to PMACS LAN
P64	Signal available to PMACS client (science node data)
P65-P72	Residual calculated for various voltages at shore station 2
P73-P80	Residual calculated for various voltages at shore station 2
P81	Residual sensitivities for variations at both shore stations known
P82	Assumed topology is the incorrect topology
P83	Assumed topology is the correct topology
T1	Topology change occurs
T2	Determine system topology
T3	Take measurements and Pass to the node controller
T4	ADC and pass to Y patch
T5	Pass signal from Y-panel to L2/L3 Switch West
T6	Pass signal from Y-panel to L2/L3 Switch East
T7	Pass signal from L2/L3 switch west to L2/L3 switch east
T8	Pass signal from L2/L3 switch east to L2/L3 switch west
T9	Pass signal from L2/L3 to OEO

Table A4.1 (Continued)

T10	Pass signal from OEO to L2/L3
T11	Pass signal from DWDM to OEO
T12	Pass signal from OEO to DWDM
T13	Pass signal from DWDM to EDFA on fiber 1
T14	Pass signal from DWDM to EDFA on fiber 2
T15	Pass signal from EDFA to DWDM on fiber 1
T16	Pass signal from EDFA to DWDM on fiber 2
T17	Pass signal from fiber 1 to EDFA
T18	Pass signal from fiber 2 to EDFA
T19	Pass signal from EDFA to fiber 1
T20	Pass signal from EDFA to fiber 2
T21	Pass signal from shore station 2 EDFA to fiber 1
T22	Not Used
T23	Not Used
T24	Pass signal from fiber 2 to shore station 2 EDFA
T25	Pass signal from shore station 2 EDFA to DWDM
T26	Pass signal from shore station 2 EDFA to DWDM
T27	Not Used
T28	Not Used
T29	Not Used
T30	Pass signal from shore station 2 DWDM to L2/L3
T31	Take measurements and Pass to the node controller
T32	ADC and pass to Y patch
T33	Pass from Y-panel to L2/L3 Switch West
T34	Pass from Y-panel to L2/L3 Switch East
T35	Pass from L2/L3 switch west to L2/L3 switch east
T36	Pass from L2/L3 switch east to L2/L3 switch west
T37	Pass signal from L2/L3 to OEO
T38	Pass signal from OEO to L2/L3
T39	Pass signal from DWDM to OEO
T40	Pass signal from OEO to DWDM
T41	Pass signal from DWDM to EDFA on fiber 1
T42	Pass signal from DWDM to EDFA on fiber 2
T43	Pass signal from EDFA to DWDM on fiber 1
T44	Pass signal from EDFA to DWDM on fiber 2
T45	Pass signal from fiber 1 to EDFA
T46	Pass signal from fiber 2 to EDFA
T47	Pass signal from EDFA to fiber 1
T48	Pass signal from EDFA to fiber 2

Table A4.1 (Continued)

T49	Pass signal from shore station 1 EDFA to fiber 1
T50	Not Used
T51	Not Used
T52	Pass signal from fiber 2 to shore station 1 EDFA
T53	Pass signal from shore station 1 EDFA to DWDM
T54	Pass signal from shore station 1 EDFA to DWDM
T55	Pass signal from shore station 1 DWDM to EDFA
T56	Pass signal from shore station 1 DWDM to EDFA
T57	Not Used
T58	Pass signal from shore station 1 DWDM to L2/L3
T59	Send signal to PMACS Server at shore station 2 via LAN
T60	Send signal to PMACS Server at shore station 1 via LAN
T61	Convert values and send to shores station 2 LAN
T62	Convert values and send to shore station 1 LAN
T63	Send signal to 10 kV Controller at shore station 2 via LAN
T64	Send signal to 10 kV Controller at shore station 1 via LAN
T65	Convert values and send to shore station 2 10 kV supply
T66	Convert values and send to shore station 1 10 kV supply
T67-T73	Decrement shore station 2 converter voltage 500V @ power supply
T74-T80	Increment shore station 2 converter voltage 500V @ power supply
T81-T87	Decrement shore station 1 converter voltage 500V @ power supply
T88-T94	Increment shore station 1 converter voltage 500V@ power supply
T95	Take measurements at shore station 2 supply, ADC, and pass to the supply controller
T96	Take measurements at shore station 1 supply, ADC, and pass to the supply controller
T97	Send signal to shore station 2 LAN
T98	Send signal to shore station 1 LAN
T99	Poll science node measurements from shore station 2 to PMACS LAN
T100	Poll science node measurements from shore station 1 to PMACS LAN
T101	Poll shore station 2 measurements to PMACS LAN
T102	Poll shore station 1 measurements to PMACS LAN
T103	New signal received at PMACS server (science node data)
T104	New signal received at PMACS server (science node data)
T105	New signal received at PMACS server (shore station voltage)
T106	New signal received at PMACS server (shore station voltage)
T107	Send raise/lower signal to shore station 2 LAN
T108	Send raise/lower signal to shore station 1 LAN
T109	Pass signal from PMACS LAN to client (shore station 2 data)

Table A4.1 (Continued)

T110	Pass signal from PMACS LAN to client (shore station 1 data)
T111	Pass signal from PMACS LAN to client (science node data)
T112-T119	Calculate residual for various voltages at shore station 2
T120-T127	Calculate residual for various voltages at shore station 2
T128	Generate residual sensitivity to variations in shore station 2 voltages
T129	Generate residual sensitivity to variations in shore station 1 voltages
T130	Determine if assumed topology is correct topology (it is not)
T131	Change assumed topology to next possible topology in queue
T132	Determine if assumed topology is correct topology (it is)
T133	Pass signal from shore station 2 L2/L3 switch to LAN
T134	Pass signal from shore station 1 L2/L3 switch to LAN

Table A4.2: Detailed PN model information

Node	FIT (1/hours)	MTBF (hours)	TP	TP(msec)
T1	N/A	N/A	N/A	20
T2	0		1	1
T3	9991.443828	100085.635	1	1000
T4	5204.189414	192152.8831	1	4
T5	1416.935	705748.6758	1	4
T6	1416.935	705748.6758	1	4
T7	2416.935	413747.1632	1	4
T8	2416.935	413747.1632	1	4
T9	1646.935	607188.5047	1	4
T10	1646.935	607188.5047	1	4
T11	1106.935	903395.4117	1	4
T12	1106.935	903395.4117	1	4
T13	976.935	1023609.554	1	4
T14	976.935	1023609.554	1	4
T15	976.935	1023609.554	1	4
T16	976.935	1023609.554	1	4
T17	516.935	1934479.19	1	4
T18	516.935	1934479.19	1	4
T19	516.935	1934479.19	1	4
T20	516.935	1934479.19	1	4

Table A4.2 (Continued)

Node	FIT (1/hours)	MTBF (hours)	TP	TP(msec)
T21	100	10000000	1	4
T22	100	10000000	1	4
T23	100	10000000	1	4
T24	100	10000000	1	4
T25	560	1785714.286	1	4
T26	560	1785714.286	1	4
T27	560	1785714.286	1	4
T28	560	1785714.286	1	4
T29	1460	684931.5068	1	4
T30	1460	684931.5068	1	4
T31	9991.443828	100085.635	1	1000
T32	5204.189414	192152.8831	1	4
T33	1416.935	705748.6758	1	4
T34	1416.935	705748.6758	1	4
T35	2416.935	413747.1632	1	4
T36	2416.935	413747.1632	1	4
T37	1646.935	607188.5047	1	4
T38	1646.935	607188.5047	1	4
T39	1106.935	903395.4117	1	4
T40	1106.935	903395.4117	1	4
T41	976.935	1023609.554	1	4
T42	976.935	1023609.554	1	4
T43	976.935	1023609.554	1	4
T44	976.935	1023609.554	1	4
T45	516.935	1934479.19	1	4
T46	516.935	1934479.19	1	4
T47	516.935	1934479.19	1	4
T48	100	10000000	1	4
T49	100	10000000	1	4
T50	100	10000000	1	4
T51	100	10000000	1	4
T52	100	10000000	1	4
T53	560	1785714.286	1	4
T54	560	1785714.286	1	4
T55	560	1785714.286	1	4
T56	560	1785714.286	1	4
T57	1460	684931.5068	1	4
T58	1460	684931.5068	1	4
T59	15635	63959.0662	1	4
T60	15635	63959.0662	1	4
T61	15635	63959.0662	1	4

Table A4.2 (Continued)

Node	FIT (1/hours)	MTBF (hours)	TP	TP(msec)
T62	15635	63959.0662	1	4
T63	5037.254414	198520.8445	1	20
T64	5037.254414	198520.8445	1	20
T65	9574.508828	104444	1	20
T66	9574.508828	104444	1	20
T67	4787.254414	208888	1	1000
T68	4787.254414	208888	1	1000
T69	4787.254414	208888	1	1000
T70	4787.254414	208888	1	1000
T71	4787.254414	208888	1	1000
T72	4787.254414	208888	1	1000
T73	4787.254414	208888	1	1000
T74	4787.254414	208888	1	1000
T75	4787.254414	208888	1	1000
T76	4787.254414	208888	1	1000
T77	4787.254414	208888	1	1000
T78	4787.254414	208888	1	1000
T79	4787.254414	208888	1	1000
T80	4787.254414	208888	1	1000
T81	4787.254414	208888	1	1000
T82	4787.254414	208888	1	1000
T83	4787.254414	208888	1	1000
T84	4787.254414	208888	1	1000
T85	4787.254414	208888	1	1000
T86	4787.254414	208888	1	1000
T87	4787.254414	208888	1	1000
T88	4787.254414	208888	1	1000
T89	4787.254414	208888	1	1000
T90	4787.254414	208888	1	1000
T91	4787.254414	208888	1	1000
T92	4787.254414	208888	1	1000
T93	4787.254414	208888	1	1000
T94	4787.254414	208888	1	1000
T95	9574.508828	104444	1	100
T96	9574.508828	104444	1	100
T97	5037.254414	198520.8445	1	10
T98	5037.254414	198520.8445	1	10
T99	250	4000000	1	0.128
T100	250	4000000	1	0.128
T101	250	4000000	1	0.128
T102	250	4000000	1	0.128

Table A4.2 (Continued)

Node	FIT (1/hours)	MTBF (hours)	TP	TP(msec)
T103	0	N/A	1	0
T104	0	N/A	1	0
T105	0	N/A	1	0
T106	0	N/A	1	0
T107	250	4000000	1	2
T108	250	4000000	1	2
T109	250	4000000	1	4
T110	250	4000000	1	4
T111	250	4000000	1	4
T112	0	N/A	1	1
T113	0	N/A	1	1
T114	0	N/A	1	1
T115	0	N/A	1	1
T116	0	N/A	1	1
T117	0	N/A	1	1
T118	0	N/A	1	1
T119	0	N/A	1	1
T120	0	N/A	1	1
T121	0	N/A	1	1
T122	0	N/A	1	1
T123	0	N/A	1	1
T124	0	N/A	1	1
T125	0	N/A	1	1
T126	0	N/A	1	1
T127	0	N/A	1	1
T128	1250	N/A	1	4
T129	1250	N/A	1	4
T130	1250	N/A	1	4
T131	1250	N/A	1	4

$$TP_{Section1} = \left(\left(TP_{SS1} + TP_{SS2}\right) - \left(TP_{SS1} \cdot TP_{SS2}\right)\right) \tag{A4.1}$$

Where:

$$TP_{SS1} = \left(\sum_{i=1}^{46} \left(\begin{array}{l} \left(TP_{31} \cdot TP_{32} \cdot \left(\begin{array}{l} \left(TP_{33} \cdot TP_{35} + TP_{34}\right) - \\ \left(TP_{33} \cdot TP_{35} \cdot TP_{34}\right) \end{array} \right) \right) \cdot \\ \left(\left(\left(\begin{array}{l} \left(TP_{41} \cdot TP_{45} \cdot TP_{46} \cdot TP_{43}\right) + \\ \left(TP_{42} \cdot TP_{48} \cdot TP_{47} \cdot TP_{44}\right) \end{array} \right) - \\ \left(\begin{array}{l} TP_{41} \cdot TP_{45} \cdot TP_{46} \cdot TP_{43} \\ TP_{42} \cdot TP_{48} \cdot TP_{47} \cdot TP_{44} \end{array} \right) \right) \cdot \prod_{k=37}^{40} \left(TP_k\right) \right)^{n_{SS1(i)}} \cdot \\ \left(\left(\left(TP_{53} + TP_{54}\right) - \left(TP_{53} \cdot TP_{54}\right)\right) \cdot TP_{58}\right) \cdot TP_{134} \end{array} \right) \right)^{15}$$

$$TP_{SS2} = \left(\sum_{i=1}^{46} \left(\begin{array}{l} \left(TP_{3} \cdot TP_{4} \cdot \left(\begin{array}{l} \left(TP_{5} \cdot TP_{7} + TP_{6}\right) - \\ \left(TP_{5} \cdot TP_{7} \cdot TP_{6}\right) \end{array} \right) \right) \cdot \\ \left(\left(\left(\begin{array}{l} \left(TP_{13} \cdot TP_{17} \cdot TP_{18} \cdot TP_{15}\right) + \\ \left(TP_{14} \cdot TP_{20} \cdot TP_{19} \cdot TP_{16}\right) \end{array} \right) - \\ \left(\begin{array}{l} TP_{13} \cdot TP_{17} \cdot TP_{18} \cdot TP_{15} \\ TP_{14} \cdot TP_{20} \cdot TP_{19} \cdot TP_{16} \end{array} \right) \right) \cdot \prod_{k=9}^{12} \left(TP_k\right) \right)^{n_{SS1(i)}} \cdot \\ \left(\left(\left(TP_{25} + TP_{26}\right) - \left(TP_{25} \cdot TP_{26}\right)\right) \cdot TP_{30}\right) \cdot TP_{133} \end{array} \right) \right)^{15}$$

$n_{SS1(i)}$: Number of relays necessary to reach shore station 1 for the i[th] node

$n_{SS2(i)}$: Number of relays necessary to reach shore station 2 for the i[th] node

$$TP_{Section2} = \left(\prod_{i=\begin{pmatrix}59,61,63,65,\\95,97,107\end{pmatrix}} (TP_i) \cdot \prod_{i=\begin{pmatrix}60,62,64,66,\\96,98,108\end{pmatrix}} (TP_i) \right)^{15} \left(\cdot \prod_{i=67}^{80} (TP_i) \cdot \prod_{i=81}^{94} (TP_i) \right) \tag{A4.2}$$

$$TP_{Section3} = \left(\begin{array}{l} \left(\begin{array}{l} \left(\left(\left(\prod_{i=\begin{pmatrix}99,101,\\103,105\end{pmatrix}} (TP_i) \cdot (TP_{59} \cdot TP_{61})^{16} \right) + \left(\prod_{i=\begin{pmatrix}100,102,\\104,106\end{pmatrix}} (TP_i) \cdot (TP_{60} \cdot TP_{62})^{16} \right) \right) \right) - \\ \left(\left(\left(\prod_{i=\begin{pmatrix}99,101,\\103,105\end{pmatrix}} (TP_i) \cdot (TP_{59} \cdot TP_{61})^{16} \right) \cdot \left(\prod_{i=\begin{pmatrix}100,102,\\104,106\end{pmatrix}} (TP_i) \cdot (TP_{60} \cdot TP_{62})^{16} \right) \right) \right) \end{array} \right) \cdot \\ (TP_{109} \cdot TP_{110})^{8} \cdot TP_{111}{}^{16} \cdot \prod_{i=112}^{129} (TP_i) \cdot TP_{132} \cdot (TP_{131} \cdot TP_{132})^{n} \cdot TP_2 \end{array} \right) \tag{A4.3}$$

Where:

n : number of incorrect topologies assumed before the correct one is found

$$TTP = \left(\begin{array}{l} \left(\begin{array}{l} \left(\left(\left(\prod_{i=\begin{pmatrix}99,101,\\103,105\end{pmatrix}} (TP_i) \cdot (TP_{59} \cdot TP_{60})^{16} \cdot TP_{SS1} \right) + \left(\prod_{i=\begin{pmatrix}100,102,\\104,106\end{pmatrix}} (TP_i) \cdot (TP_{60} \cdot TP_{62})^{16} \cdot TP_{SS2} \right) \right) \right) - \\ \left(\left(\left(\prod_{i=\begin{pmatrix}99,101,\\103,105\end{pmatrix}} (TP_i) \cdot (TP_{59} \cdot TP_{60})^{16} \cdot TP_{SS1} \right) \cdot \left(\prod_{i=\begin{pmatrix}100,102,\\104,106\end{pmatrix}} (TP_i) \cdot (TP_{60} \cdot TP_{62})^{16} \cdot TP_{SS2} \right) \right) \right) \end{array} \right) \cdot \\ \left((TP_{109} \cdot TP_{110})^{8} \cdot TP_{111}{}^{16} \cdot \prod_{i=112}^{129} (TP_i) \cdot TP_{132} \cdot (TP_{131} \cdot TP_{132})^{n} \cdot TP_2 \cdot \right) \\ \left(\left(\prod_{i=\begin{pmatrix}59,61,63,65,\\95,97,107\end{pmatrix}} (TP_i) \right)^{15} \cdot \prod_{i=67}^{80} (TP_i) \right) \cdot \left(\left(\prod_{i=\begin{pmatrix}60,62,64,66,\\96,98,108\end{pmatrix}} (TP_i) \right)^{15} \cdot \prod_{i=81}^{94} (TP_i) \right) \end{array} \right) \tag{A4.4}$$

$$TP_{SS1}=\left(\sum_{i=1}^{46}\left(\begin{matrix}\left(TP_3\cdot TP_4\cdot\left(\begin{matrix}\left(TP_5\cdot TP_7+TP_6\right)-\\ \left(TP_5\cdot TP_7\cdot TP_6\right)\end{matrix}\right)\right)\cdot\\ \left(\left(\left(\begin{matrix}\left(TP_{13}\cdot TP_{17}\cdot TP_{18}\cdot TP_{15}\right)+\\ \left(TP_{14}\cdot TP_{20}\cdot TP_{19}\cdot TP_{16}\right)\end{matrix}\right)-\\ \left(\begin{matrix}TP_{13}\cdot TP_{17}\cdot TP_{18}\cdot TP_{15}\\ TP_{14}\cdot TP_{20}\cdot TP_{19}\cdot TP_{16}\end{matrix}\right)\right)\cdot\prod_{k=9}^{12}\left(TP_k\right)\right)^{n_{SS1i_{(i)}}}\cdot\\ \left(\left(\left(TP_{25}+RP_{26}\right)-\left(TP_{25}\cdot TP_{26}\right)\right)\cdot TP_{30}\right)\cdot TP_{133}\end{matrix}\right)\right) \tag{A4.5}$$

$$TP_{SS2}=\left(\sum_{i=1}^{46}\left(\begin{matrix}\left(TP_{31}\cdot TP_{32}\cdot\left(\begin{matrix}\left(TP_{33}\cdot TP_{35}+TP_{34}\right)-\\ \left(TP_{33}\cdot TP_{35}\cdot TP_{34}\right)\end{matrix}\right)\right)\cdot\\ \left(\left(\left(\begin{matrix}\left(TP_{41}\cdot TP_{45}\cdot TP_{46}\cdot TP_{43}\right)+\\ \left(TP_{42}\cdot TP_{48}\cdot TP_{47}\cdot TP_{44}\right)\end{matrix}\right)-\\ \left(\begin{matrix}TP_{41}\cdot TP_{45}\cdot TP_{46}\cdot TP_{43}\cdot\\ TP_{42}\cdot TP_{48}\cdot TP_{47}\cdot TP_{44}\end{matrix}\right)\right)\cdot\prod_{k=37}^{40}\left(TP_k\right)\right)^{n_{SS2(i)}}\cdot\\ \left(\left(\left(TP_{53}+RP_{54}\right)-\left(TP_{53}\cdot TP_{54}\right)\right)\cdot TP_{58}\right)\cdot TP_{134}\end{matrix}\right)\right) \tag{A4.6}$$

$$TT_{SS1}=\left(\left(20\cdot\sum_{k=37}^{40}\left(TT_k\right)\right)+\left(\sum_{k=\begin{pmatrix}31,32,34,41,\\ 43,45,46,53,\\ 54,58,134\end{pmatrix}}\left(TT_k\right)\right)\right) \tag{A4.7}$$

$$TT_{SS2}=\left(\left(13\cdot\sum_{k=9}^{12}\left(TT_k\right)\right)+\left(\sum_{k=\begin{pmatrix}3,4,6,13,\\ 15,17,18,\\ 25,26,30,133\end{pmatrix}}\left(TT_k\right)\right)\right) \tag{A4.8}$$

$$TT_{SS1} = \left(\sum_{i=\left(\substack{60,62,64,66,\\88,96,98,108}\right)} (TT_i) \right) \quad \text{(A4.9)}$$

$$TT_{SS2} = \left(\sum_{i=\left(\substack{59,61,63,65,\\67,95,97,107}\right)} (TT_i) \right) \quad \text{(A4.10)}$$

$$TT_{PMACS} = \begin{pmatrix} \sum_{i=\left(\substack{99,101,\\103,105}\right)} (TT_i) + (16 \cdot (TT_{59} + TT_{60})) + (8 \cdot (TT_{109} + TT_{110})) + \\ (16 \cdot TT_{111}) + \sum_{i=112}^{129} (TT_i) + TT_{132} + (n \cdot (TT_{131} + TT_{132})) + TT_2 \end{pmatrix} \quad \text{(A4.11)}$$

Where:

n : number of incorrect topologies assumed before the correct one is found

$$TTT = \begin{pmatrix} \left(\left(13 \cdot \sum_{k=37}^{40} (TT_k)\right) + \left(\sum_{k=\left(\substack{31,32,34,41,\\43,45,46,53,\\54,58,134}\right)} (TT_k) \right) \right) + \left(\sum_{i=\left(\substack{59,61,63,65,\\67,95,97,107}\right)} (TT_i) \right) + \\ \begin{pmatrix} \sum_{i=\left(\substack{99,101,\\103,105}\right)} (TT_i) + (16 \cdot (TT_{59} + TT_{60})) + (8 \cdot (TT_{109} + TT_{110})) + \\ (16 \cdot TT_{111}) + \sum_{i=112}^{129} (TT_i) + TT_{132} + (n \cdot (TT_{131} + TT_{132})) + TT_2 \end{pmatrix} \end{pmatrix} \quad \text{(A4.12)}$$

$$TTP=\left(\left(\begin{array}{l}(((TP_{59}\cdot TP_{61}\cdot TP_{99}\cdot TP_{105})\cdot TP_{SS1})+((TP_{60}\cdot TP_{62}\cdot TP_{100}\cdot TP_{104})\cdot TP_{SS2}))-\\(((TP_{59}\cdot TP_{61}\cdot TP_{99}\cdot TP_{105})\cdot TP_{SS1})\cdot((TP_{60}\cdot TP_{62}\cdot TP_{100}\cdot TP_{104})\cdot TP_{SS2}))\end{array}\right)\cdot\right.\\\left.\prod_{i=109}^{112}(TP_i)\cdot TP_{128}\cdot TP_{132}\cdot(TP_{131}\cdot TP_{132})^n\cdot TP_2\right) \quad \text{(A4.13)}$$

$$TTT=\left(\left(\left(13\cdot\sum_{k=37}^{40}(TT_k)\right)+\left(\sum_{k=\begin{pmatrix}31,32,34,41,\\43,45,46,53,\\54,58,134\end{pmatrix}}(TT_k)\right)\right)+\left(\sum_{i=\begin{pmatrix}59,61,63,65,\\67,95,97,107\end{pmatrix}}(TT_i)\right)+\right.\\\left.(TT_{111}+TT_{112}+TT_{132}+(n\cdot(TT_{131}+TT_{132}))+TT_2)\right) \quad \text{(A4.14)}$$

Vita

Kevin Schneider was born in London England in 1973 and soon after moved to the United States. After graduating from Bellingham High School in 1992 he enlisted in the United States Navy. His initial assignment was in the Navy's nuclear power training program which took just under 2 years. The remainder of the six year commitment was spent assigned to the nuclear submarine U.S.S. Los Angeles (SSN-688) as a member of the Electrical Division, Engineering Department.

Upon discharge from active duty he enrolled at the University of Washington as a Freshman Physics Major in the autumn of 1998. While an undergraduate he worked for Professor Paul Boynton studying Non-Newtonian Gravity. In the Winter Quarter of 2001 he completed his B.S. degree in Physics and transferred to the Department of Electrical Engineering. In 2002 he completed his M.S. in Electrical Engineering while studying aspects of distributed generation under Professor Chen-Ching Liu. With the competition and successful defense of this dissertation he will have completed his Ph.D. in Electrical Engineering, also under Professor Chen-Ching Liu.